HYDROSTRATIGRAPHY OF THE PARIS MORAINE

IN THE GUELPH AREA, ONTARIO, CANADA

HYDROSTRATIGRAPHY OF THE PARIS MORAINE IN THE GUELPH AREA, ONTARIO, CANADA

By

Andrew T. Trapp, B.Sc.

A Thesis

Submitted to the School of Graduate Studies

In partial Fulfillment of the Requirements

For the Degree

Master of Science

McMaster University

MASTER OF SCIENCE (2015) **McMaster University**

Earth and Environmental Science **Hamilton, Ontario**

Title: Hydrostratigraphy of the Paris Moraine in the Guelph area, Ontario, Canada.

AUTHOR: Andrew T. Trapp, B.Sc. (McMaster University)

SUPERVISOR: Professor James E. Smith

NUMBER OF PAGES: 179

ABSTRACT

Many growing southern Ontario communities, including Guelph, rely on fractured bedrock aquifers for drinking water. Contamination and overexploitation pose a threat to these water resources, necessitating characterization of vulnerability, risks, and recharge areas. Quaternary sediments southeast of the City of Guelph, including the Paris Moraine, were investigated in order to delineate hydrostratigraphy. This was achieved through study of 9 cored-holes, as well as existing MOE, GRCA, and University of Guelph data. Falling head permeameter measurements and empirical grain-size distribution measurements and analysis were employed for determination of K_{sat} values, which were used to construct a hydrostratigraphy. Of 19 methods evaluated, The Kozeny-Carman empirical grain-size method for determining K_{sat} was found to be more representative of measured values for the study area. The area is dominated by a conductivity regime of 2.72×10^{-7} – 1.40×10^{-6} m/s with local heterogeneity present on the scale of 10's to 100's of meters. The Paris Moraine, particularly its backslope, is at higher risk due to its relatively high conductivity, greater occurrence of aquifer units, as well as prevalence of small-scale topographic (hummocky topography), and bedrock topographic lows.

ACKNOWLEDGMENTS

There are a number of individuals who I must recognize. I must thank my supervisor, Dr. James E. Smith, for providing me this great opportunity and for helping to develop my skills as a student and researcher alike. Dr. Smith must also be thanked for his support of my personal goals. I must also thank Dr. Emmanuelle Arnaud for allowing me to collaborate on this project and for providing me with unwavering support and encouragement throughout this process.

Thank you to Anna Best and Steve Sadura for guiding and assisting me with fieldwork and sampling activities, as well as Anna's contribution to key figures and maps presented in the study.

I would also like to thank the Ontario Research Fund, and NSERC for funding this project, as well as OMAFRA for funding drilling activities.

Thank you to the GRCA for providing access to geotechnical reports and grain-size data.

Additionally, thank you to previous G360 students, including: Mike McGill, Adam Gilmour, and Kelsey MacCormack for your contribution to sample collection.

Last, but certainly not least, I must thank my family and friends for supporting me through this endeavor, especially my parents and girlfriend; whose love and patience have made all the difference.

TABLE OF CONTENTS

LIST OF FIGURES

LIST OF TABLES

LIST OF APPENDICES

1.0 INTRODUCTION

An ever-growing world population drives an increasing demand for water supply. Surface water bodies can meet the majority of this demand, however, spatial variability causes certain regions to rely heavily on groundwater resources (Wada, 2010). Roughly 30% of the Canadian population is reliant on groundwater for drinking (Statistics Canada, 2003). As the Canadian population grows, and the impact on surface water deepens, this reliance will only increase. Land use changes accompanying the growing population will simultaneously amplify reliance on groundwater resources and increasingly threaten them. Overexploitation and increased contamination are the main threats and must be mitigated (Wada, 2010; Honisch et al., 2002).

Urban development, industrial development, increased agriculture intensity, and aggregate extraction, all accompany population growth (Blackport 2009). These factors cause a variety of changes in the regional and local hydrologic cycle including changes in water demand and decreased water quality due to; changes in interception and recharge, evapotranspiration, contaminated runoff, contamination spills, increased erosion, and intensified water use (USGS, 2014).

1.1 Objectives

This study aims to investigate Quaternary sediment deposits in the Guelph area for the purpose of groundwater protection and risk management. This will be carried out in two stages: 1) Analysis of existing empirical grain-size methods

for applicability to the study area. 2) Integration and application of existing geologic and hydrogeologic data, with new calculated and measured K_{sat} values, towards delineation of high-resolution hydrostratigraphy. This will inform future use of empirical grain-size methods in the local area. It will provide insight into the heterogeneous nature of hydraulic conductivity in these complex glacial deposits, informing contaminant fate and transport, and recharge, into underlying bedrock aquifers.

1.2 Thesis Organization

This thesis consists of two main chapters. Chapter 2 focuses on assessment of 19 empirical grain-size methods for calculation of K_{sat} and identification of the most appropriate method for use in the study area. Chapter 3 focuses on delineation of Quaternary hydrostratigraphy using K_{sat}, and associated implications for risk and recharge.

2.0 Calculating Hydraulic Conductivity by Empirical Grain-Size Analysis

2.1.0 INTRODUCTION

There are various methods used to determine K_{sat} including: pump tests, lab permeameter tests, and grain-size analysis. Empirical grain-size methods are often used to determine K_{sat} from grain-size analysis. This is due to their simplicity, low cost, and availability of data from existing sedimentological studies.

Multiple empirical grain-size methods are found in the literature to calculate K_{sat}. The majority are derived from field or lab investigations, and nearly all the studies fail to outline the conditions and assumptions under which the study took place (Kasenow, 2002). The wide use of these empirical grain-size methods in the hydrogeologic industry calls for a comprehensive understanding of the uses and limitations of each method as well as their relation to accepted measurement methods (ie. pump tests, permeameter tests).

It needs to be stated that K_{sat} values determined from empirical grain-size methods are regarded as the least accurate when compared to methods of direct measurement (Kasenow, 2002). This is in part due to the isotropic, structure independent nature of these methods. Sample scale also has a great effect on observed discrepancies between empirically calculated K_{sat} values and measured values. Generally, empirical grain-size methods underestimate values measured in pump tests, where higher flow along layers dominate. Simultaneously, flow limiting heterogeneities are minimized due to large sample volume. Conversely, empirical grain-size methods overestimate permeameter

tests, which are dominated by lower flow across layers. These empirical grain-size methods are also conducted on a much smaller scale, increasing the effect of small-scale heterogeneities (Vukovic and Soro, 1992).

In this study, 19 grain-size methods were evaluated in order to determine the method that best approximates the values for the Paris Moraine data from 9 high quality boreholes (Figure 2.0). This was accomplished by comparison of 164 calculated values from grain-size data, to those measured by falling head permeameter tests on 104 corresponding samples across all sites. Each empirical method was then calibrated to adjust the calculated mean *log-*K_{sat} to the permeameter measured mean *log-*K_{sat} values. Additionally, soil water retention curves, and K_{unsat} functions were calculated to evaluate variation of unsaturated hydraulic parameters of sediments with similar grain-size and for potential use in numerical modeling.

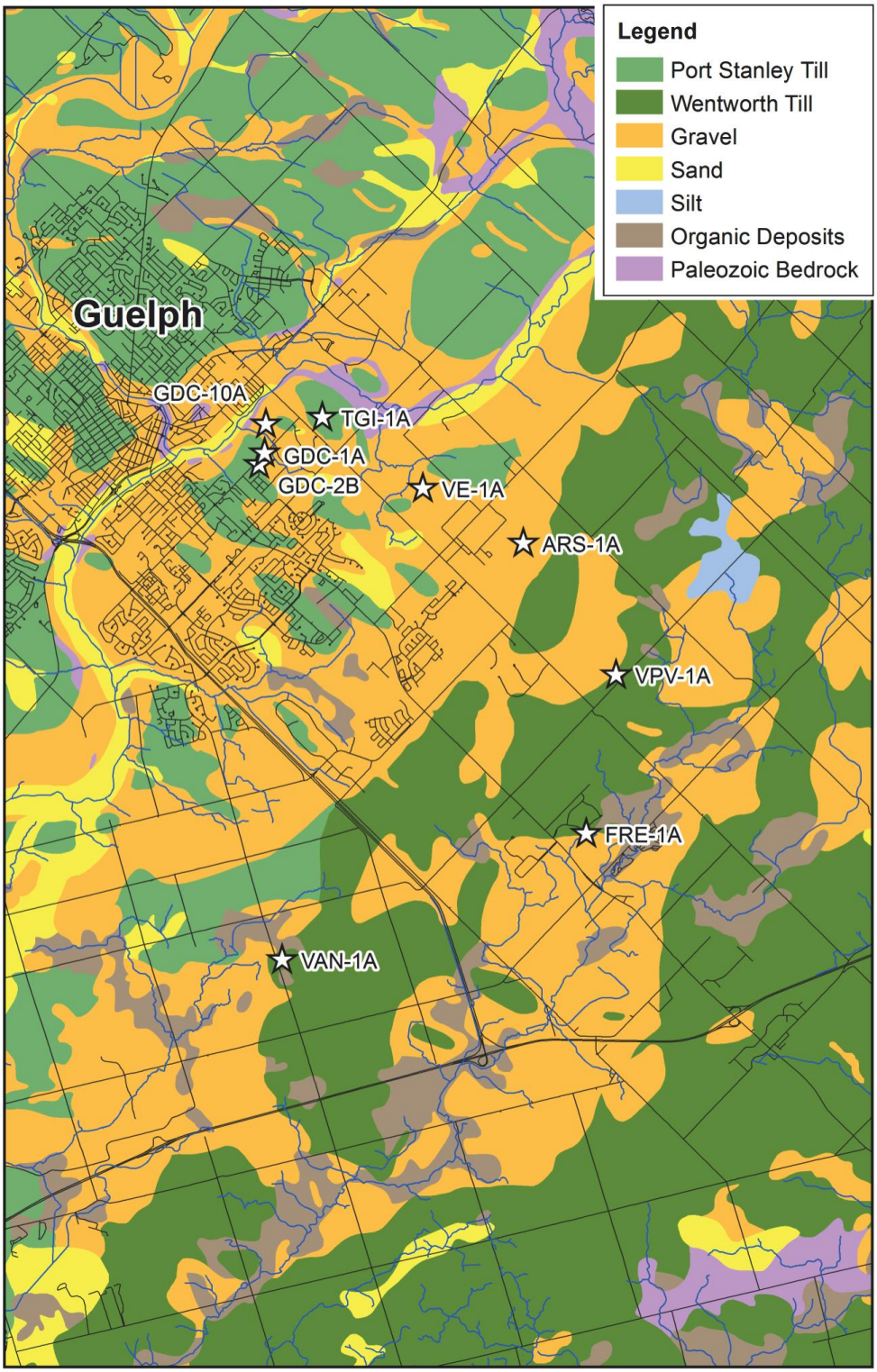

Figure 2.0: Surficial geology map of the study are with high quality borehole locations (stars). Modified from maps created by Anna Best using ESRI ArcMap 9.3 with data from the Ontario Geological Survey (2003).

2.2.0 BACKGROUND

2.2.1 The General Empirical Grain-Size Equation

The empirical grain-size equations were developed for a range of materials, and for differing characteristics of porous media (Vukovic and Soro, 1992). As a result, the literature contains multiple forms of each empirical equation. Vukovic and Soro (1992) present a "general formula" allowing direct comparison of the various empirical equations:

$$K = \frac{g}{v} \text{ x } C \text{ x } f(n) \text{ x } d_e^2 \tag{1}$$

Where, g = acceleration of gravity (m/s^2)

v = kinematic coefficient of viscosity (m^2/s)

C = coefficient of proportionality (cited as dimensionless; dimension analysis reveals embedded dimensions associated with dimension conversions)

$f(n)$ = porosity function

And, d_e = effective grain-size diameter (mm)

Expression of K_{sat} in the form of equation (1) is dimensionally homogeneous, as the authors (Vukovic and Sorro, 1992) modified the form of the original equations to facilitate comparative analysis.

2.2.2 Parameters of Empirical Grain-Size Equations

2.2.2.1 Coefficient of Uniformity (C_u)

The coefficient of uniformity expresses the degree of homogeneity of a soil sample. Due to its relationship to porosity (Equation 4), some authors (Beyer, 1964; Pavchich, 1966) use C_u in place of, or as part of, the porosity function ($(f(n))$ in their empirical grain-size equation (Equation 1). The following ratio was proposed by Hazen (1911) to represent coefficient of uniformity from grain-size data:

$$C_u = \frac{d_{60}}{d_{10}} \tag{2}$$

Where, d_{60} = 60% passing by weight

And, d_{10} = 10% passing by weight

A large C_u value represents a large range of grain-sizes within the sample. This would be described as being more heterogeneous, poorly sorted, or well graded. A small $C_u$value represents a small range of grain-sizes within the sample. This is described as being more homogeneous, well sorted, or poorly graded. A C_u value of “1” represents a perfectly uniform sample (Vukovic and Soro, 1992).

2.2.2.2 Porosity (n)

It is well known that porosity significantly impacts K_{sat} of a sample (Vukovic and Soro, 1992). Porosity is represented as the ratio of pore volume (V_p) per unit total volume (V_t):

$$n = \frac{V_p}{V_t} \tag{3}$$

In natural soils, the porosity is dependent on several factors including the: C_u, degree of compactness, and shape of the grains (Vukovic and Soro, 1991).

It is important to note the relationship between the C_u of a sample and its porosity. Kasenow (2002) cites the degree of uniformity as the factor with the greatest effect on porosity of natural materials. In homogeneous samples the pore spaces between grains are filled by fluid. However, in heterogeneous samples the pore spaces between large grains tend to be filled in by smaller grains. This decreases the pore space of the sample and therefore, decreases the porosity.

Istomina (1957) presents the following equation for estimation of porosity from grain-size analysis:

$$n = 0.255\ (1 + 0.83^{C_u}) \tag{4}$$

Equation 4 offers reasonable results for natural sand, gravely sand, and gravel (Kasenow, 2002).

The compactness of a sample also contributes significantly to its porosity. Figure 2.1 demonstrates the effects of compactness or packing on porosity:

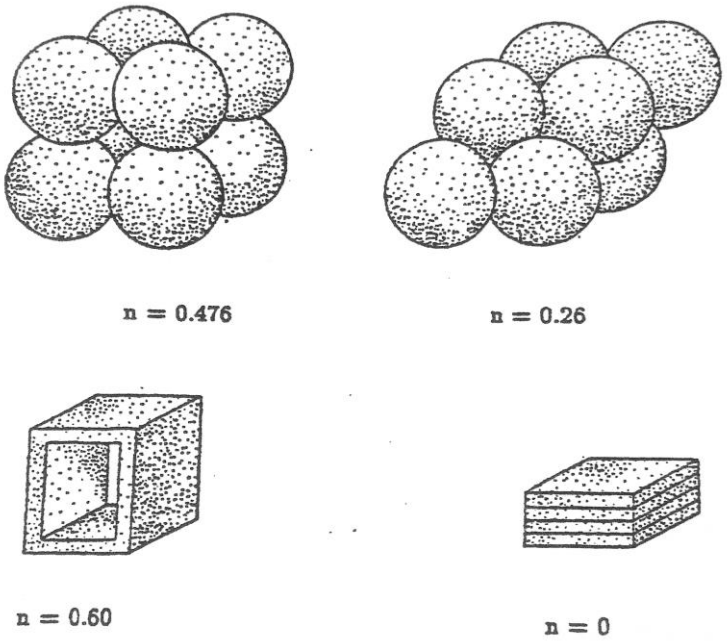

Figure 2.1: Effects of grain structure on porosity (Vukovic and Soro, 1992)

Figure 2.1 shows that if a sample is composed of uniform spherical grains the porosity is dependent on compactness. Therefore, porosity can range from n = 0.476 (unstable structures) to n = 0.26 (full compact structure). Conversely, if the grains are shaped like square plates, the porosity due to varying compactness ranges from n = 0.60 (ideally forming rectangular pores) to n = 0 (ideally stacked plates) (Vukovic and Soro, 1992).

While the previous explanation provides a basic understanding of the relationship between compactness and porosity, it is important to realize that natural materials are never composed of ideally spherical or plate-like grains. The grains are usually oval in shape with irregular and sometimes sharp edges (Vukovic and Soro, 1992).

Grain shape has also been shown to have a significant effect on porosity (Kansenow, 2002). Vault-like structures tend to be created by grains of irregular shape. This leaves larger voids that would not normally be present with ideal spherical grains. Grains with sharp edges have been shown to have porosities 2 – 5% higher than ideally spherical grains (Vukovic and Soro, 1992).

2.2.2.3 Porosity Function (*f (n)*)

The porosity function introduces the concept of hydraulic radius and uses it analogously to flow in conduits. The purpose of this is to relate the flow through pore spaces in porous media to conduit flow dynamics. The ratio of water volume in the pores to the wet surface, specific surface area of the grains, weight content of the individual fractions are combined to obtain the hydraulic radius of a porous medium (Kasenow, 2002):

$$R = \left(\frac{n}{1-n}\right) \frac{1}{6 \sum_{i=1}^{i=n} \frac{f_i}{d_i}} \quad (5)$$

Where, f_i = % weight retained on *i*th fraction

And, d_i = diameter of *i*th fraction

The linear relationship between conduit radius and hydraulic radius (R) can be used to calculate the effective flow velocity (average linear pore-water velocity) (v) through the porous media by dividing velocity (Darcy flux) (V) by the porosity (n) (Kasenow, 2002):

$$v = \frac{V}{n} \tag{6}$$

The relationship between hydraulic loss of energy in the porous media is then substituted into the hydraulic radius of porous media equation (5). From this, the effect of porosity on hydraulic conductivity is expressed in the form of the following porosity function ($f(n)$) (Kasenow, 2002):

$$f(n) = \frac{n^3}{(1-n)^2} \tag{7}$$

Equation 7 is the result of theoretical analysis, however, different forms of this relationship have been found by numerous authors (e.g. Hazen, 1892; Kozeny, 1953; NAVFAC, 1974; Slichter, 1899). The empirical grain-size equations used in this study employ $f(n)$ in various forms (Table 2.1).

2.2.2.4 Effective Grain-Size Diameter (d_e)

The effective grain-size diameter represents the spherical grain diameter of a uniform porous medium with the same K_{sat} as the equivalent natural material (Kasenow, 2002). Many authors recommend a single representative grain-size diameter, corresponding to a specific percent passing by weight from a grain-size distribution analysis. For example: Hazen recommends: $d_e = d_{10}$, Sauerbrei recommends: $d_e = d_{17}$ and, USBR recommends $d_e = d_{20}$.

There are other authors who express effective grain-size diameter by including all fractions of the sample (Vukovic and Soro, 1992; Kasenow, 2002). The fundamental difference between these approaches that include all fractions

is the definition of the “mean” grain diameters that represent the material. As shown in Table 2.1, Kruger recommends the arithmetic mean, while Kozeny, Zamarin, and Zunker recommend means that set the diameter closer to the lower limit of the fractions (Vukovic and Soro, 1992).

2.2.2.5 Coefficient of Proportionality (C)

The coefficient of proportionality (C) is included in the empirical equations to represent all other secondary factors that have an effect on K_{sat} (Vukovic and Soro, 1992). These secondary factors include grain shape and structure, packing, and clay content. C is used as a fitting parameter allowing authors of these empirical grain-size methods to fit their calculated values to measured values. By doing this, the methods are calibrated to the measured data, which may represent a specific set of grain-sizes, type of distribution (e.g. well/poorly sorted), type of sediment (based on origin), or physical area. While some authors recommend a range of C values based on sample characteristics, many express C as a constant. Representing C as a constant is problematic due to the highly variable nature of these secondary factors. Thus, it becomes necessary to locally calibrate C values in order maintain accuracy of these empirical methods when calculating K_{sat}.

2.2.3 Unsaturated Soil Hydraulic Parameters and Models

2.2.3.1 Unsaturated Soil Hydraulic Parameters

Water retention characteristics and hydraulic conductivity functions of unsaturated soils are essential components in modeling efforts of water flow and solute transport in the unsaturated zone (Van Genuchten et al., 1991). Direct measurement of unsaturated conductivity and its related parameters is a time consuming, and expensive process (Kumar and Mittal, 2010; Schapp et al., 2001). Unsaturated zone studies generally utilize large sample areas, which display significant spatial variability in soil hydraulic parameters (Schapp et al., 2001). Processing the number of samples needed to meaningfully characterize such large areas is virtually impossible due to excessive time and expense. Therefore, inexpensive and fast methods are needed to determine unsaturated soil hydraulic properties (Schapp et al., 2001).

Many indirect methods have been developed to determine unsaturated soil hydraulic properties (Schapp et al., 2001). Most of these are classified as pedotransfer functions, which convert existing easily obtainable data (particle-size distributions, bulk density, organic matter, etc.) into usable soil hydraulic data. Pedotransfer functions are developed empirically, being calibrated using existing databases (Schapp et al., 2001). They are broken down into multiple linear regression and extended nonlinear regression equations.

A more recent approach is an empirical pedotransfer function called artificial neural networks (ANN) (Schapp et al., 2001). An advantage of ANNs is

that they require no a priori model concept. Input data in linked to output data by an iterative calibration process. This allows the model to use the maximum amount of data in calculation of output data. Schapp et al. (1999) used neural network analysis to estimate Van Genuchten (1980) water retention parameters and K_{unsat}. Application of these parameters to additional predotransfer functions yields K_{unsat} functions.

A commonly used ANN is the computer model ROSETTA (1999), which uses a hierarchical structure to allow input of either more limited or more extensive data inputs. ROSETTA (1999) has been shown to produce relatively accurate estimates of soil hydraulic parameters (Schapp et al, 1999).

2.2.3.2 Soil Water Retention Models

Unsaturated soil hydraulic functions are used to represent the water retention characteristics and K_{unsat} properties in unsaturated or partly saturated soils. The controlling factors in these functions include the soil matric potential and water content relationship, and the hydraulic conductivity and water content relationship (Kumar and Mittal, 2010). K_{unsat} is controlled by resistive force due to matric potential, which ultimately originates from surface tension of the menisci formed between grains. This resistance greatly increases as soil water content decreases due to the decreased radii and increased angle of menisci (Freeze and Cherry, 1979).

The two most common soil water retention models used to relate the water content of a soil to matric potential are the Brooks Corey (1966) and Van Genuchten (1980):

Brooks Corey Equation (1966)

$$\theta = \theta_r + (\theta_s - \theta_r)\left(\frac{\psi}{h_b}\right)^{-\lambda} \tag{8}$$

Where, $\theta =$ volumetric water content

$\theta_s =$ volumetric water content at saturation

$\theta_r =$ irreducible minimum water content

$\psi =$ matric potential

And, $h_b =$ bubbling pressure

λ = experimentally derived parameter representing capillary behavior

In the literature, the Brooks Corey Equation (8) has shown to be accurate for materials with narrow grain-size distributions (Schapp, 1999).

Van Genuchten Equation (1980)

$$\theta = \theta_r + \frac{\theta_s - \theta_r}{(1 + (\alpha\psi)^n)^m}$$

$$m = 1 - \frac{2}{n}$$

$$\alpha = \frac{1}{h_b}\left(2^{\frac{1}{m}} - 1\right)^{1-m} \tag{9}$$

Where, $m =$ empirical curve calibration factor

$n =$ empirical curve calibration factor

And, $\alpha =$ empirical curve calibration factor representing air entry pressure (cm^{-1})

The Van Genuchten equation (9) in this form is cited as providing more accurate estimation for soils with wider grain-size distributions than the Brooks Corey (1966) or alternative forms where the definition of m varies (Schapp, 1999).

The Brooks Corey (1966) and Van Genuchten (1980) equations can be rewritten to yield effective saturation as shown in equations 10 and 11:

Brooks Corey (1966)

$$S_e = \begin{cases} (\alpha h)^{-\lambda} & (\alpha h > 1) \\ 1 & (\alpha h \leq 1) \end{cases} \quad (10)$$

Where, S_e = saturation ratio $\left(\frac{\theta}{\theta_s}\right)$

Van Genuchten (1980)

$$S_e = \frac{1}{(1 + (\alpha h)^n)^m} \quad (11)$$

Both forms of the Brooks Corey (1966) and Van Genuchten equations provide the data necessary to plot the soil water retention characteristics of soils as $\theta(h)$ or $S_e(h)$ (Schapp, 1999).

2.2.3.3 Unsaturated Hydraulic Conductivity Models

Unsaturated hydraulic conductivity functions are used to predict K_{unsat} in conjunction with one of the aforementioned water retention functions. K_{unsat}, plotted against either Ψ or S_e/θ, provides important information as to K_{unsat} variation with changes in water content. The Mualem (1976) model applied to van Genuchten water retention functions (Equation 9) and Burdine (1953) model applied to Brooks-Corey water retention function (Equation 8) are most commonly used in the literature to express relative K_{unsat} in terms of soil water pressure head, or soil water effective saturations (Schapp, 1999):

Mualem Equation (1976)

$$K(h) = \frac{K_s\{1-(\alpha h)^{mn}[1+(\alpha h)^n]^{-m}\}^2}{[1+(\alpha h)^n]^{ml}} \tag{12}$$

and,

$$K(S_e) = K_s S_e^l\left[1-\left(1-S_e^{\frac{1}{m}}\right)^m\right]^2 \tag{13}$$

Where, l = pore connectivity parameter, -1 (Schapp and Leij, 2000)

Burdine Equation (1953)

$$K(h) = \frac{K_s\{1-(\alpha h)^{n-2}[1+(\alpha h)^n]^{-m}\}}{[1+(\alpha h)^n]^{ml}} \tag{14}$$

and,

$$K(S_e) = K_s S_e^l \left[1 - \left(1 - S_e^{\frac{1}{m}}\right)^m\right] \quad (15)$$

Where, l = pore connectivity parameter, 2 (Van Genuchten et al., 1991)

2.3.0 METHODS

2.3.1 Sample Collection

Prior to the commencement of this study, G360 students and staff, through the University of Guelph, completed the majority of drilling activities and grab sampling (June 2010 to January 2013). Drilling sites were chosen based on a variety of factors including: land access, historic OGS surficial geology mapping, and location relative to geomorphic elements (McGill, 2012). The distribution of drill sites was chosen in order to more fully characterize the Quaternary sediments of the Paris Moraine and all its elements (outwash, frontslope, hummocky terrain, back slope, Galt moraine outwash) (McGill, 2012). Due to the high cost of drilling, site selection was subject to the input of a number of researchers involved in this ORF project.

Due to the variability of sediments in the area, two types of drilling were employed to obtain 4-inch diameter cores, PQ coring and roto-sonic. PQ coring consists of advancing a series of PQ-size rods with a cutting bit, by rotation and lubrication with drilling mud (McGill, 2012). Within these rods is a 5 foot long inner tube which traps the core sample, which is then brought to the surface via a wireline system (McGill, 2012). Roto-sonic drilling consists of advancing a drill string containing inner and outer rods. The drill bit both rotates and vibrates at a high frequency. The inner rods are used to capture the core sample and raise it to the surface (McGill, 2012). Boreholes GDC-1A, GDC-2B, and VPV-1A were

collected using PQ coring. Boreholes GDC-10A, ARS-1A, TGI-1A, VAN-1A, FRE-1A, and VE-1A were collected using roto-sonic.

Once samples were removed from the drilling rods they were field logged, photographed, and stored in wooden boxes for transportation back to the University of Guelph. Grab samples were collected at the University of Guelph. Grab samples that were selected based on observed heterogeneities (layer transitions) in the cores as well as layers deemed significant to characterization of the borehole. Thick layers may contain multiple grab samples based on visually perceived potential variation in conductivity within the layer. Samples varied in size from ~100 to 500g, and typically occupied a ~0.5ft (0.15m) interval of core. Sample size and interval varied with thickness of layers. While sampling, the outside of the core was scraped to remove mud or rock flour present from drilling. The samples were placed in Ziplock bags, labeled, and stored at 4^{o}C. The elevations of the samples within the boreholes were recorded. The samples were later transported to McMaster University in coolers and stored at 4^{o}C for subsequent grain-size and falling head permeameter analyses.

2.3.2 Grain-Size Analysis: Sieve and Hydrometer Analysis

Methods used for grain-size analysis were adapted from methods described in Best (2013) and SSSA (2002) for consistency within the ORF project. Best (2013) adapted these methods from the standard methods described in Kroetsch and Wang (2008).

1. Wet samples were air-dried. If consolidated, sample was crushed carefully with mortar and pestle in an up and down motion into <2mm pieces.
2. Obvious large gravel clasts were removed.
3. Sample trays were pre-weighed.
4. Samples were riffled into subsamples of ~100g for sandy material, and ~50g for muddy material.
5. Samples were dried at 105^{o}C overnight.
6. Dried samples were weighed in trays.
7. Samples were soaked overnight in 100ml of 50g/L sodium metaphosphate solution (Calgon).
8. Sample was added to a mixing cup with 300ml distilled water.
9. Slurry was mixed with electric mixer for 5 minutes.
10. Slurry was rinsed through a 45µm sieve into a 1L cylinder using a large funnel (until passing water was clear). The inside of the funnel was also rinsed into the cylinder.
11. The sand retained in the sieve was rinsed into a pre-weighed tray.
12. The sand fraction:
    a. Dried overnight at 105^{o}C and weighed in tray.
    b. Sieves were checked for tears and cleaned.
    c. Weight of sieves was recorded.

d. Sieve stack was assembled, the sample was added to the top, and shaken for 10 minutes on motorized sieve shaker (Humboldt MFG. CO.; Model: H-4325; Serial #: 00094325; Specs.: ASTM) .
e. Each sieve was weighed and recorded.
f. Silt collected in the bottom of the stack was added to the corresponding 1L cylinder.

13. The mud fraction:

a. Distilled water was added to the 1L mark on the cylinder.
b. A blank cylinder was set up with 100ml of 50g/L sodium metaphosphate solution and 900ml distilled water mixed.
c. Sample cylinder was mixed thoroughly with a plunger using an up and down motion along the entire length of the cylinder (avoiding splashing at the surface).
d. Time was recorded when the mixing rod was removed.
e. Hydrometer measurements were taken at the following intervals after mixing (minutes): 0.5, 1, 90 (1.5hrs), 420 (7hrs), 1440 (24hrs).

Particle-size distribution curves (% passing curves) were constructed from the combined sieve analysis and hydrometer analysis data by plotting sieve analysis data from 2mm - 45µm with hydrometer data data <45µm (hydrometer measurements >45µm were disregarded).

2.3.3 Falling Head Permeameter Analysis

The falling head permeameter methods were adapted from SSSA (2002) in accordance with standard methods (ASTM D5084-03). Permeameter analysis was performed on samples with at least ~40g of unused sample after sieve analysis.

1. Wet samples were air-dried. If consolidated, sample was crushed carefully with a mortar and pestle in an up and down motion <2mm pieces.
2. Obvious large gravel clasts were removed.
3. Samples were riffled into subsamples of ~40-100g subsamples.
4. Sandy samples:
    a. J-cloth was used fixed to the end of a 6.5cm x 4.5cm(diameter) piece of PVC pipe using an elastic band.
    b. The dry sample is then poured into the PVC pipe.
    c. A piece of 53µm mesh was used to cover the sample.
    d. The stem apparatus (consisting of a 61.5cm x 1.75cm (diameter) glass tube which perforates through a #9 rubber stopper) was pressed firmly into the top of the open PVC pipe containing the sample.
5. Silty samples:
    a. J-cloth was used fixed to the end of 61.5cm x 2.1cm (diameter) glass tube using an elastic band.

b. The dry sample was then poured into the glass tube with the open end up.
c. A piece of 53µm mesh was used to cover the sample.

6. Using a retort stand, the sample/tube apparatus was suspended resting inside a 500ml beaker with the surface of the sample resting ~ 1cm below the beaker opening.
7. To hydrate the sample, the beaker was filled bringing the water level to half the height of the sample with sodium adsorption ratio adjusted water.
8. After 2hrs the water level was raised to the surface of the sample.
9. After another 2hrs the water level was brought to the surface of the beaker and allowed to stand until the water level in the glass tube had equilibrated.
10. A paper clip straightened into a slight curve, wrapped in a small piece of J-cloth, was draped over the edge of the beaker to facilitate free flow of water.
11. Water was poured carefully into the top of the glass tube, bringing the water level to the top of the tube. This height above datum (counter surface) was recorded.
12. The start time was recorded.
13. The time and height dropped from the top of the tube (at least 4 intervals) were recorded as the water level drops in the glass tube.

14. This data was used to directly calculate measured K_{sat}.

2.3.4 Calculating K_{sat} from Grain-Size Distribution

Table 2.1 (adapted from Rosas et al., 2014) outlines the 19 empirical grain-size methods used to calculate K_{sat} from grain-size distribution. It is important to note that the units are not consistent across all methods. For ease of comparison, all K_{sat} values were calculated in m/s. Values were first calculated in the units shown in Table 2.1, then converted to m/s. This was to ensure correct usage of constants and coefficients as the literature cites many of these coefficients and calibration factors without units, i.e. as being dimensionless. However, dimensional analysis reveals that they are not dimensionless; the units were just not reported.

2.3.5 Calculating Calibration Factors

Calibration factors were calculated for each empirical grain-size method (Table 2.1). Permeameter measurements are more accurate than calculated values (Kasenow, 2002). Therefore, calculated grain-size K_{sat} values were adjusted to match measured permeameter K_{sat} values using equation 16:

$$Calibration\ Factor = \frac{GM_{measured}}{GM_{calculated}} \quad (16)$$

Where, GM = geometric mean K_{sat}

This calibration factor was applied to the existing coefficients in each equation to yield a local calibration coefficient for the Guelph/Paris Moraine area.

2.3.6 Calculated and Measured Porosity Values

As discussed in Section 2.2.2.2, the literature (Kasenow, 2002; Vukovic and Soro, 1992) commonly uses the equation presented by Istomina (1957) for estimation of porosity from grain-size analysis:

$$n = 0.255\ (1 + 0.83^{C_u}) \tag{4}$$

Where, C_u = coefficient of uniformity ($\frac{d_{60}}{d_{10}}$)

This equation was applied to all sieved samples to determine their "calculated" porosity value and was used in calculation of K_{sat} for all empirical grain-size methods.

The "measured" porosity value was determined from in lab falling-head permeameter tests for comparison to calculated porosity values using:

$$n = \frac{V_{voids}}{V_{total}} \tag{17}$$

$$V_{voids} = V_{total} - V_{solids} \tag{18}$$

$$V_{total} = \pi r^2 \text{ x } H \tag{19}$$

$$V_{solids} = \frac{M}{\rho_p} \tag{20}$$

Where, r = radius of sample in PVC pipe/glass tube

H = height of sample in PVC pipe/glass tube

M = mass of sample

And, ρ_p = particle density, 2.65 g/cm^3 (average particle density soil) is used (Freeze and Cherry, 1979)

These values are displayed in Appendix B.

2.3.7 Unsaturated Soil Hydraulic Parameters and Functions

The ANN model, ROSETTA (1999), was used to estimate soil hydraulic parameters ($\theta_r, \theta_s, \alpha, n$) from the sand, silt, and clay percentages of each sample (Appendix C). The output parameters were used as inputs for Van Genuchten (1980) (equation 11) – Mualem (1976) (equation 13) model and the Brooks Corey (1966) (equation 10) – Burdine (1953) (equation 15) model to produce $S_e(h)$ and K_{unsat} (S_e) plots in order to evaluate the unsaturated behavior of sediments with similar grain-sizes and provide modeling parameters for future simulations.

Many of the empirical equations rely on d_{10} as the effective grain-size for their calculation of K_{sat}, therefore, d_{10} was used to group samples into similar grain-sizes (0.001 - 0.005mm, 0.005 – 0.01mm, 0.01 – 0.05mm and, $\geq$0.05mm) for analysis of unsaturated characteristics.

Table 2.1
Methods used to calculate K_{sat} from grain-size distribution data

Method	Equation	Variable and Unit Definition	Usage Criteria
Alyamani and Sen (1993)	$K\ (\frac{m}{d}) = 1300[I_o + 0.025\ (d_{50} - d_{10})]^2$	I_o is the intercept in mm of the line formed by d_{50} and d_{10} with the grain-size axis on an arithmetic plot	Well distributed sample
Beyer (1964)	$K\ (\frac{m}{s}) = \frac{g}{v}$ x 6 x $10^{-3} log\left(\frac{500}{C_u}\right) d_{10}^2$		0.06mm < d_{10}< 0.6mm 1 < C_u < 20
Chapuis et al. (2005)	$K\ (\frac{cm}{s}) = 2.46$ x $\left(\frac{d_{10}^2 e^3}{1+e}\right)^{0.7825}$ $e = \frac{n}{1-n}$	e is the void ratio d_{10} is in mm	0.03mm < d_{10}< 3mm 0.3 < e < 0.7
Harleman et al. (1963)	$K\ (\frac{m}{s}) = \frac{g}{v}$ x 6.54 x $10^{-4} d_{10}^2$	d_{10} is in m	

Method	Equation	Variable and Unit Definition	Usage Criteria
Hazen-Original (1892)	$K\,(\frac{m}{s}) = \frac{g}{v}$ x 6 x $10^{-4}[1 + 10(n - 0.26)]d_{10}^2$	d_{10} is in m	0.1mm < d_{10} < 3mm C < 5
Hazen-New (modified) (Rosas et al., 2014)	$K\,(\frac{cm}{s}) = C d_{10}^2$	C is the Hazen coefficient in *1/[cm*s]* d_{10} is in cm	C = 125
Kozeny (1953)	$K\,(\frac{m}{s}) = \frac{g}{v}$ x 8.3 x $10^{-3}\left[\frac{n^3}{(1-n)^2}\right] d_e^2$ $\frac{1}{d_e} = \frac{3}{2}$ x $\frac{\Delta g_1}{d_1} + \sum \Delta g_i \frac{d_i^g + d_i^d}{2 \text{ x } d_i^g \text{ x } d_i^d}$	d_1 is the largest diameter of the finest fraction in m Δg_1 is the weight of the finest fraction in parts of total weight Δg_i is the weight of the i fraction, in parts of total weight d_i^g is the maximum grain diameter of the corresponding fraction in m	Large grain sand

Method	Equation	Variable and Unit Definition	Usage Criteria
Kozeny (1953) continued		d_i^d is the minimum grain diameter of the corresponding fraction in m	
Kozeny-Carman (Vukovic and Soro, 1992)	$K\left(\frac{m}{s}\right) = \frac{g}{v}$ x 5.56 x $10^{-3}\left[\frac{n^3}{(1-n)^2}\right] d_{10}^2$		Silts, sands, and gravelly sands d_{10} < 3mm
Kozeny-Carman (Carrier, 2003)	$K\left(\frac{cm}{s}\right) = 1.99$ x $10^4\left(\frac{1}{S_o^2}\right)$ x $\left(\frac{e^3}{[1+e]}\right)$ $S_o = \left(\frac{SF}{d_e}\right)$ $\frac{1}{d_e} = \frac{3}{2}$ x $\frac{\Delta g_1}{d_1} + \sum \Delta g_i \frac{d_i^g + d_i^d}{2 \text{ x } d_i^g \text{ x } d_i^d}$	$S_o$is in cm $d_e$is in cm	SF = 7
Kruger (Vukovic and Soro, 1992)	$K\left(\frac{m}{s}\right) = \frac{g}{v}$ x 4.35 x $10^{-5}\left[\frac{n}{(1-n)^2}\right] d_e^2$ $\frac{1}{d_e} = \sum \Delta g_i \frac{2}{d_i^g + d_i^d}$	g_i is the fraction % weight retained on *i* sieve d_i^g and d_i^d, max and min grain diameters of the fraction in m	C > 5 Medium grain sands

Method	Equation	Variable and Unit Definition	Usage Criteria
Krumbein and Monk (1943)	$K\ (darcy) = 760 \text{ x } GM^2\ e^{-1.31\sigma_\phi}$	GM is the geometric mean in mm ϕ is the phi standard deviation	
NAVFAC (1974)	$K\ (\frac{m}{s}) = \ 10^{1.291e-0.6435} d_{10}^{0.5504-0.2937e}$ $e = \frac{n}{1-n}$	e is the void ratio d_{10} is in mm	0.1 mm < d_{10} < 2mm 0.3 < e < 0.7 2 < C < 12 $\frac{d_{10}}{d_5}$ > 1.4
Pavchich (Pravedney, 1966)	$K\ (\frac{m}{s}) \ = \frac{g}{v} \text{ x } 0.35 \text{ x } \sqrt[3]{C_u} \left[\frac{n^3}{(1-n)^2}\right] d_{17}^2$	d_{17} is in m	0.06mm < d_{17} < 1.5mm
Sauerbrei (Vukovic and Soro,1992)	$K\ (\frac{m}{s}) \ = \frac{g}{v} \text{ x } 3.75 \text{ x } 10^{-3} \left[\frac{n^3}{(1-n)^2}\right] \ d_{17}^2$	d_{17} is in m	Sand and sandy clay d_{17} < 0.5mm
Slichter (1899)	$K\ (\frac{m}{s}) = \frac{g}{v} \text{ x } 1 \text{ x } 10^{-2}\ n^{3.287}\ d_{10}^2$	d_{10} is in m	0.01mm < d_{10} < 5mm

Method	Equation	Variable and Unit Definition	Usage Criteria
Terzaghi (1925)	$K\,(\frac{m}{s}) = \frac{g}{v}$ x 8.4 x 10^{-3} x $\left(\frac{n-0.13}{\sqrt[3]{1-n}}\right)^2 d_{10}^2$	d_{10} is in m	Large grain sands
USBR (Vukovic and Soro,1992)	$K\,(\frac{m}{s}) = \frac{g}{v}$ x 4.8 x 10^{-4} x $d_{20}^{0.3}$ x d_{20}^2	d_{20} is in m	Medium grain sands C < 5
Zamarin (Vukovic and Soro,1992)	$K\,(\frac{m}{s}) = \frac{g}{v}$ x 8.2 x $10^{-3}\left[\frac{n^3}{(1-n)^2}\right]$ x $(1.275 - 1.5n)^2\, d_e^2$ $\frac{1}{d_e} = \frac{3}{2}$ x $\frac{\Delta g_1}{d_1} + \sum \Delta g_i \frac{\ln d_i^g - \ln d_i^d}{d_i^g - d_i^d}$	d_1 is the largest diameter of the finest fraction in m Δg_1 is the weight of the finest fraction in parts of total weight d_i^g and d_i^d, max and min grain diameters of the fraction in m Δg_i is the fraction weight in parts of total weight	Large grain sands

Method	Equation	Variable and Unit Definition	Usage Criteria
Zunker (Vukovic and Soro,1992)	$K\left(\frac{m}{s}\right) = \frac{g}{v}\ \text{x}\ 1\ \text{x}\ 10^{-3}\left[\frac{n}{(1-n)}\right]^2\ d_e^2$ $\frac{1}{d_e} = \frac{3}{2}\ \text{x}\ \frac{\Delta g_1}{d_1} + \sum \Delta g_i \frac{d_i^g - d_i^d}{d_i^g\ \text{x}\ d_i^d(\ln d_i^g - \ln d_i^d)}$	$d_1$is the largest diameter of the finest fraction in m d_i^g and d_i^d, max and min grain diameters of the fraction in m Δg_i is the fraction weight in parts of total weight	Fine and medium grain sands

2.4.0 RESULTS AND DISCUSSION

Review of the literature reveals significant variability between methods when calculating K_{sat} from grain-size distribution data (Alyamani and Sen, 1993; Cheng and Chen, 2007; Eshaku et al., 2007; Kasenow, 2002; Rosas et al. 2014; Vukovic and Soro, 1992). Figures 2.2 – 2.4 displays the calculated K_{sat} values from 10 of 19 methods (the other 7 cannot be used on the Guelph/Paris Moraine data due to the limitations in Table 2.1) plotted against permeameter measured K_{sat} values. Figures 2.2 – 2.4 shows that the variability seen in the literature is also present in the Guelph/Paris Moraine data. Calculated K_{sat} of a single sample can vary by up to 2 orders of magnitude dependent on the empirical method used. Some methods also show insensitivity to changes in input (grain-size, porosity, void ratio, etc) as they calculate similar K_{sat} values over a wide range of measured values. Generally, these methods under/over estimate the measured values by 0 to 2 orders of magnitude. These observations highlight inherent inaccuracy in these methods when compared to measured permeameter data.

Variability in precision of these methods is also present in Figures 2.2 – 2.4 Some methods display large scatter from the observed linear trend while others are relatively small.

2.4.1 Calculated vs Measured K_{sat}

Figure 2.2 – 2.4 shows calculated values from empirical grain-size methods plotted against measured permeameter data. Evaluation of the

empirical grain-size methods is based on 3 main criteria: relative slope of calculated values, accuracy (mean), and precision (variance).

Alyamani and Sen (1993) underestimates measured K_{sat} at lower conductivities (<10^{-6}m/s) and overestimates it at higher conductivities (>10^{-6}m/s) (Figure 2.2a). Its slope of 0.4519 is the closest to that of the measured data (slope=1). The y-intercept of -0.351 indicates inaccuracy, as it should be consistent with that of the measured data (y=0), where zero measured conductivity corresponds with zero measured conductivity. This method has poor precision; with measured values have corresponding calculated values ranging over 1-4 orders of magnitude.

Chapuis et al. (2005) overestimates measured K_{sat} at lower conductivities (<10^{-6}m/s) and underestimates it at higher conductivities (>10^{-6}m/s) (Figure 2.2b). Its trend-line has a slope of 0.1213, which represents variation in the sample similarly to other methods. The y-intercept is -5.27, which indicates inaccuracy. Calculated values vary by ~1 order of magnitude for measured values, indicating quite high precision.

Harleman et al. (1963) tends to underestimates measured values. Its slope (0.1621) is similar in accuracy to other methods (Figure 2.2c). The y-intercept of -5.48 indicates inaccuracy. This method is relatively precise as calculated values vary by ~1.5 orders of magnitude for measured values.

Hazen – new (Rosas et al., 2014) displays a very similar trend to the Harleman et al. (1963) method but slightly vertically shifted (Figure 2.2d). The

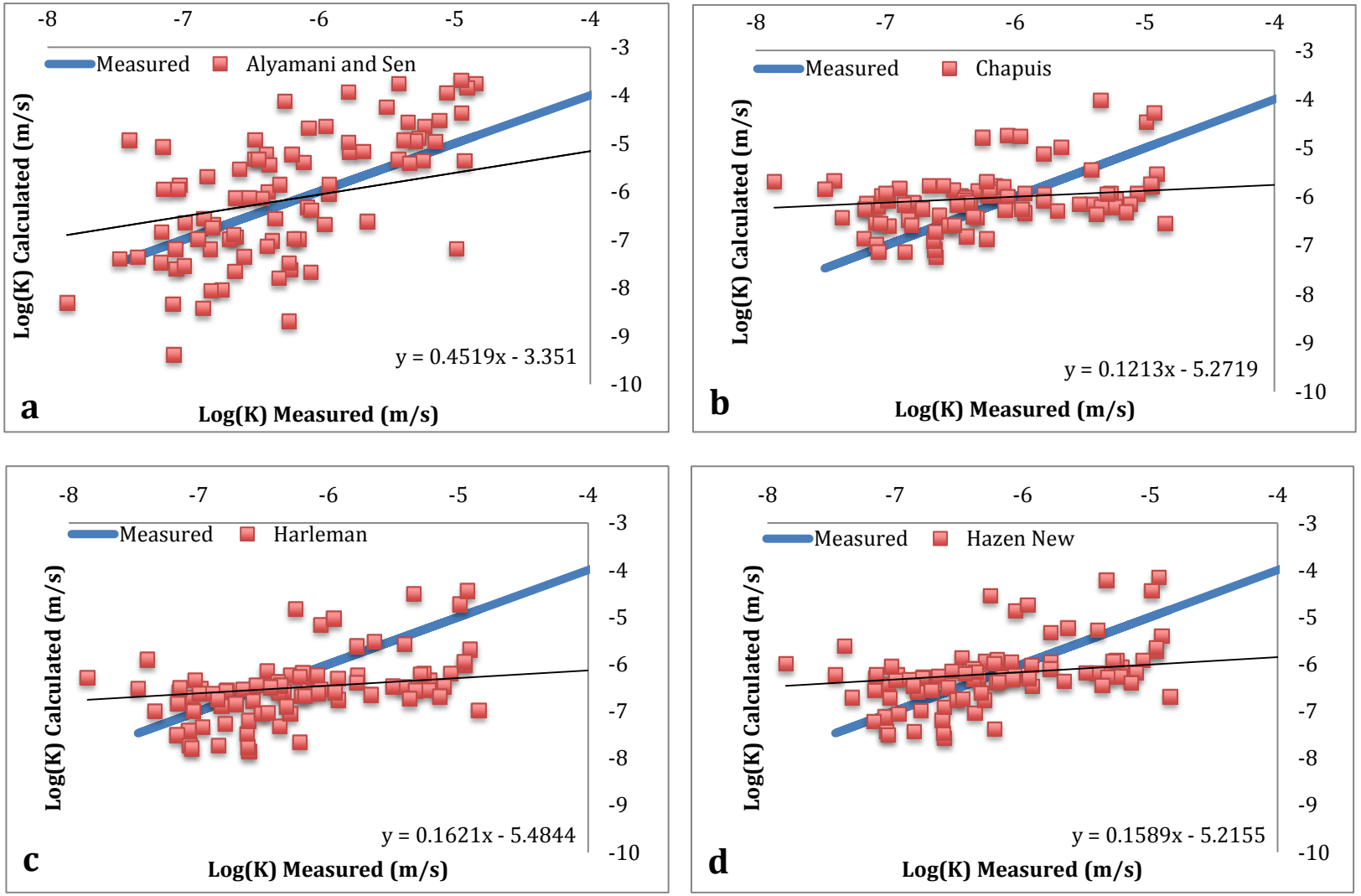

Figure 2.2 a,b,c,d: Calculated K_{sat} values of individual methods, plotted against measured permeameter values.

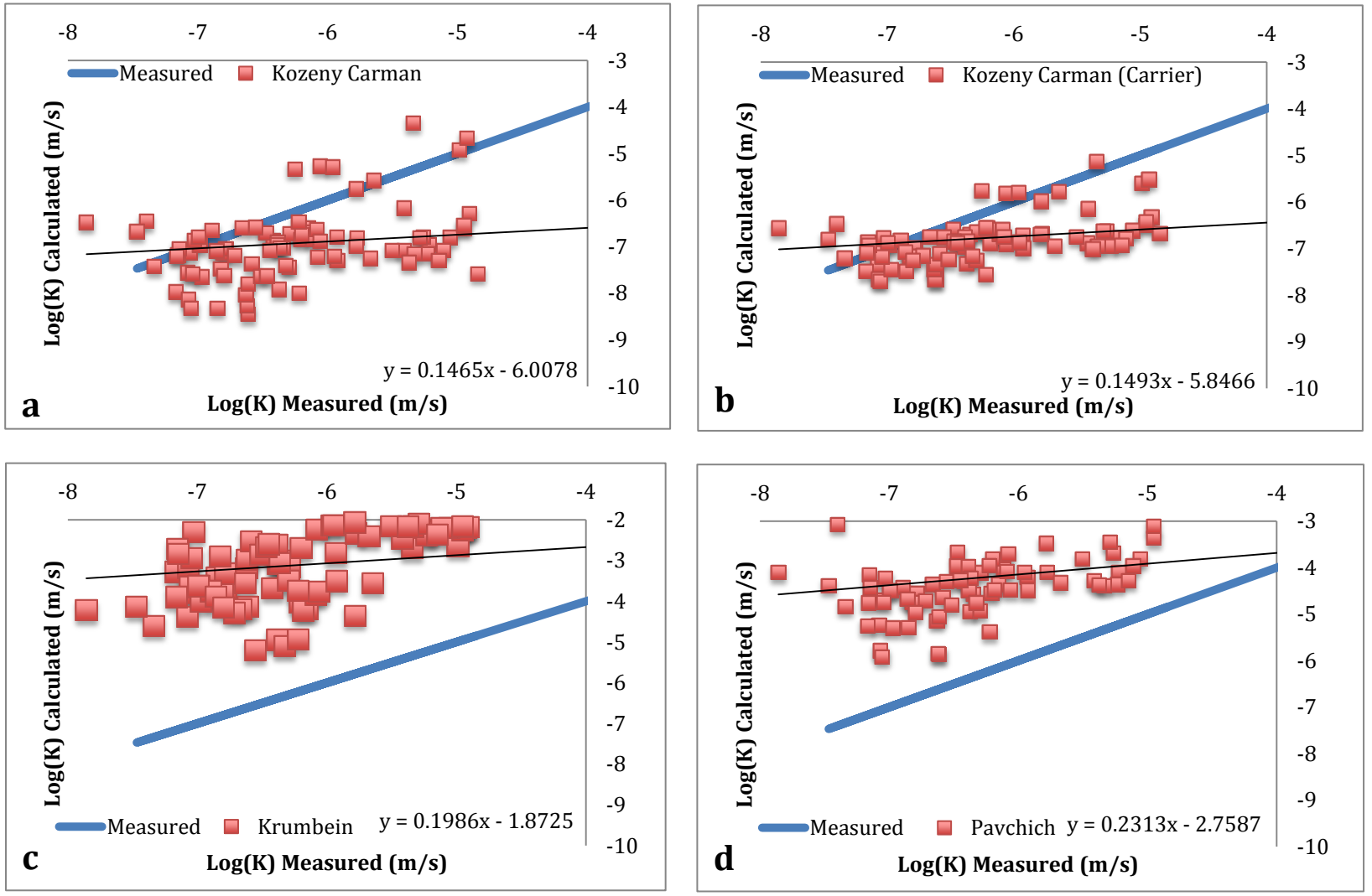

Figure 2.3 a,b,c,d: Calculated K_{sat} values of individual methods, plotted against measured permeameter values.

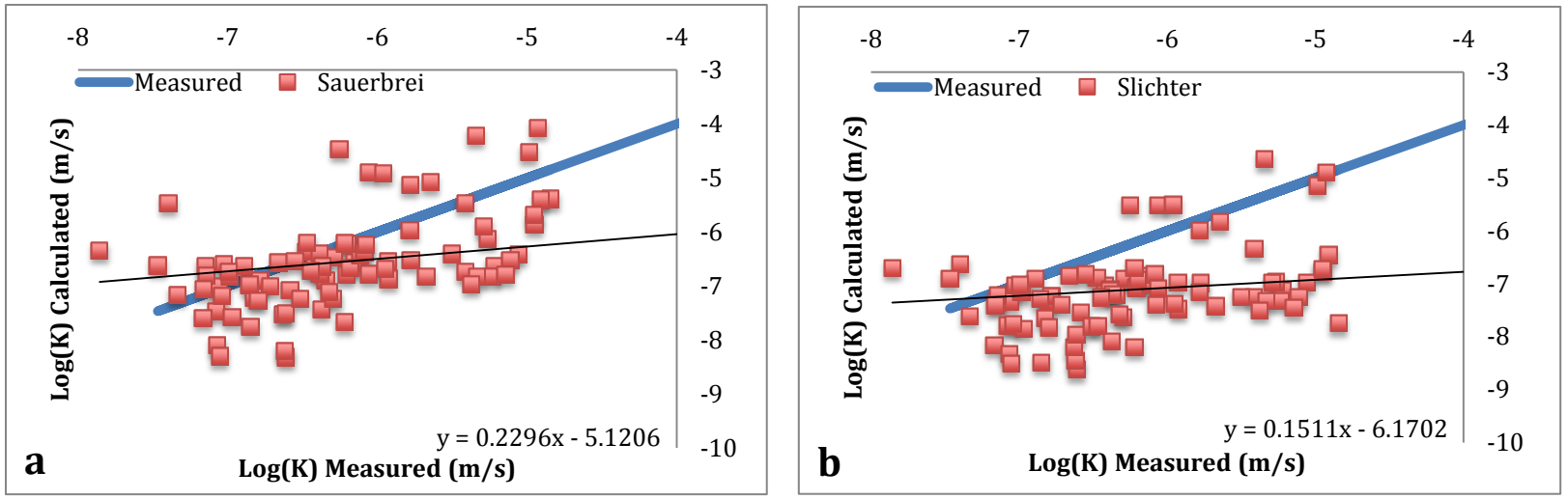

Figure 2.4 a, b : Calculated K_{sat} values of individual methods, plotted against measured permeameter values.

trend shows underestimation of measured values at higher conductivities (>10^{-6} m/s) with a slope of 1.1589. The y-intercept is -5.22 making it slightly more accurate than Harleman et al. (1963) but with a similar slope. Precision is relatively high as calculated values deviate from measured values by approximately 1 order of magnitude.

The Kozeny-Carman (Vukovic and Soro, 1992) equation tends to underestimate measured values (Figure 2.3a). It has a slope of 0.1465 (similar to other methods) and a y-intercept of -6.01. Scatter is present in the data as calculated K_{sat} values range over 1.5 orders of magnitude showing relative precision.

The Kozeny-Carman, method as found in Carrier (2003), tends to underestimate calculated values (Figure 2.3b). It has a slope of 0.1493 and a y-intercept of -5.85. Its precision is within 1 order of magnitude for a single measured value.

Krumbein and Monk (1943) tends to overestimate measured values (Figure 2.3c). Its slope is 0.1986, and its y-intercept of -1.87 makes it relatively accurate. The precision of this method increases at higher conductivity values, with data falling within 2 order of magnitude for a given value.

Pavchich (Pravedney, 1966) is one of the methods that overestimates the data. It has a slope of 0.2313 and y-intercept of -2.758 (Figure 2.3d). It shows similar precision compared to other methods as the of data falls within 1.5 orders of magnitude for a discrete measured value.

The Sauerbei (Vukovic and Soro, 1992) method tends to underestimate measured values (Figure 2.4a). The slope of 0.2296 indicates relative accuracy compared to other methods, however, the y-intercept of -5.12 shows underestimation of data. Precision is fairly low with values ranging over ~2 orders of magnitude.

The Slichter (1899) method underestimates measured values, with a slope of 0.1511 and y-intercept of -6.17 (Figure 2.4b). Data scatter is over 1.5 orders of magnitude indicating similar precision to other methods.

The Hazen – original (1892), Beyer (1964), Kozeny (1953), NAVFAC (1974), Terzaghi (1925), USBR, Kruger, Zamarin, and Zunker (Vukovic and Soro, 1992) methods all lack sufficient data to form a significant trend. This is due to the application of restrictions on their usage shown in Table 2.1. Use of these restrictions is fundamental to calculation of the most accurate values possible. Each empirical method was developed under differing conditions on a variety of materials. As such, each method should only be used on materials, on which they have been shown to produce reliable results.

These methods all use some variation of the same parameters to calculate K_{sat}. In varying degrees, they all attempt to account for effective grain-size diameter, flow pathway (porosity/void ratio/surface area), and grain structure/shape. Therefore, it is expected that many of them produce similar data trends with a vertical transformation about the measured data. This vertical transformation is due to the coefficient of proportionality (*C*) applied by the original authors in order to fit their data to measured or known values. The range

of values produced by these methods, from identical input data, dictates that an informed decision is made when grain-size data is used to calculate K_{sat}.

2.4.1.1 Variability in Calculated and Measured Porosity Values

It is well established that K_{sat} is greatly affected by the porosity of a sample, which is determined by a variety of factors including uniformity, degree of compactness, and shape of the grains (Vukovic and Soro, 1991; Section 2.2.2.2). As such, the majority of empirical grain-size methods account for porosity, either directly or indirectly. The variability in K_{sat} values between measured and calculated values is attributable not only to the inherent lack of accuracy in empirical grain-size methods (Kasenow, 2003; Vukovic and Soro, 1993), but also by differences in porosity values between the empirical grain-size methods and lab measured permeameter tests (Appendix B).

The empirical grain-size equations utilize the equation presented by Istomina (1957) to calculate porosity based on grain-size distribution data (Section, 2.2.2.2; Section 2.3.6), while the porosity of samples used in falling-head permeameter tests was determined by the amount of packing during free pouring of the sample (Section 2.3.3). As such, the empirically calculated porosity values are expected to differ from those present in the falling-head permeameter tests, contributing to the deviation between calculated and measured K_{sat} values.

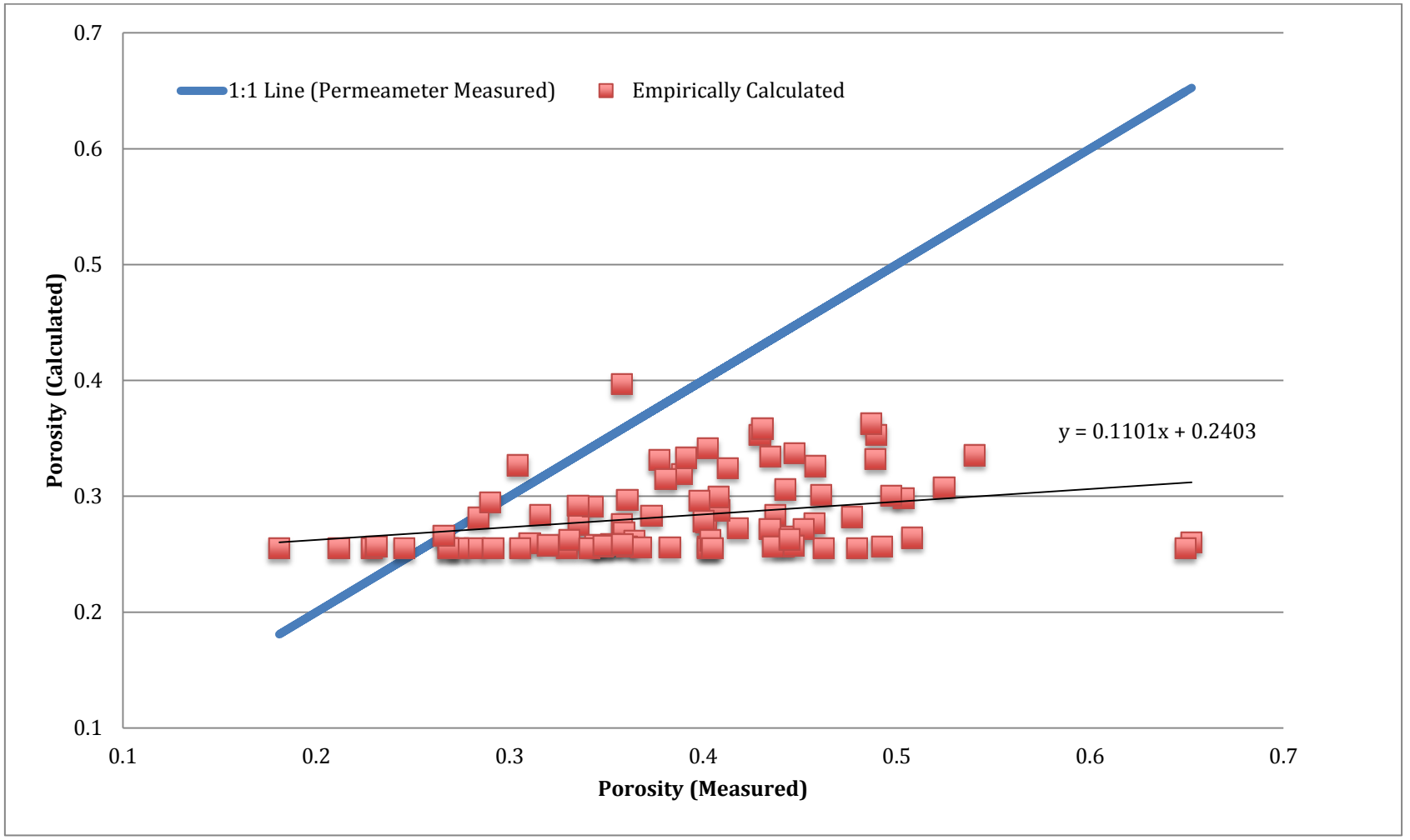

Figure 2.5: Empirically calculated (using Istomina, 1957) and lab measured (from free poured falling-head permeameter samples) porosity value (Appendix B). Measured porosity is plotted as 1:1.

Figure 2.5 shows that measured values are generally higher than empirically calculated values. The measured porosity values are set as 1:1 and therefore have a slope of 1. The calculated porosity values have a slope of 0.11 which shows underestimation of measured porosity values >0.28. This ranges from 0% underestimation of measured values (at the intersection of the two data sets), increasing relatively linearly to ~40% underestimation of measured values (at a measured porosity of 0.5.).

The equation from Istomina (1957) used to calculate porosity values from grain-size analysis (Section 2.3.6) is cited as providing reasonable porosity estimates for natural materials (Kasenow, 2002). Istomina's (1957) porosity equation relies exclusively on the coefficient of uniformity ($C_u = \frac{d_{60}}{d_{10}}$), which has been shown to have the greatest effect of all parameters (ie. uniformity, degree of compactness, and shape of the grains) relating to porosity. However, the measured porosity values, encountered in the free pour falling head permeameter analysis, are the combined result of all porosity related parameters. Therefore, degree of compactness and the shape of grains are also intrinsically incorporated into measured porosity values.

Hence, the observed outcome, calculated values underestimating measured values, is expected. With all other parameters assumed to be equal, natural materials, as approximated by Istomina's (1957) equation, are more tightly packed than those used in the free pour falling head permeameter analysis in this study. Therefore, higher porosity values are present in the falling head permeameter analysis, resulting in higher K_{sat} values.

The underestimation of calculated porosity values, compared to measured values, suggests that measured K_{sat} values would overestimate calculated values. However, it is clear from Figure 2.4 that measured K_{sat} values both overestimate and underestimate calculated values; both within a single empirical grain-size method, and between methods. This is seen in the Chapuis method (Figure 2.4) which overestimates measured values where K_{sat} = <1x10^{-6} m/s and underestimates values >1x10^{-6} m/s. Over and underestimation between methods is seen in the Kozeny Carman method (calculated values underestimate measured values) and the Pavchich method (calculated values overestimate measured values).

As such, it is likely that the deviation in porosities between empirically calculated and lab measured values play a role in deviations in K_{sat} (between measured and calculated values). However, it is difficult to determine the degree of this effect as it varies between empirical grain-size methods depending on the influence of porosity on K_{sat} relative to other parameters utilized by each equation. Additional variation in this effect lies in the characteristics of each measured sediment sample where the relative influence of each porosity parameter (uniformity, degree of compactness, and shape of the grains) is unknown and therefore cannot be accounted for in any systematic way.

2.4.2 Kozeny-Carman (Vukovic and Soro, 1992) Method for Guelph/Paris Moraine

Evaluation of relative slope, accuracy, and precision of calculated values in Figures 2.2 – 2.4 deems the Kozeny-Carman (Vukovic and Soro,1992) method to be the most appropriate for use on the Guelph/Paris Moraine data. This method provides a trend-line with a slope that is similar in accuracy to other methods, accounting for natural variability of the samples reasonably well. The Kozeny-Carman (Vukovic and Soro, 1992) method is one of the most widely used and accepted in the literature (along with Hazen (1892)) and is considered accurate over a wide range of sediments (Chapuis and Aubertin, 2003). Thus, its use on all sediments in this study is valid. Additionally, use of the Kozeny-Carman (Vukovic and Soro, 1992) method in this study will facilitate comparison to literature values.

2.4.2.1 Limitations of Empirical Grain-size Methods: Overconsolidated Sediments

It must be noted that the empirical grain-size methods, including the Kozeny Carman equation (Vukovic and Soro, 1992), require the use of disturbed sediment samples. As such, they contain inherent limitations when applied to overconsolidated sediments, including many of the diamicts found in the Guelph/Paris Moraine study area. During sieve analysis, overconsolidated sediments must be crushed with a mortar and pestle (Section 2.3.2). Crushing overconsolidated sediments into an unconsolidated state often results in break down of sediment grains into smaller grain-sizes, or conversely, larger

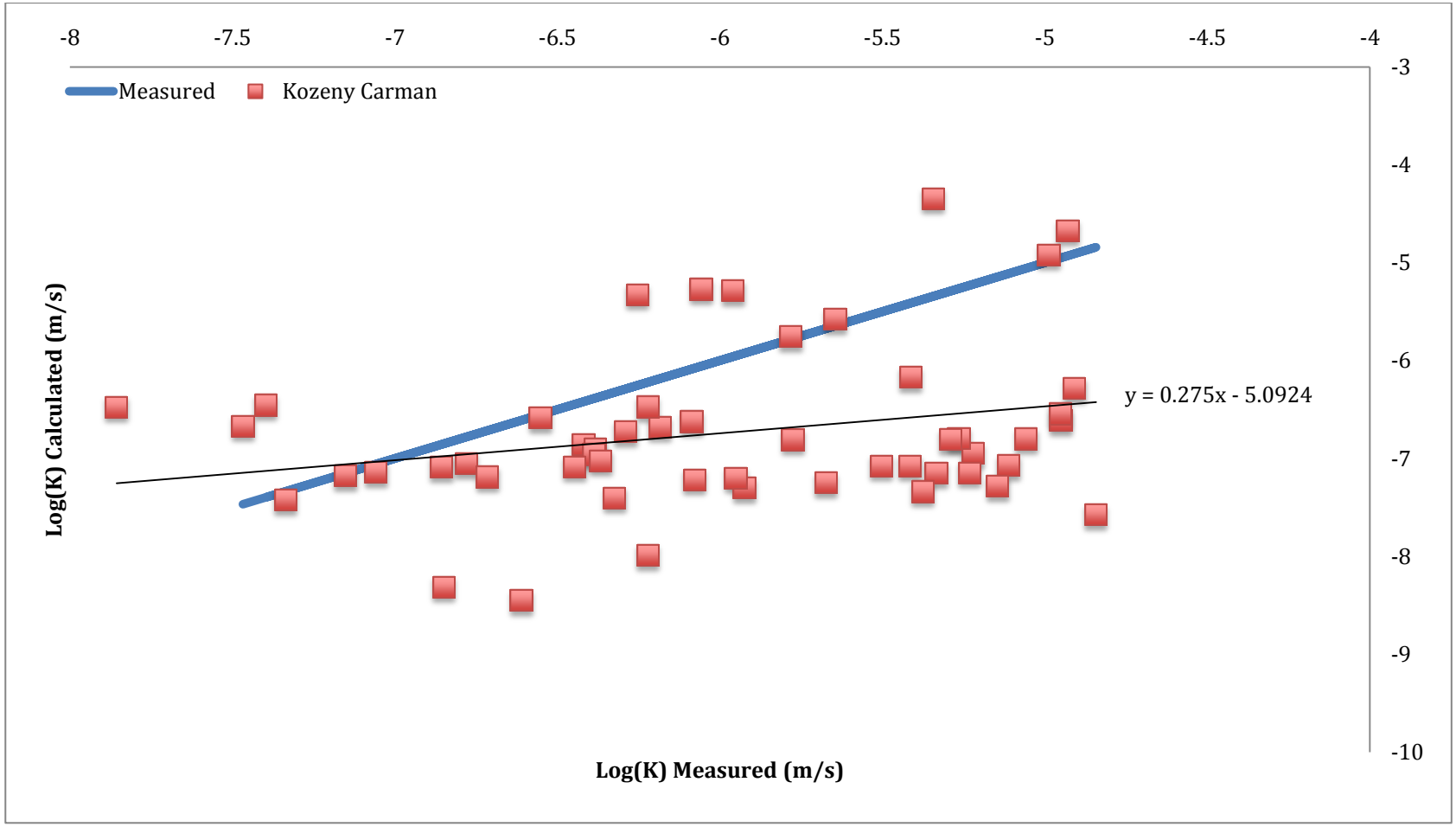

Figure 2.6: Calculated K_{sat} values of the Kozeny Carman method (Vukovic and Soro, 1992), plotted against measured permeameter values, with overconsolidated samples (diamict samples) removed.

grain-sizes if the samples are insufficiently crushed. This results in misrepresentation of the natural sample during grain-size analysis, and therefore poor estimation of K_{sat} values calculated from empirical grain-size analysis.

Figure 2.5 shows the effect on calculated K_{sat} values when diamict samples (many of which were overconsolidated) are removed from the plot of the Kozeny Carman method (Vukocic and Soro, 1992) against measured permeameter data. The result is a much more favorable slope 0.275 (versus 0.146 with diamict data) indicating that the accuracy of empirical grain-size methods are decreased by the aforementioned issues inherent in crushing overconsolidated sediment samples.

2.4.3 Calculating Calibration Factors

Calibration factors were calculated for each empirical grain-size method as outlined in Section 2.3.5. The literature states that permeameter (measured) values are more accurate than values calculated by empirical grain-size methods (Kasenow, 2003). Therefore, the empirically calculated values are adjusted or "calibrated" to reflect the measured permeameter values in the study area. This ensures the greatest possible accuracy when employing the empirical grain-size methods for calculation of K_{sat} in the Guelph/Paris Moraine area. These calibration factors shift the geometric mean of calculated values onto the geometric mean of the measured values (Equation 16). This vertically transforms the distribution without affecting the slope or relative values of the data. These calibration factors are presented in Table 2.2. The resulting distributions are

seen in Figures 2.6 – 2.8 and corresponding values are in Appendix A. This makes application of each method accurate as possible (within existing limitations) on the Guelph/Paris Moraine data. Table 2.3 shows the calibrated empirical formulas accounting for the calibration factor in the equations' coefficient. Therefore, if a particular method is used in the Guelph/Paris Moraine area, the form presented in Table 2.3 ensures maximum accuracy of that method. Additionally, void of other data, these calibration factors can also be applied in similar glacial sediments at other sites.

Method	Calibration Factor (m/s)	Method	Calibration Factor (m/s)
Alyamani and Sen	0.48	Krumbein and Monk	0.00044
Beyer	N/A	NAVFAC	N/A
Chapuis	0.53	Pavchich	0.0068
Harleman et al.	1.46	Sauerbrei	1.62
Hazen-Original	N/A	Slichter	6.22
Hazen-New	0.75	Terzaghi	N/A
Kozeny	N/A	USBR	N/A
Kozeny-Carman	3.86	Zamarin	N/A
Kozeny-Carman (Carrier)	3.12	Zunker	N/A
Kruger	N/A		

Table 2.2: Calibration Factors. Methods showing "N/A" cannot be applied to the Guelph/Paris Moraine data due to restriction of their application (Table 2.1)

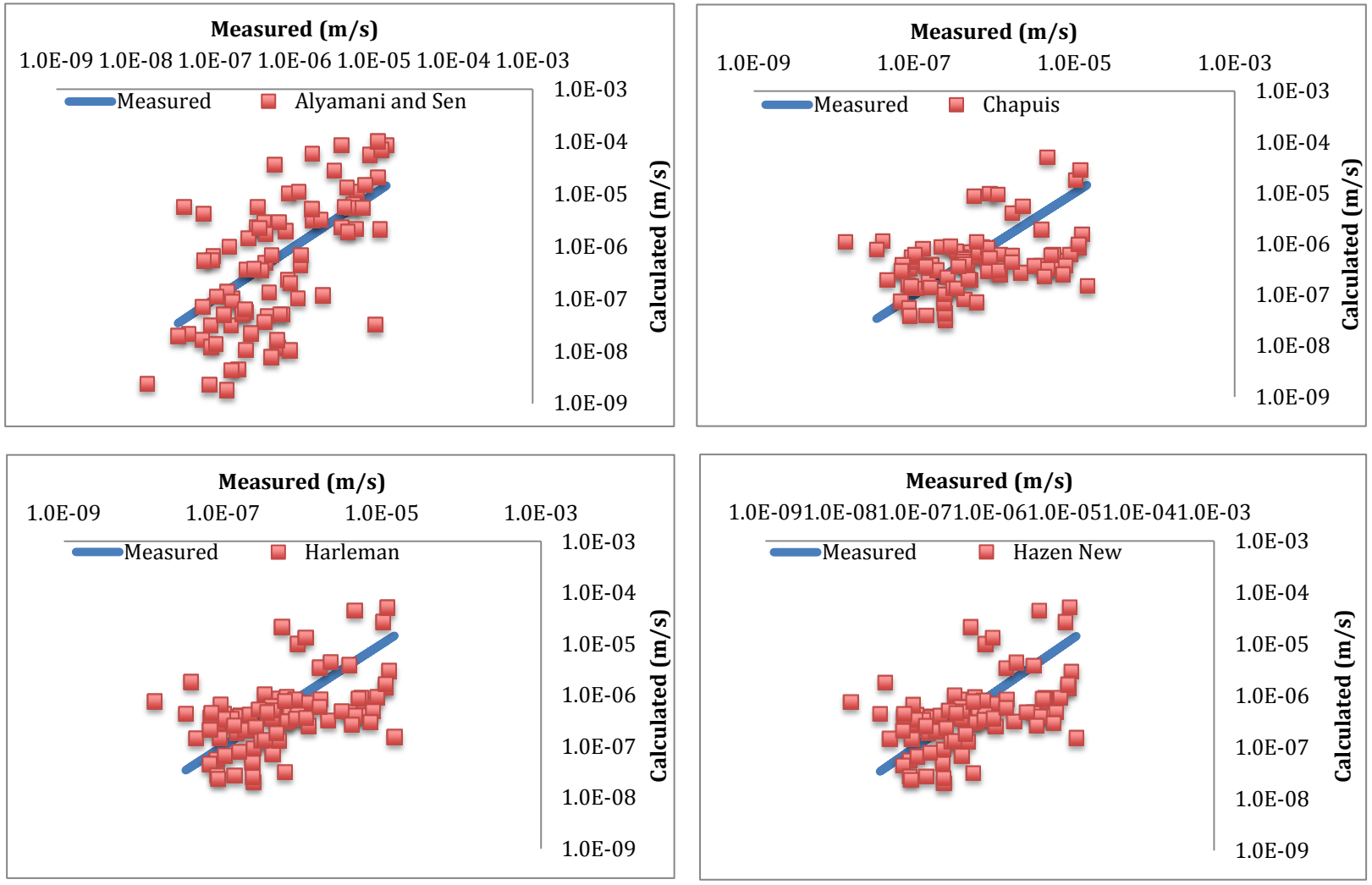

Figure 2.7: Calibrated K_{sat} values of individual methods, plotted against measured permeameter values.

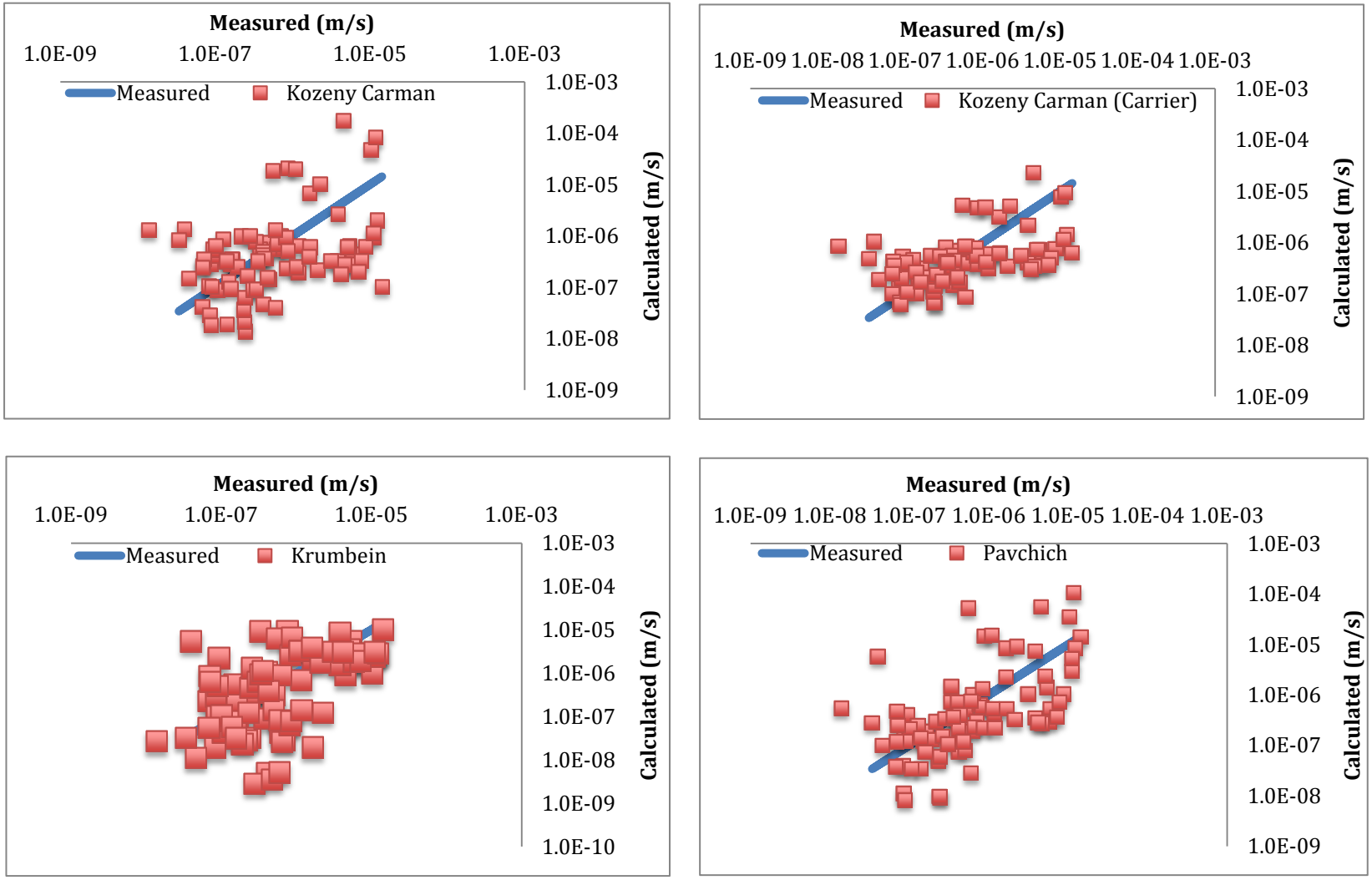

Figure 2.8: Calibrated K_{sat} values of individual methods, plotted against measured permeameter values.

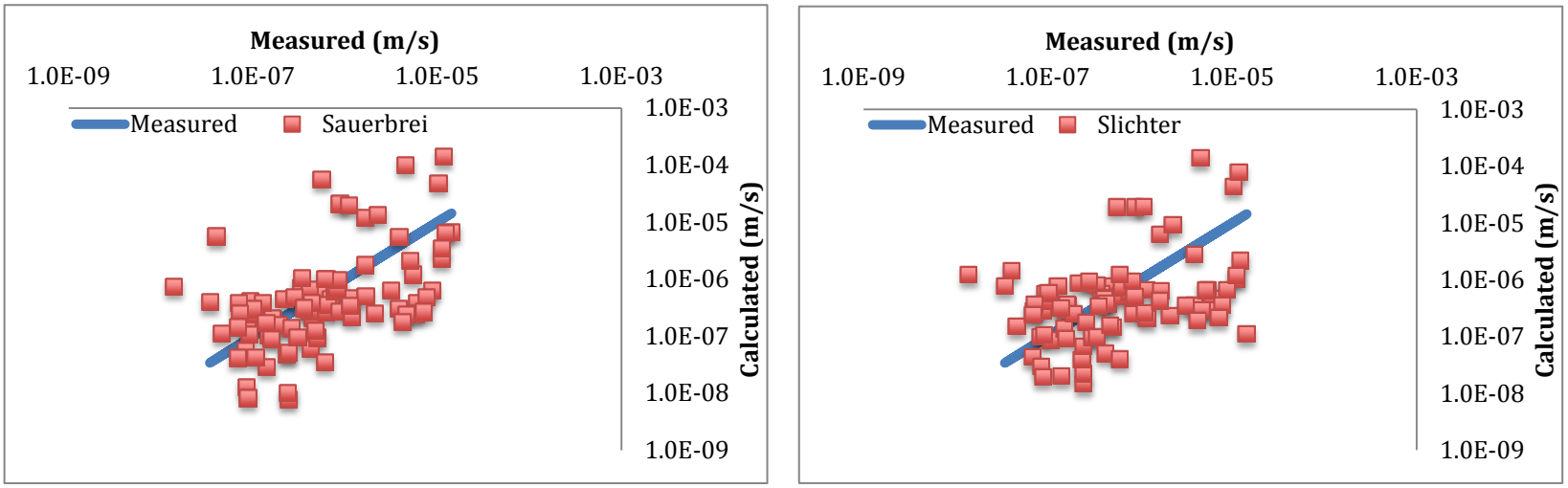

Figure 2.9: Calibrated K_{sat} values of individual methods, plotted against measured permeameter values.

Table 2.3
Calibrated Methods to Calculate K_{sat} from Grain-Size

Method	Equation	Variable and Unit Definition	Usage Criteria
Alyamani and Sen (1993)	$K\left(\frac{m}{s}\right) = 6.27 \text{ x } 10^2[I_o + 0.025\ (d_{50} - d_{10})]^2$	I_o is the intercept in mm of the line formed by d_{50} and d_{10} with the grain-size axis on an arithmetic plot	Well distributed sample
Beyer (1964)	N/A		0.06mm < d_{10} < 0.6mm 1 < C_u < 20
Chapuis et al. (2005)	$K\left(\frac{m}{s}\right) = \frac{g}{v} \text{ x } 1.31 \left(\frac{d_{10}^2 e^3}{1+e}\right)^{0.7825}$ $e = \frac{n}{1-n}$	e is the void ratio d_{10} is in m	0.03mm < d_{10} < 3mm 0.3 < e < 0.7
Harleman et al. (1963)	$K\left(\frac{m}{s}\right) = \frac{g}{v} \text{ x } 9.54\text{x}10^{-4}\ d_{10}^2$	d_{10} is in m	

Method	Equation	Variable and Unit Definition	Usage Criteria
Hazen-Original (1892)	N/A	d_{10} is in m	0.1mm < d_{10} < 3mm C < 5
Hazen-New (modified) (Rosas et al., 2014)	$K\left(\frac{m}{s}\right) = 9.32 \text{ x } 10^{1}\ d_{10}^{2}$	C is the Hazen coefficient in *1/[cm*s]* d_{10} is in cm	
Kozeny (1953)	N/A	d_1 is the largest diameter of the finest fraction in m Δg_1 is the weight of the finest fraction in parts of total weight Δg_i is the weight of the i fraction, in parts of total weight d_i^g is the maximum grain diameter of the corresponding fraction in m	Large grain sand

Method	Equation	Variable and Unit Definition	Usage Criteria
Kozeny (1953) continued		d_i^d is the minimum grain diameter of the corresponding fraction in m	
Kozeny-Carman (Vukovic and Soro, 1992)	$K\left(\frac{m}{s}\right) = \frac{g}{v}$ x 2.15 x $10^{-2}\left[\frac{n^3}{(1-n)^2}\right] d_{10}^2$		Silts, sands, and gravelly sands d_{10} < 3mm
Kozeny-Carman (Carrier, 2003)	$K\left(\frac{m}{s}\right) = \frac{g}{v}$ x 6.21 x 10^4 $\left(\frac{1}{S_o^2}\right)$ x $\left(\frac{e^3}{[1+e]}\right)$ $S_o = \left(\frac{SF}{d_e}\right)$ $\frac{1}{d_e} = \frac{3}{2}$ x $\frac{\Delta g_1}{d_1} + \sum \Delta g_i \frac{d_i^g + d_i^d}{2 \text{ x } d_i^g \text{ x } d_i^d}$	S_o is in mm d_e is in mm	SF = 7
Kruger (Vukovic and Soro, 1992)	N/A	g_i is the fraction % weight retained on *i* sieve d_i^g and d_i^d, max and min grain diameters of the fraction in m	C > 5 Medium grain sands

Method	Equation	Variable and Unit Definition	Usage Criteria
Krumbein and Monk (1943)	$K\ (\frac{m}{s}) = 3.34 \text{ x } 10^{-1} GM^2\ \ e^{-1.31\sigma_\phi}$	GM is the geometer mean in m $_\Phi$ is the phi standard deviation	
NAVFAC (1974)	N/A	e is the void ratio d_{10} is in mm	0.1 mm < d_{10} < 2mm 0.3 < e < 0.7 2 < C < 12 $\frac{d_{10}}{d_5}$ > 1.4
Pavchich (Pravedney, 1966)	$K\ \left(\frac{m}{s}\right) = \frac{g}{v} \text{ x } 2.36 \text{ x} 10^{-3}\ \sqrt[3]{C_u}\left[\frac{n^3}{(1-n)^2}\right] d_{17}^2$	d_{17} is in m	0.06mm < d_{17} < 1.5mm
Sauerbrei (Vukovic and Soro,1992)	$K\ \left(\frac{m}{s}\right) = \frac{g}{v} \text{ x } 6.1 \text{ x } 10^{-3}\left[\frac{n^3}{(1-n)^2}\right]\ d_{17}^2$	d_{17} is in m	Sand and sandy clay d_{17} < 0.5mm
Slichter (1899)	$K\ \left(\frac{m}{s}\right) = \frac{g}{v} \text{ x } 6.22 \text{ x } 10^{-2}\ n^{3.287}\ d_{10}^2$	d_{10} is in m	0.01mm < d_{10} < 5mm

Method	Equation	Variable and Unit Definition	Usage Criteria
Terzaghi (1925)	N/A	d_{10} is in m	Large grain sands
USBR (Vukovic and Soro,1992)	N/A	d_{20} is in m	Medium grain sands $C < 5$
Zamarin (Vukovic and Soro,1992)	N/A	d_1 is the largest diameter of the finest fraction in m Δg_1 is the weight of the finest fraction in parts of total weight d_i^g and d_i^d, max and min grain diameters of the fraction in m Δg_i is the fraction weight in parts of total weight	Large grain sands

Method	Equation	Variable and Unit Definition	Usage Criteria
Zunker (Vukovic and Soro,1992)	N/A	d_1 is the largest diameter of the finest fraction in m d_i^g and d_i^d, max and min grain diameters of the fraction in m Δg_i is the fraction weight in parts of total weight	Fine and medium grain sands

2.4.4 Unsaturated Soil Hydraulic Parameters and Functions

Soil water retention characteristics and K_{unsat} are widely employed in modeling of unsaturated zone processes. These modeling efforts cover a range of important issues including chemical transport and dissolution, water flow and partitioning, biological processes and remediation, and climate change (Wosten et al., 2001). The spatial and temporal variability of unsaturated hydraulic parameters highlights the importance of reporting and understanding the implications of these values (Wosten et al., 2001). Estimated unsaturated soil hydraulic parameters are shown in Appendix C. These are not commonly calculated in grain-size analysis, however, it is important to report these values for use in the modeling context (ie. contamination and water flow partitioning).

As outlined in Section 2.3.7, ROSETTA (1999) was used to estimate soil hydraulic parameters ($\theta_r, \theta_s, \alpha, n$) from the sand, silt, and clay percentages of each sample (Appendix C). The output parameters were used as inputs for Van Genuchten (1980) (equation 11) – Mualem (1976) (equation 13) model:

$$S_e = \frac{1}{(1 + (\alpha h)^n)^m} \tag{11}$$

$$K(S_e) = K_s S_e^l \left[1 - \left(1 - S_e^{\frac{1}{m}}\right)^m\right]^2 \tag{13}$$

and the Brooks Corey (1966) (equation 10) – Burdine (1953) (equation 15) model:

$$S_e = \begin{cases} (\alpha h)^{-\lambda} & (\alpha h > 1) \\ 1 & (\alpha h \leq 1) \end{cases} \quad (10)$$

$$K(S_e) = K_s S_e^l \left[1 - \left(1 - S_e^{\frac{1}{m}}\right)^m\right] \quad (15)$$

to produce $S_e(h)$ and K_{unsat} (S_e) plots.

2.4.4.1 The Van Genuchten-Mualem Model (Equations 11,13)

Figure 2.9 shows the Van Genuchten retention characteristics ($S_e(h)$) of samples with d_{10} values of 0.001 - 0.005mm (top left) and 0.005 – 0.01mm (top right). These represent the finer samples in the study. The $S_e(h)$ functions of these sediments are relatively similar, with variation in the slope reflecting small heterogeneities (sorting) in grain-size composition of the samples. The slope of these functions is relatively shallow compared to those of larger grain-sizes. These functions also indicate the requirement for higher *h* values to reach residual saturation when compared to larger grain-sizes.

Figure 2.9 shows the Van Genuchten retention characteristics ($S_e(h)$) of samples with d_{10} values of 0.01 - 0.05mm (bottom left) and >0.05mm (bottom right). The $S_e(h)$ of these sediments show increased variability compared to finer samples. This is likely to do a combination of variable sorting of the samples, as well as the more highly variable pore-drainage characteristics of larger grain materials. The slope of these functions range from: similar to those seen finer

sediments (0.005 and 0.01mm), to much steeper. The majority of these samples lose saturation at much lower *h* values than finer samples.

Figure 2.10 shows the Mualem $K_r(S_e)$ functions, where K_r= K_{unsat}/K_{sat}, for samples with d_{10} values of 0.001 – 0.005mm (top left) and 0.005 – 0.01mm (top right). These functions represent the finer samples. The slopes of these samples show a relatively high variation, due to variable sorting as well as differential pore drainage associated with varying pore sizes. The slopes of these functions are generally the most smooth and shallow, dictating that a greater drop is saturation is required for a given drop is K_r. However, there are steeper functions present in this set of samples. The conductivity of these samples, with steeper slopes, decrease more drastically with decreasing saturation.

Figure 2.10 shows the Mualem $K_r(S_e)$ functions for samples with d_{10} values of 0.01 – 0.05mm (bottom left). The functions show relatively low variation when compared to samples of other grain-sizes. The slopes of these functions are generally relatively steep compared to smaller grain-sizes. The conductivity of these samples decreases drastically with decreasing saturation.

Figure 2.10 shows the $K_r(S_e)$ functions for samples with d_{10} values of >0.05mm (bottom right). The functions show a low degree of variation. The slopes of these functions are generally steep, indicating that they will rapidly lose conductivity with decreases in saturation (resulting from changes in *h)*.

2.4.4.2 The Brooks Corey-Burdine Model (Equations 10-15)

The Van Genuchten-Mualem model is cited in the literature as providing the most accurate K_{unsat} values for heterogeneous samples (Shapp, 1999). The Brooks Corey-Burdine model is more accurate on homogeneous samples (Shapp, 1999). The Brooks Corey-Burdine $S_e(h)$ and $K_r(S_e)$ functions are shown in Figures 2.11 and 2.12.

The $S_e(h)$ functions seen in Figure 2.11 show much less variability between samples through all grain-sizes when compared to the Van Genuchten - Mualem model. Generally, the lower grain-sizes have greater water retention as *h* increases (more shallow slopes). Additionally, the Brooks Corey-Burdine model calculates zero saturation at much lower values than the Van Genuchten-Mualem model. In the Brooks Corey model, the moisture content drops much more abruptly than is seen with the Van Genuchten-Mualem model, and therefore does not represent retention at S_e values >60% in as much detail. This type of behavior is characteristic of uniform grain-size distributions which lose much of their moisture very abruptly at a given *h* value. This is unlikely the case as the Guelph/Paris Moraine sediments are not uniform.

$K_r(S_e)$ functions in Figure 2.12 shows less variation between individual samples relative to the Van Genuchten-Mualem model. However, the slopes of the functions do not vary, with changes in grain-size, to a similar degree as when the Van Genuchten-Mualem model is applied. Therefore, the Brooks Corey-Burdine model lacks the ability to accurately represent the poorly sorted

sediments encountered in this study. Additionally, the Brooks Corey-Burdine model indicates that samples will reach zero conductivity at a saturation ~30% lower than indicated by the Van Genuchten-Mualem model. Therefore, it can be concluded that the Van Genuchten-Mualem model most accurately estimates the unsaturated soil hydraulic characteristics in the Guelph/Paris Moraine area.

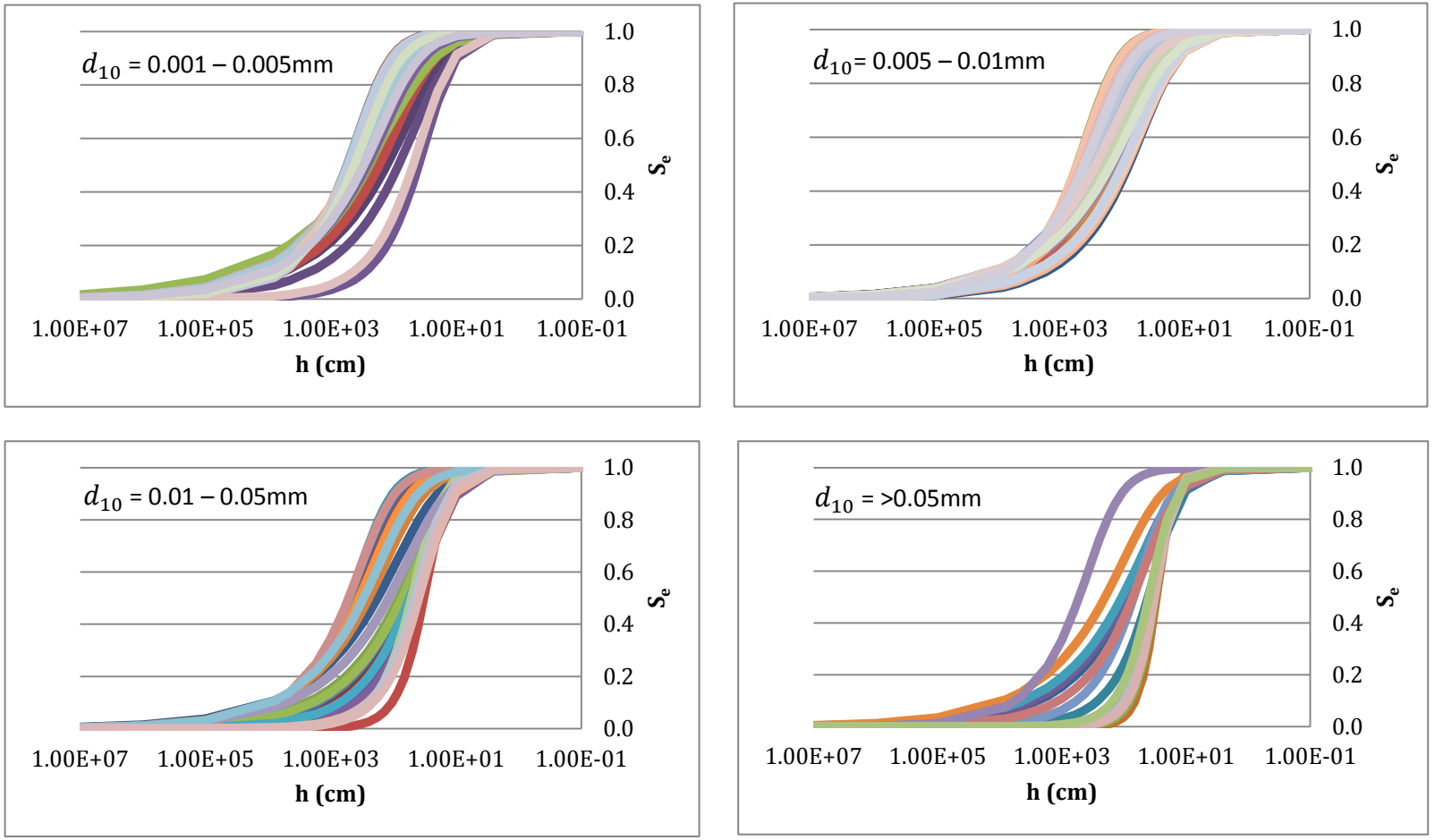

Figure 2.10: Effective saturation as a function of capillary suction, ($S_e(h)$), as calculated by Van Genuchten (1980). Input parameters were estimated by sand/silt/clay % using the ROSETTA (1999) model. Curves represent individual sediment samples from high quality boreholes.

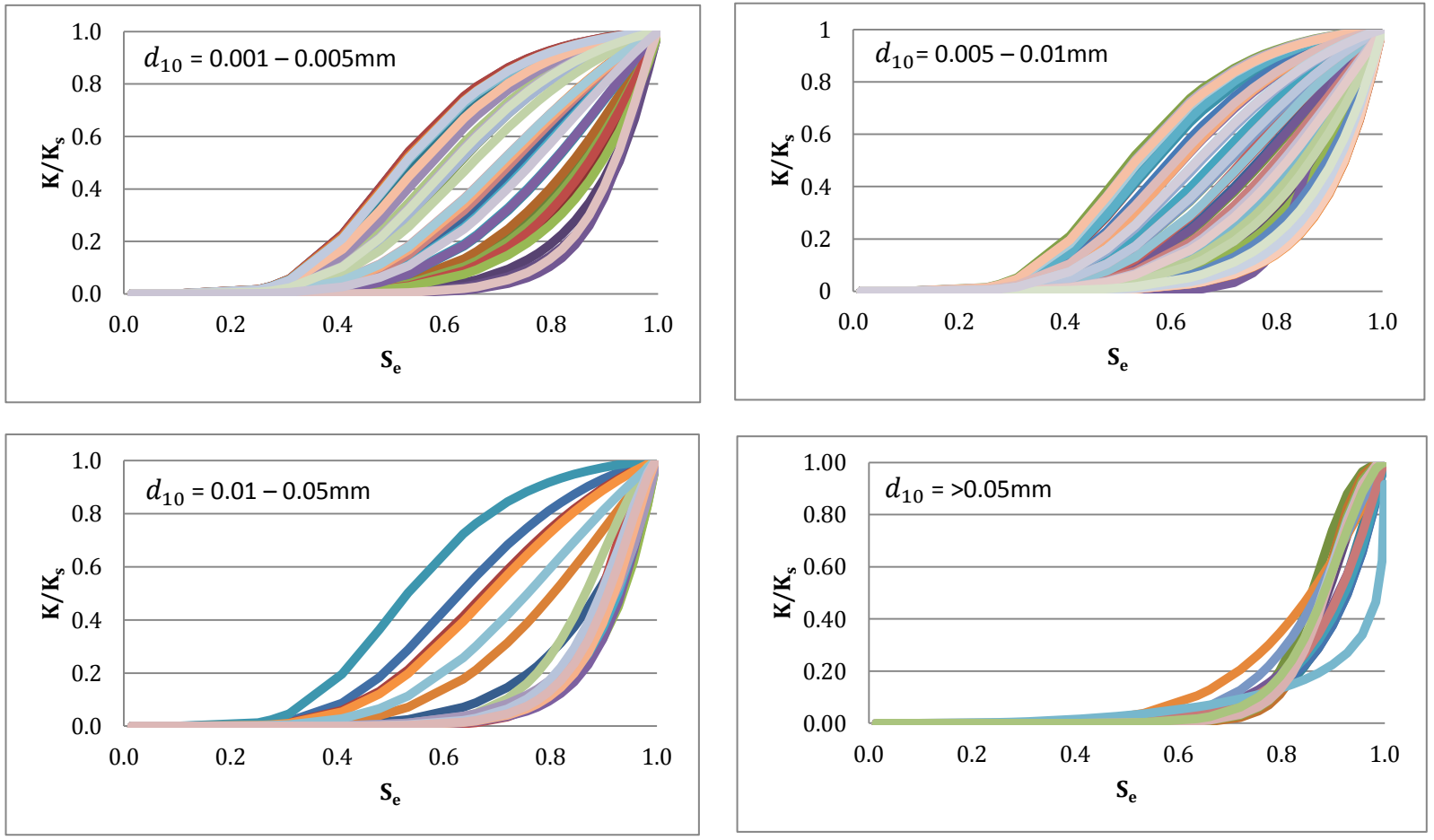

Figure 2.11: Relative hydraulic conductivity as a function of effective saturation, $K_r(S_e)$, as calculated by Mualem (1976). Input parameters were estimated by sand/silt/clay % using the ROSETTA (1999) model. Curves represent individual sediment samples from high quality boreholes.

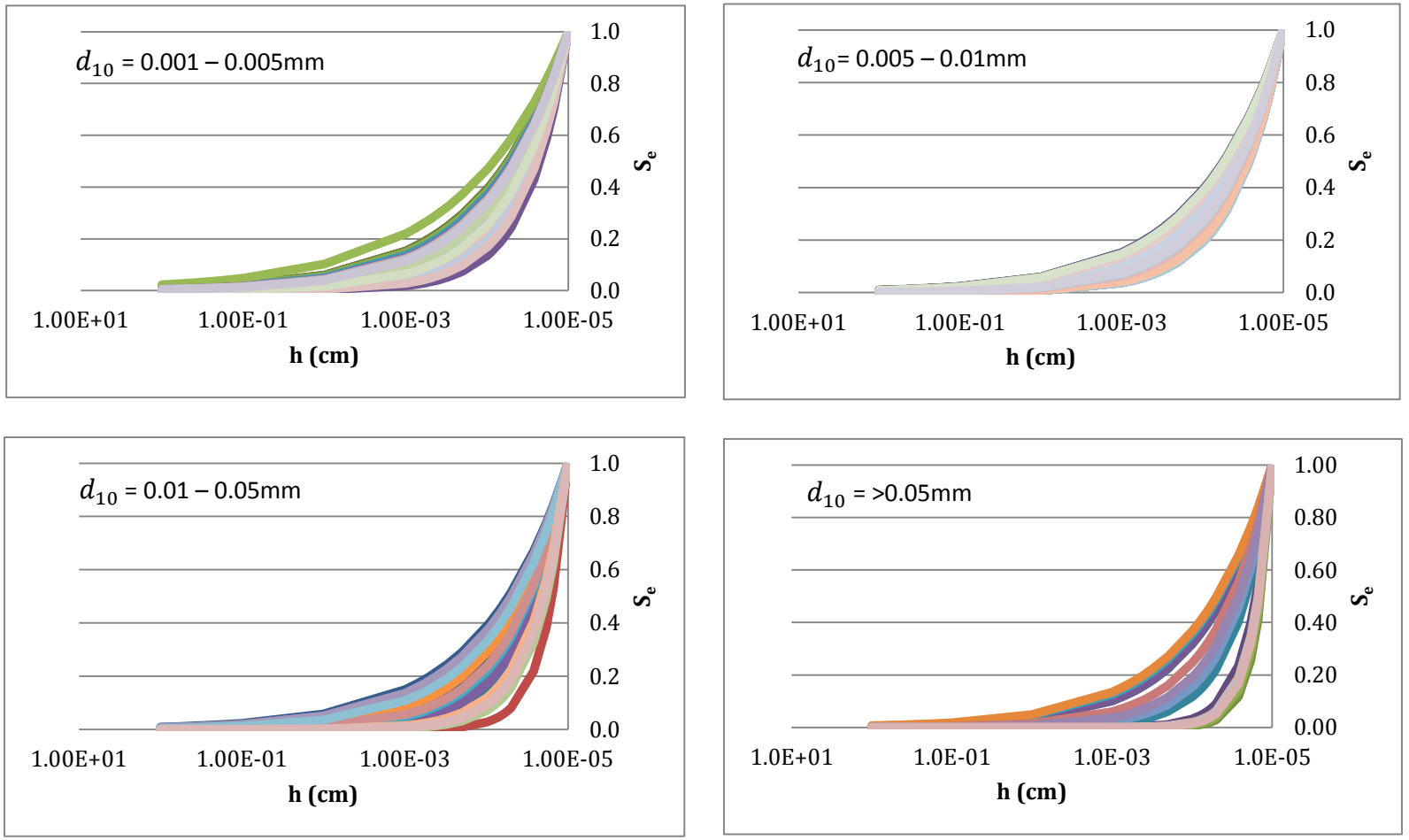

Figure 2.12: Effective saturation as a function of capillary suction, ($S_e(h)$), as calculated by Brooks Corey (1966). Input parameters were estimated by sand/silt/clay % using the ROSETTA (1999) model. Curves represent individual sediment samples from high quality boreholes.

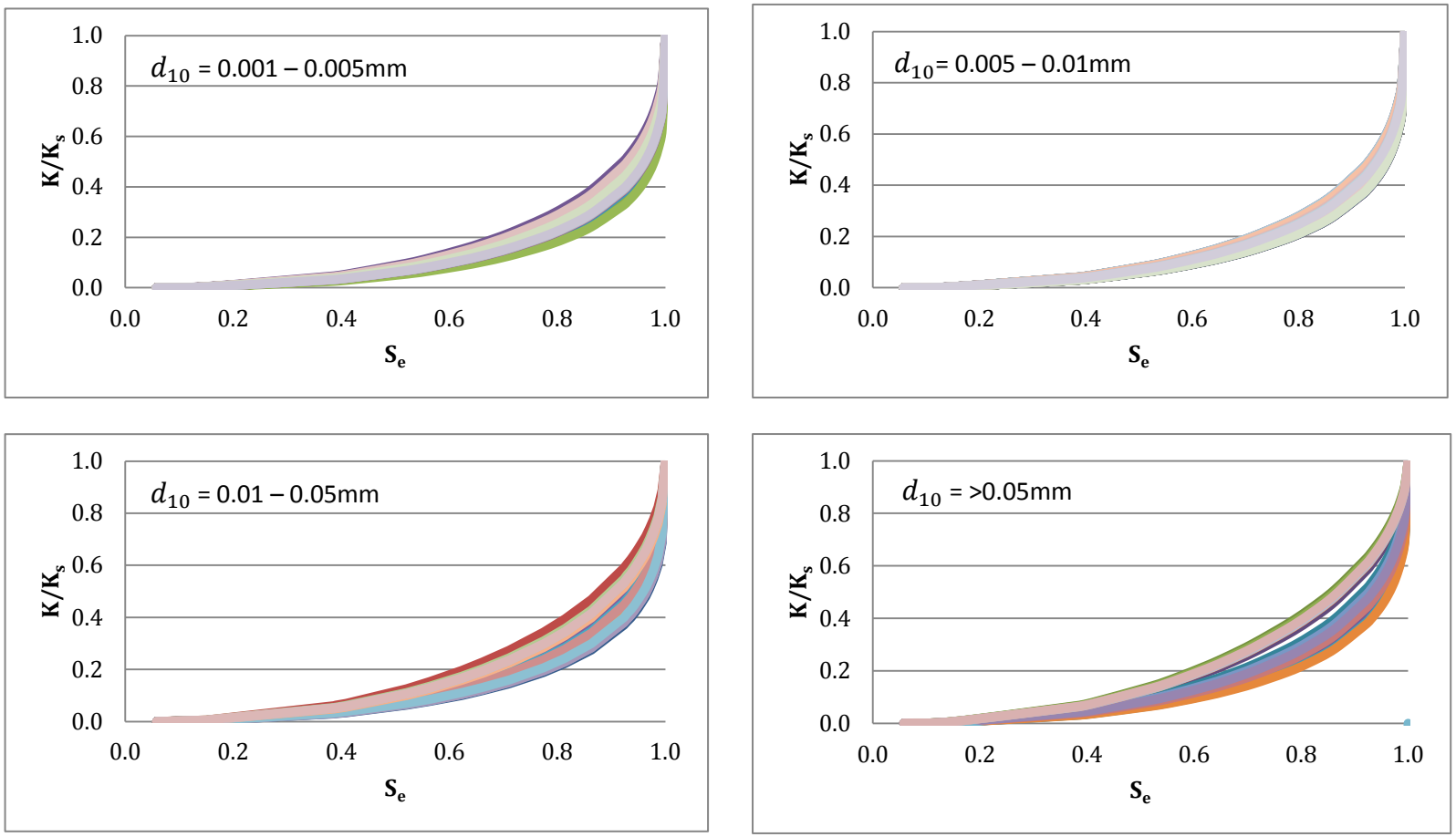

Figure 2.13: Relative hydraulic conductivity as a function of effective saturation, $K_r(S_e)$, as calculated by Burdine (1953). Input parameters were estimated by sand/silt/clay % using the ROSETTA (1999) model. Curves represent individual sediment samples from high quality boreholes.

2.5.0 CONCLUSIONS

The purpose of this study was to investigate the 19 most common empirical grain-size methods used to calculate K_{sat} in order to identify the most suitable method for use on the Paris Moraine data. This was accomplished by evaluation of calculated values from empirical grain-size methods, against measured values from falling head permeameter tests. Each method was calibrated for the Guelph/Paris Moraine data to ensure maximum accuracy in their use. Unsaturated soil hydraulic parameters and functions were estimated using the ROSETTA (1999) model, and Van Genuchten-Mualem/Brooks Corey-Burdine models.

The literature cites the Kozeny-Carman method as the most popular and widely accepted (Vukovic and Soro, 1992; Kasenow, 2002; Carrier, 2003), therefore its use facilitates comparison to the literature. It has also been found to yield accurate K_{sat} estimates for a wide range of sediments (Chaupis and Aubertin, 2003). This study finds the Kozeny-Carman (Vukovic and Soro, 1992) method to yield estimates with similar accuracy and precision to other methods. Its use provides reasonable estimates of K_{sat} for the Guelph/Paris Moraine sediments.

The C value of these methods can easily be modified for calibration of to specific sites based on measured values. However, these methods fall short with respect to estimating heterogeneity of samples based on the complex interactions of grain-size, grain structure/shape, packing, and clay content. This

suggests that some factors are unknown, or cannot be adequately accounted for. Thus, a purely empirical approach should be the focus of further research, as opposed to the semi-empirical/physical approach, which is used in the majority of these methods. Furthermore, efforts to improve precision of these approaches should be in the forefront of future study, which should accompany advances in characterization of heterogeneity.

It should be noted that grain-size analysis contains inherent limitations, as it cannot capture heterogeneities found in the field. Both grain-size analysis and falling head permeameter analysis require disturbed samples, therefore, the ability to observe and characterize fractures and macropore effects is lost. Small-scale heterogeneities such as bedding are destroyed by these methods and therefore cannot be characterized. Additionally, the differences in empirically calculated and lab measured porosity values likely contributes to the variability observed between measured and calculated K_{sat} values.

Calculated calibration factors shown in Table 2.2 were applied to 10 of the 19 empirical grain-size methods to ensure maximum accuracy of all methods in the Guelph/Paris Moraine area. The remaining 9 methods could not be calibrated as their lack of applicability to the study area sediments (Table 2.1) discounted them from use. This does not rectify inherent issues with each method; therefore, selection of the most appropriate method based on site-specific data is required where data is available.

Estimated unsaturated hydraulic parameters and functions from grain-size in are not commonly reported, and as such contribute to the scope of this study in characterizing hydraulic parameters of the Guelph/Paris Moraine. The literature suggests that the Van Genuchten-Mualem model more accurately represents heterogeneous samples (Schapp, 1999) and therefore, is superior to the Brooks Corey-Burdine model for use in the Guelph/Paris Moraine sediments. While samples display significant variation in unsaturated characteristics, there is a general trend of greater retention and more gradual drainage with smaller grain-sizes, and less retention with more drastic drainage as grain-size increases.

3.0 Hydrostratigraphy in the Paris Moraine

3.1.0 INTRODUCTION

3.1.1 Problem Scope

The city of Guelph, Ontario, sources most of its drinking water from bedrock aquifers. Characterization of these aquifers is essential to groundwater management. It must also be considered that due to the glacial history of this region, significant Quaternary glacial deposits cover much of the land surface (Karrow, 1968, 1987). As such, these overlying deposits have a significant effect on the fate and transport of both contaminants and recharge as water infiltrates toward bedrock aquifers.

Hydraulic properties of unconsolidated sediments influence groundwater flow paths. Hydraulic properties are highly variable throughout the Guelph region due to the glacial origin of this unconsolidated material. This high spatial variability requires high-resolution characterization of geologic and hydraulic properties in order to accurately represent groundwater and contaminant flow pathways.

Historically, hydrogeologists have overlooked small-scale spatial trends in porous media, as it has little use in water resource applications, which tend to be more regional in scope. More recent concerns with contaminant fate and transport have led to the incorporation of this heterogeneity into hydrogeologic study (Anderson, 1989). Conceptual stratigraphic cross sections and depositional facies can provide control and guidance in the development of

improved hydrostratigraphic cross sections by integrating these small-scale spatial trends (Russell et al., 2001).

3.1.2 Objectives

As part of the ORF (Ontario Research Fund) project entitled Sustainable Bedrock Water Supplies for Ontario Communities, this study will contribute to the objective of characterizing Quaternary sediment deposits in the Guelph area for the purpose of groundwater protection and risk management by the municipality by providing detailed data on the hydraulic conductivity of Quaternary sediments. The study will build on the previous ORF funded research of McGill (2012), which focused on the geological and geomorphic characteristics of Quaternary sediments in the Guelph area. The current study will synthesize geologic and hydrogeologic information, as well as integrate new high quality hydraulic data. Characterization of high-resolution hydrostratigraphy in the Guelph area will provide insight into the heterogeneous nature of hydraulic conductivity in these complex glacial deposits, informing flow, contaminant fate and transport, and recharge, into the underlying bedrock aquifers.

3.1.3 Study Area

The City of Guelph, Ontario, is located approximately 70 km southwest of Toronto. Guelph has been identified as one area in the Ontario Places to Grow Act (Ministry of Infrastructure, 2012) and has therefore, undergone significant

land use change and urbanization in recent years. Its forecasted growth has caused concern with regards to sustainability of its groundwater supplies. The ORF program was undertaken to investigate the bedrock water supply system in the area and to provide much needed data on which evidence-based decisions can be made for future water resources management. Investigation of the overlying Quaternary hydrogeology is central to understanding recharge and contaminant transport in the area.

The unconsolidated sediments in the Guelph area are of glacial origin, with the Paris Moraine as its most prominent glacial landform (Karrow, 1968, 1987). The Paris Moraine system extends approximately 150 km from Caledon in the Northeast to Port Rowan on the Lake Erie shoreline and thus runs through the Credit River and Grand River watersheds (Blackport, 2009). The Paris Moraine is generally comprised of hummocky belts and ridges (Chapman and Putnam, 1984). In the Guelph area, the Paris Moraine is expansive with up to a 4 km width (Blackport, 2009) and can have topographic relief of up to 30-40m. Substantial outwash sand and gravel is associated with the Paris Moraine, as well as wetland features and kettle lakes that have developed over time since the retreat of glaciers. Historically, land use in the Guelph area has been largely agricultural. More recently, significant urbanization has taken place as the population of Guelph has grown (Ministry of Infrastructure, 2012).

3.2.0 BACKGROUND

3.2.1 Geologic History

3.2.1.1 Regional Quaternary Stratigraphy

Quaternary sediments in the Guelph area range from 0 to 76.20m thick (Karrow 1968, 1987). This is mainly due to variations in erosional and bedrock features. Wentworth Till and Port Stanley Till are typically found at the surface with a range of other tills appearing at depth. The regional stratigraphic till sequence from oldest to youngest is: Canning Till, Catfish Creek Till, Maryhill Till, Tavistock Till, Port Stanley Till, Wentworth Till, alluvial deposits, and swamp/bog deposits (Karrow, 1968, 1987), though not all are present throughout the Guelph area. Table 3.1 outlines the typical characteristics of these stratigraphic units.

Table 3.1: Stratigraphic till layers of the Guelph area

Stratigraphic Units	Description
Canning Till	Coarse textured, often confused with the Catfish Creek Till (Bajc and Dodge, 2011)
Catfish Creek Till	Stony, silty sand; hard, olive coloured (Karrow, 1987) ; Average of 38% sands, 16% clay (Bajc, 2007); regionally extensive (Burt, 2001)
Maryhill Till	Clayey silt to clay, low in pebbles (Karrow, 1968); not as regionally extensive as the Catfish Creek Till (Burt, 2001).
Tavistock Till	Fine textured silt or clayey silt rich (Burt, 2011);

	7% sand, 54% clay (Karrow, 1987)
Port Stanley Till	Sandy; ~40% sand (Karrow, 1987); Stone poor, clayey silt with high plasticity (Bajc and Dodge, 2001); regionally variable (Karrow, 1987)
Wentworth Till	Sandy to silty sand till, buff in colour, often bouldery or stony (Karrow, 1968, 1987); stony, sandy diamicton in the Guelph area (Sadura et al., 2006)

This till stratigraphy provides a regional framework for the local stratigraphy and can provide further insight on local heterogeneity.

3.2.1.2 Local Quaternary Stratigraphy

The oldest Quaternary sediments in the Guelph area are spatially variable consisting of diamict, stratified sediment infill (Eramosa/Speed River), or gravel infill (bedrock valley) directly overlying bedrock. The basal diamict is thought to be Catfish Creek Till (Karrow, 1968, 1987), though the older Canning Till may be present in some places (Burt, 2011; McGill, 2012). The next oldest are sediments infilling the bedrock valley and the sediments of the drumlinized till plains north of the Paris Moraine (Karrow, 1968, 1987). These are interpreted as subglacial traction tills (McGill, 2012). These consist of sandy to gravel rich diamict and are likely of the Port Stanley Till or older.

The Paris Moraine frontslope is characterized by a bedrock-diamict-troughfill-diamict sequence (McGill, 2012). Trough fill sediments originate from a range of ice marginal fluvial and lacustrine processes (McGill, 2012).

The hummocky terrain of the Paris Moraine in the Guelph area is the product of localized and uneven melting of debris rich ice, creating topographic highs and lows. The topographic lows are filled with sediment deposited from meltwater streams or mass flows from high relief slumping (McGill, 2012). Paul (1984) outlines the sedimentary sequence of this relief process where the lower diamict is of subglacial origin, trough fill sediments are either waterlain or mass flow produced, and surface diamict is of high relief debris flow origin. The Paris Moraine sediments are associated with the Wentworth Till at surface and older subtraction tills (possibly Catfish Creek Till) above the bedrock (Karrow, 1987) and a highly variable sequence of sediments in between (McGill, 2012). As the same time as deposition of the Wentworth Till, outwash sediments would have eroded into and aggraded onto the Port Stanley Till and older deposits to the NW of the Paris Moraine (Karrow, 1968, 1987). Consequently, the drumlinized till plain and outwash plain sediments are characterized by both buried and surficial pre-Paris Moraine sediments, and proglacial fluvial sediments (McGill, 2012).

The Paris Moraine backslope is characterized by a bedrock-diamict-troughfill-diamict sequence. The slopes are formed by surficial mass flows. Small-scale subaqueous sediment deposition and hummocks have also been suggested for the area.

3.2.2 Hydrostratigraphy

Hydrostratigrapic units are defined as bodies of rock with significant extent that compose a geological framework for a reasonably distinct hydrologic system (Atkinson et al., 2014; Maxey, 1964). Hydrogeologists and hydrologists have long recognized the close relationship between lithologic units and the movement of groundwater. However, analysis has revealed that interpretation of hydrostratigraphy cannot be satisfactorily accomplished by lithologic factors alone (Atkinson et al., 2014; Maxey, 1964). Hydraulic parameters (such as conductivity or permeability) are not commonly included in lithologic facies but are essential to the delineation of hydrostratigraphy.

Often, single lithologic units function as aquifers or confining units. However, a variety of conditions, such as pre-glacial weathering of carbonate rock surfaces or diagenetic processes since time of deposition, can cause hydrostratigraphic units to encompass the boundaries of multiple lithologic formations or occur within single lithologic units (Atkinson et al., 2014; Maxey, 1964). The previous assumption that lithology could accurately represent hydraulic properties is misleading and can lead to incorrect conclusions regarding water supply and contaminant fate and transport (Atkinson et al., 2014; Maxey, 1964).

Mapping of units with similar hydraulic parameters is used to identify hydrostratigraphy. These maps or models identify interconnected units with relatively homogeneous hydraulic properties, which form high conductivity zones.

These pathways control groundwater flow and channeling of contaminants (Anderson et al., 1999). In establishing hydrostratigraphic units, hydrogeologists must incorporate and quantify heterogeneity within those units. This is accomplished by lumping heterogeneities into parameters such as hydraulic conductivity (Anderson et al., 1999). Difficulty arises when scaling up parameters from a measurement scale (meters) to a modeling scale (thousands of meters) and representing the accompanying heterogeneity. This is commonly accomplished by stochastic modeling to fill in geological and hydrogeological information between measurement points (Anderson et al., 1999).

Another problem arises when hydrogeologists refer to the sedimentological literature. This literature often consists of qualitative and descriptive data, while hydrogeology relies more heavily on quantitative data to describe and delineate hydrostratigraphy. This qualitative data is often used, but its application is subjective and depends on expert knowledge that can evolve over time. Ideally, hydrogeologists undertake further studies to obtain direct measurements of hydraulic parameters (Anderson et al., 1999) to supplement these subjective data. However, various budgetary or logistical constraints usually limit these direct measurements and thus the hydrogeologist's characterization of the heterogeneity of hydraulic parameters.

3.2.2.1 Quaternary Hydrogeology in the Guelph/Paris Moraine Area

Singer et al. (2003) present a detailed investigation of the hydrostratigraphy of southern Ontario in which the authors attempt to identify important aquifers in the Quaternary sediments. As previously stated, a large portion of bedrock in southern Ontario is covered by unconsolidated Quaternary sediments. Within these unconsolidated sediments, clay, and compact tills with high clay contents, tend to be characterized by low hydraulic conductivities (K_{sat}) while sand and gravel deposits tend to be highly permeable (high K_{sat}). It should be noted that while tills are often characterized as low K_{sat}, they are highly variable and can be relatively coarse-grained (Karrow, 1968, 1987). The low K_{sat} layers impede vertical infiltration of water, reducing recharge and form impermeable layers causing localized ponding or lateral groundwater flow. The high K_{sat} layers are highly permeable, and if underlain by impermeable materials, form the water table. Generally, unconsolidated sediment aquifers in southwestern Ontario occur within the sand and/or gravel deposits of glaciofluvial or glaciolacustrine origin (Singer et al., 2003). These aquifers are highly variable in size and spatial distribution, and can yield enough water for a single home or up to a whole town (Singer et al., 2003).

Blackport (2009) suggests the following contextual details of the Guelph/Paris Moraine area: 1. The Wentworth Till is a relatively expansive unit and become more fine-grained to the south, and therefore is more permeable in the north and less permeable in the south; 2. The internal structure of the Paris

Moraine is highly complex, consisting of a mixture of till, stratified drift, and localized layers of more permeable material; 3. A less permeable till unit exists at the bedrock interface overlain by higher permeability material. This till unit is likely to be variable in continuity.

Potential for large-scale aquifers within the Paris Moraine Quaternary sediments is limited to adjacent melt water channel sand and gravel deposits. On a smaller scale, the permeable deposits within the Moraine do support private wells and a small number of municipal wells (Blackport, 2009). The majority of producing aquifers are otherwise found in the underlying bedrock. The overlying sediments lack a continuous permeable unit and this limits its ability to supply water.

A study by (Golder, 2006) concludes that while there are a number of unconsolidated sediment wells in the area, it is impossible to interpret individual aquifer units within the Paris Moraine. The complexity of the stratigraphy implies that there may be hydraulic connections between apparently discrete sand lenses, and the potential for larger scale-but still relatively localized- groundwater production zones. The study also concluded that underlying bedrock aquifers may or may not be hydraulically connected to overlying unconsolidated sediment aquifers. This reflects the limitations of delineating complex hydrostratigraphy based solely on geologic stratigraphy (Blackport, 2009).

These previous studies provide a qualitative assessment of the local hydrostatigraphy using common or average values for sediments of various

textures, origins, and structures. This approach is useful as it provides very rough estimates of hydraulic parameters, particularly if insufficient data exists to more accurately characterize hydraulic parameters. However, it lacks the ability to provide accuracy in its estimates due to the highly variable nature of sediments. As seen in Figure 3.1, each sediment type exhibits a range of K_{sat} values over several orders of magnitude. Thus, it becomes very difficult to delineate hydrostratigraphy if solely inferring hydraulic conductivity from textural data. This approach is however useful to inform extent and connectivity of hydrostratigraphic units between higher quality data that are based on direct measurement or empirically based calculation of hydraulic parameters based on grain size distribution curves.

3.2.2.2 Delineating Hydrostratigraphy

Seaber (1988) defines hydrostratigraphic units as rock units distinguished by their porosity and permeability. Hydrostratigraphic units can be separated into aquifers (water bearing, K_{sat} = >10^{-6} m/s) or aquitards (water retarding relative to adjacent strata, K_{sat} = <10^{-6} m/s) (Singhal and Gupta, 2010). Models tend to delineate units based on its status as an aquifer or aquitard. This approach is powerful on a regional scale for water resource development. However, it is not sufficient to represent the complexity found in previously glaciated areas like Guelph and the Paris Moraine, especially for addressing contaminant transport and fate problems.

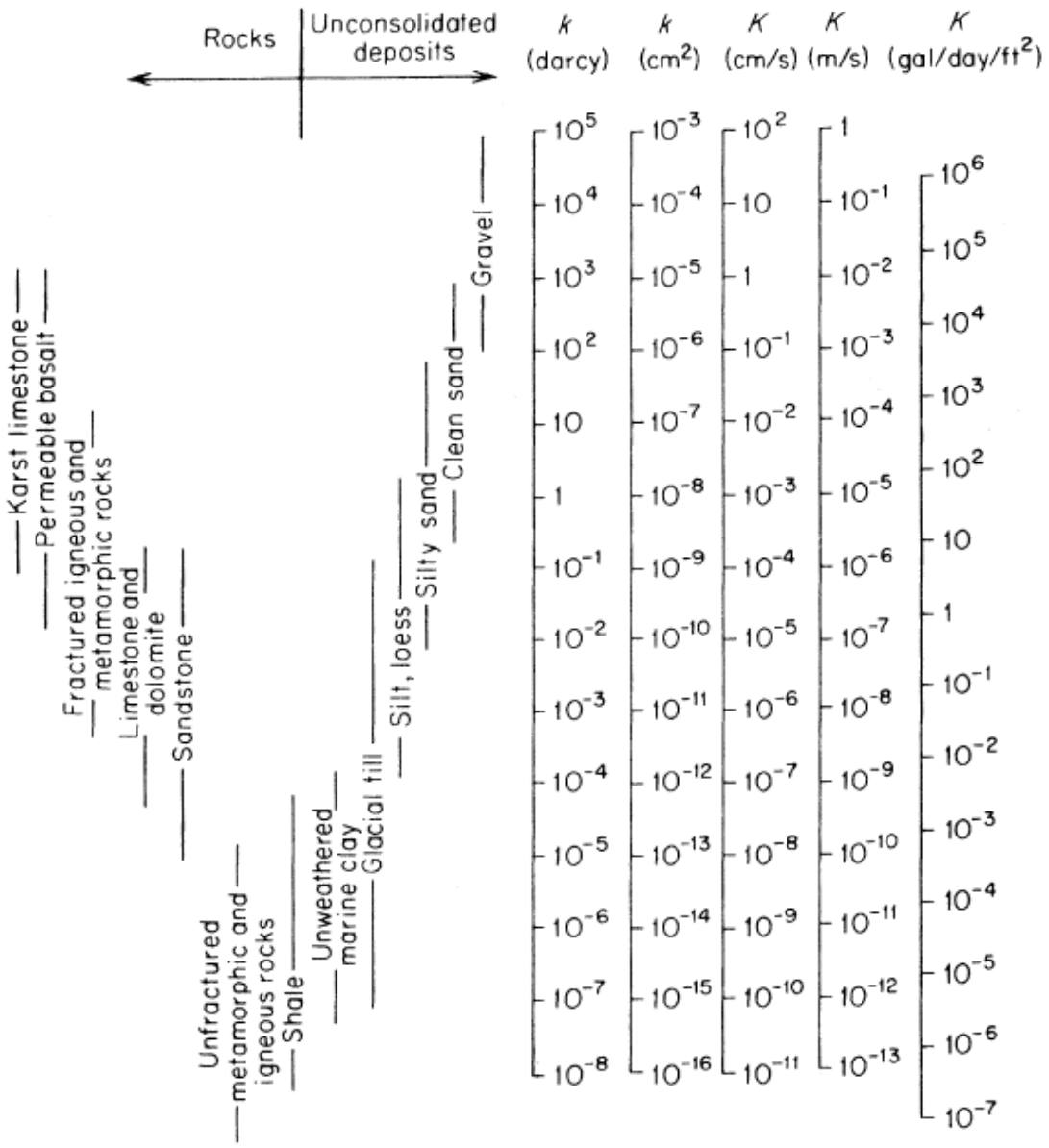

Figure 3.1: Ranges of Hydraulic Conductivity and Permeability for various sediment and rock types (Freeze and Cherry, 1979)

3.3.0 METHODS

3.3.1 High Quality Boreholes

Nine new boreholes were drilled in the Guelph/Paris Moraine area as part of the ORF research program (Figure 3.2). These are considered high quality boreholes as they were logged in detail from cores that were recovered during drilling as opposed to pre-existing lower quality boreholes that were collected for various purposes (e.g. geotechnical or water well) and are often based on cuttings rather than recovered whole core. PQ coring and roto-sonic drilling was used to obtain 4-inch diameter cores. Cores from GDC-1A, GDC-2B, and VPV-1A were collected using mud rotary (PQ) drilling, whereas cores from GDC-10A, ARS-1A, TGI-1A, VAN-1A, FRE-1A, and VE-1A were collected using roto-sonic drilling. Cores were logged in the field, photographed, and sampled for future lab analyses; sediment samples were subsequently stored at the University of Guelph (at 4^{o}C).

K_{sat} values of high quality borehole sediment samples were calculated using empirical grain-size analysis. The grain-size distribution of each sample was determined by sieve (Best, 2013; Kroetsch and Wang, 2008) and hydrometer analysis (SSSA, 2002) using standard methods. The locally calibrated form of the Kozeny-Carman (Vukovic and Soro, 1992) (Chapter 2) method was used to calculate K_{sat} from the grain-size distributions.

K_{sat} values of high quality borehole sediment samples were also directly measured by falling head permeameter tests using standard methods (SSSA, 2002).

3.3.2 Low Quality Boreholes

In order to characterize heterogeneity of the lithology, and inform heterogeneity in hydraulic parameters of the Guelph/Paris Moraine, a variety of low quality borehole sources were incorporated to fill the lithological gaps in information between the high quality boreholes along or close to the chosen transect. Some low quality boreholes contained grain-size data, however, none of these were present close to or along the chosen transect. Therefore, these values were not used directly in characterization of the hydrostratigraphy. Rather, the inferred lithology from the low quality data (in close proximity to the chosen transect) was used to inform regional-scale correlation of the hydrostratigraphy identified in the high quality boreholes. This low quality data was acquired through the Ministry of the Environment (MOE) waterwell database, geotechnical reports available through the Grand River Conservation Authority (GRCA), and piezometer data from past University of Guelph projects (Whiteley, unpublished report; Opazo Gonzalez, 2012).

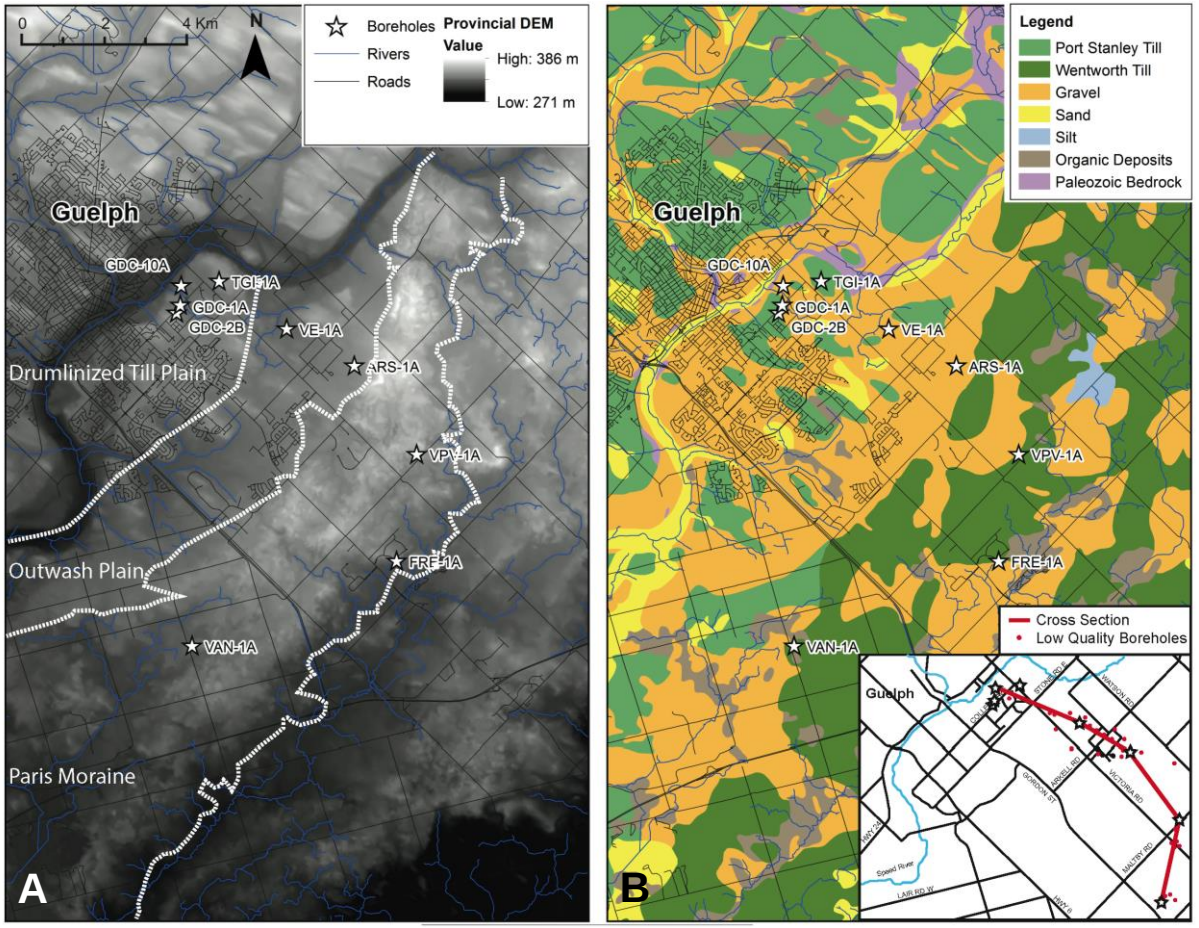

Figure 3.2: A) Digital Elevation Model (DEM) showing extent of Paris Moraine and **B)** surficial geology map of the study area with high (stars) and low quality (inset) borehole locations and the location of the study cross section (inset). The outwash plain in (A) is dominated by surficial sand and gravel deposits, whereas the drumlinized till plain is dominated by surficial Port Stanley Till deposits. Modified from maps created by Anna Best using ESRI ArcMap 9.3 with data from the Provincial Digital Elevation Model (2007) and the Ontario Geological Survey (2003).

3.3.3 Lithologic Cross Section Construction

Construction of the lithological cross section was based on the nature and distribution of materials encountered in both the high and low quality boreholes. The Guelph/Paris Moraine lithologic cross section was constructed in two steps. Firstly, a cross section was made based on high and low quality boreholes. Correlations between similar units were made tentatively.

The second step was iterative review of the drawn correlations based on previous geologic/sedimentological framework of the area. The till stratigraphy established in Karrow (1968, 1987), McGill (2012), and Sadura (2006) were used heavily to help identify the presence of the aforementioned till stratigraphy, and sediments resulting from outwash plain/drumlin field formation processes. Consideration of these processes is essential to characterization of the Guelph/Paris Moraine lithological cross section as they provide insight regarding likely heterogeneity, scale, and constraints on connectivity between adjacent lithological layers.

3.3.4 Hydrostratigrahic Cross Section Construction

Construction of the hydrostatigraphic cross section was based on the measured and calculated K_{sat} values for high quality boreholes, and correlated between high quality boreholes using the inferred lithologic geometries and sediment types from low quality boreholes.

3.3.4.1 Delineating Hydrostratigraphy in Lithologic Logs

The following method was used to delineate hydrostratigraphy in the high quality boreholes, drawing heavily on concepts developed by Mukherjee (2011):

1. When both measured and calculated K_{sat} values are available for a sample, the measured value is given priority.
2. K_{sat} values were differentiated on an order of magnitude scale.
3. Hydrostratigraphic units were delineated by grouping adjacent lithologic units with similar K_{sat} values (+/- an order of magnitude).
4. If differing K_{sat} values occur in a single lithologic unit, they are separated in distinct hydrostratigraphic units at the half way-point between the two sample points.
5. Where a unit has a single K_{sat} value differing from the next unit in succession, these are separated at the lithologic boundary.
6. When a measured or calculated K_{sat} value is unavailable for a lithologic unit, it is grouped with adjacent units, as little variation in K_{sat} exists between lithology types (see Section3.4.4 for more detail regarding this lack of variability).
7. Hydrostratigraphic units within each borehole are assigned a K_{sat} value calculated as the geometric mean of the measured and calculated K_{sat} values within the unit. The following notation is used for K_{sat} values of hydrostratigraphy:

K_{Gm} = Geometric Mean K_{sat} for measured values

K_{Gc} = Geometric Mean K_{sat} for calculated values

K_{Ga} = Geometric Mean K_{sat} for all values (both measured and calculated)

3.3.4.2 Hydrostratigraphic Cross Section Construction

The hydrostratigraphic cross sections was constructed with two specific applications in mind: 1) site specific flow in the context of contamination on the local individual borehole scale; and 2) flow for regional groundwater management applications.

Delineation of aquifer and aquitard layers was done in two steps: 1) by applying high quality borehole conductivity data to their respective lithologic spatial distributions based on the lithology cross section; and 2) using low quality lithologic data to infer additional K_{sat} heterogeneities by considering the type (gravel, sand, silt/clay, or diamict) and nature of the sediments (sorting/uniformity, consolidation/packing). The incorporation of these smaller-scale heterogeneities provides site specific flow, incorporating local scale lithologic considerations, for use in the context of contaminate transport.

K_{Gm}, K_{Gc} and, K_{Ga} values were calculated for each geomorphic region (drumlinized till/outwash plain, outwash plain, and Paris Moraine) in order to inform regional groundwater management. These were calculated using the geometric mean K_{sat} values of all high quality boreholes in each geomorphic element (including those not displayed on the cross-section itself). This provides

a reasonable “background” conductivity that can be applied where there is no high quality borehole data. This also provides a context for regional groundwater meanagement applications.

Hydrostratigraphy of the individual high quality boreholes was incorporated into the cross section including their respective K_{Ga} values in order to inform small-scale local flow regimes.

3.4.0 RESULTS AND DICUSSION

The 9 boreholes examined in this study will be discussed in relation to their physiographic location (drumlin/till plain, outwash plain, Paris Moraine; Figure 3.3). All 9 boreholes were drilled 3.05m (10ft) into bedrock and range in thickness from 8 to 37m. Each physiographic region (drumlinized till plain, outwash plain, and Paris Moraine) will be analyzed first by lithology, and then by hydrostratigraphy. After evaluation of individual high quality boreholes, low quality data will be incorporated to develop a hydrostratigraphic cross section through the study area.

3.4.1 Lithology

3.4.1.1 Drumlinized Till Plain

High quality data in the drumlinized till plain is comprised of the GDC-2B, GDC-1A, and TGI-1A boreholes (Figure 3.3). GDC-2B is characterized by multiple layers of diamict, defined by texture variability, and a few sand layers from 16.25 - 1.5m. A relatively thick soil profile is present from 0 – 1.5m. GDC-1A is characterized by a basal gravel layer from 44 – 37.5m. A thick, relatively uniform diamict layer is present from 37.5 – 8m, which in turn is overlain by a fine layer (silt/clay) from 8 – 6.5m. The uppermost section is composed of a coarser diamict layer at 6.5 – 4.5m and a gravel layer (4.5 - 0m). TGI-1A is characterized by several relatively thick diamict layers, defined by different texture, that alternate with relatively thin coarse layers (sand and gravel) from 19 – 0.5m. A

thin soil profile is found at the top from 0.5m to 0m. Two of the three holes have diamict at the bedrock-sediment interface. The gravel at the base of GDC-1A infills a significant bedrock low; GDC-1A is ~200-300% deeper when compared to other local boreholes and a localized buried bedrock valley has been identified (Steelman, unpublished data).

As a whole, the drumlinized till plain is characterized by layers of diamict of varying thicknesses and origins, interbedded with relatively thin coarse-grained layers of sand or gravel. McGill (2012) identifies the diamict layers in the subsurface of the drumlinized till plain as subglacial traction till, melt-out till, or sediment gravity flows. These diamict have likely been deposited during a number of glacial events, and are therefore variable in texture. It is likely that the observed basal till corresponds to the Catfish creek Till, and that the surficial and upper tills likely correspond to Port Stanley Till (McGill, 2012). Boreholes from geotechnical reports and the MOE waterwell database in the area support this trend of laterally extensive diamict units with localized stratified sediments. These stratified sediments occur on a relatively small scale in terms of lateral (tens of meters) and vertical (<10 meters) extent and are scattered throughout the drumlinized till plain.

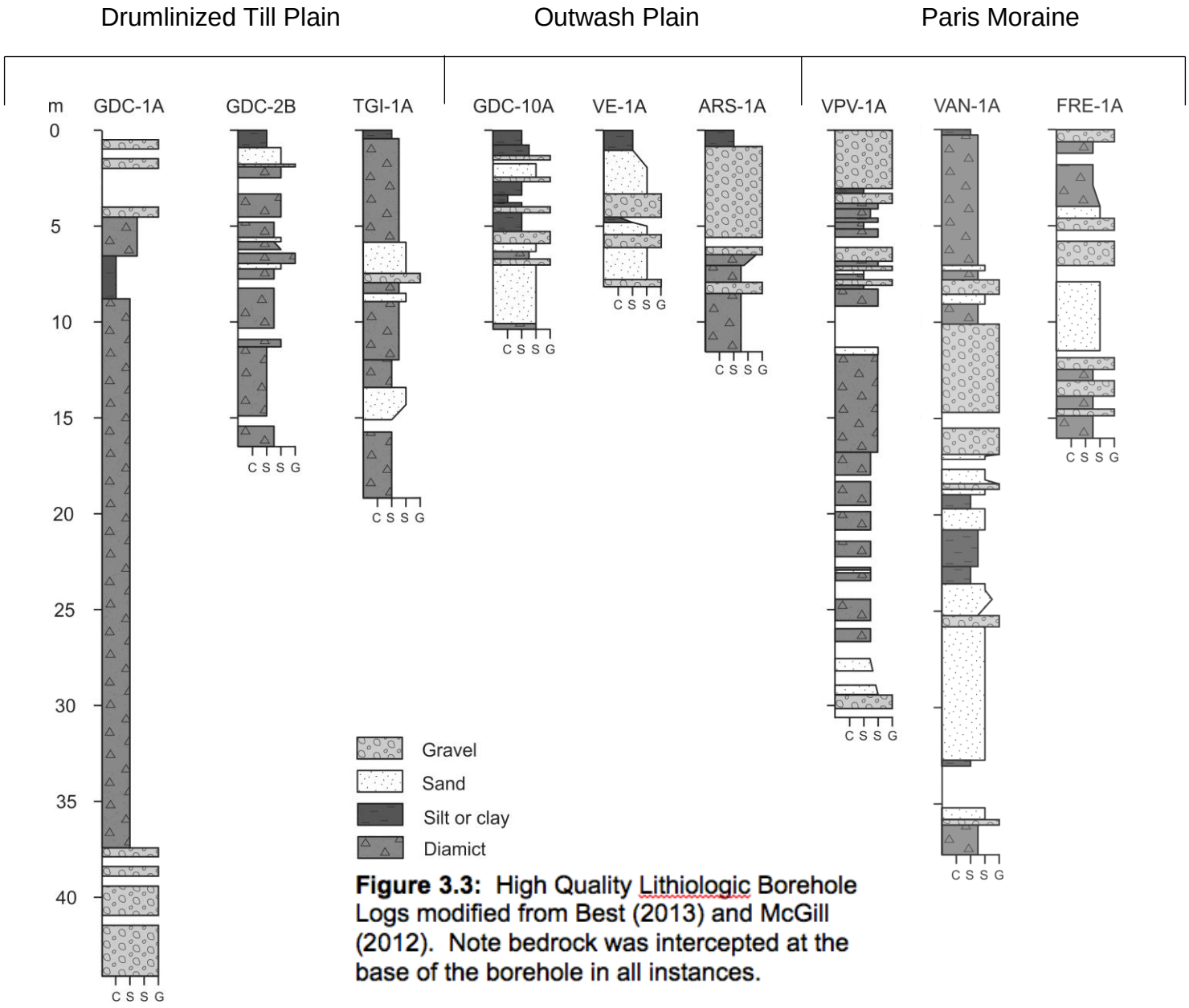

Figure 3.3: High Quality Lithiologic Borehole Logs modified from Best (2013) and McGill (2012). Note bedrock was intercepted at the base of the borehole in all instances.

3.4.1.2 Outwash Plain

High quality borehole data in the outwash plain is comprised of the GDC-10A, VE-1A and ARS-1A boreholes (Figure 3.3). GDC-10A is characterized by a thin diamict layer from 10.5-10m, a thick sand layer from 10 – 7m and alternating layers of fine sediments (silt/clay and diamict) with thin-layered coarse sediments (sands and gravels) from 7 - 0m. VE-1A is characterized by relatively thick sand layers interbedded with relatively thin gravel and silt layers from 9 – 1.5m. A relatively thick soil profile is found from 1.5 – 0m. ARS-1A is characterized by a lower section composed of diamict units defined by variable texture, and interbedded with thin gravel layers from 10.3 – 5.3m and an upper section dominated by a thick gravel unit (5.3 – 1.5m). A relatively thick soil profile is found from 1.5 – 0m. Two of the three holes have diamict at the bedrock-sediment interface.

Generally, the outwash plain is characterized by semi-extensive stratified sediments, likely caused by a braided river system cutting into underlying diamict. High and low quality boreholes in the outwash plain suggest that while stratified sediments dominate, there is still significant diamict present on the scale of hundreds of meters laterally, and meters to tens of meters vertically..

3.4.1.3 Paris Moraine

High quality borehole data in the Paris Moraine is comprised of the VPV-1A, VAN-1A, and FRE-1A boreholes (Figure 3.3). VPV-1A and VAN-1A are both

located on the moraine itself, whereas, FRE-1A is located on the back slope of the moraine. VPV-1A is characterized by gravel (30.5 – 29.5m), and sand (29.5 – 26.5m) at the base and overlain by two thick diamict layers defined by variable texture (26.5 – 8m). The uppermost 8m are dominated by a thick gravel unit with thin various thin interbedded diamict layers from 8 – 3m. VAN-1A is highly heterogeneous with a basal diamict from 37.5 – 36m, a thick sand unit (36 – 26m) a middle unit composed mostly of fine grained mud, a thick gravel unit (17 – 10.1m) and lastly a thick, relatively uniform diamict layer (10.1 – 0.2m), with minor gravel and sand layers from 7 – 9m. A relatively thin soil profile is found from 0.2 – 0m. FRE-1A is characterized by approximately 16m of interbedded diamict and gravel layers interrupted by a thick sand unit from 12 – 7m. Two of the three holes have diamict at the bedrock-sediment interface.

The Paris Moraine is highly variable in its lithology. The variability seen between these boreholes, as well as adjacent low quality boreholes on the moraine make it difficult to characterize the moraine as a whole. The hummocky terrain and the variable subsurface sediments suggest formation of topographic lows due to differential melting of the glacial ice surface and subsequent infilling by sediments from gravity flows, ponding, and melt-water (Stalker, 1960; Karrow, 1968, McGill, 2012). Thus, infilling of the resulting topographic lows by different processes is likely responsible for the lithological variability seen in VAN-1A, FRE-1A, and the top of VPV-1A. The lower potion of VPV-1A and local low quality boreholes suggest that thick and variable diamict units are present in the

Paris Moraine, similar to other physiographic regions. Upper and surficial diamict units likely correspond to the Wentworth till (Karrow, 1968). Although FRE-1A displays high variability in its layering, much like VAN-1A, the processes responsible for that variability likely also include back slope failure and mass flow associated with the retreat of the ice front.

3.4.2 Lithologic Cross Section

As discussed in the methods section, GDC-10A, TGI-1A, VE-1A, ARS-1A, VPV-1A, and FRE-1A comprise the backbone of the lithologic cross section (Figure 3.4), and the remainder of high and low quality boreholes were used to inform the scale of heterogeneity in the area. Due to the highly heterogeneous nature of sediments, spatial distribution of boreholes away from the transect leads to significant variability in lithology. Therefore, the power of this cross section is not as a site-specific characterization, but in establishing trends in lithology and scale of heterogeneity within the area.

The subsurface of the study area is characterized predominantly by diamict units with some stratified sediments, and a high degree of localized heterogeneity. This heterogeneity is expressed by relatively larger and more coarse-grained outwash channel infills in the outwash plain, more extensive coarse to fine grained diamict units in the drumlinized till plain, and smaller coarse- and fine-grained icemelt depression infills in the Paris Moraine. The material in the stratified sediment lenses ranges from gravels to clays. This

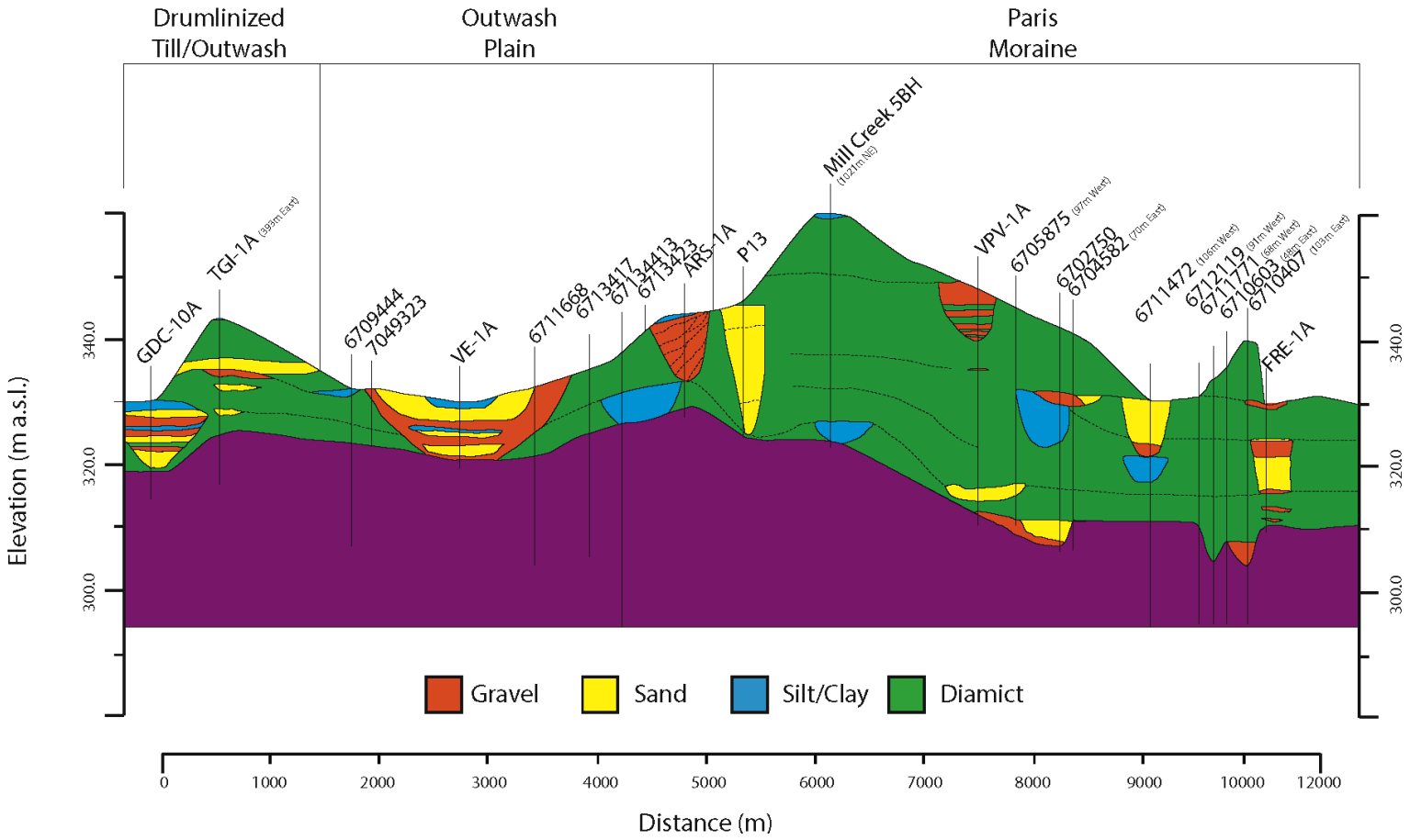

Figure 3.4: Lithological cross section of study area. Vertical exaggeration is 6x.

localized heterogeneity is on the scale of tens to hundreds of meters. Multiple diamict layers, defined by changes in texture, are present within both high and low quality boreholes. The regional till stratigraphy identified by Karrow (1968, 1987) and others is difficult to confirm in these boreholes because of their inherent spatial variability across the region. Radiocarbon dating would be the only reliable way to differentiate between these diamict layers. The literature suggests that the basal diamict layer is likely the Catfish Creek till, whereas, the surficial layer is likely the Wentworth till in the SE portion (Karrow, 1987; McGill, 2012) and the Port Stanley Till in the NW portion of the study area. The middle diamict layers have likely been extensively reworked by glacial and non-glacial processes and therefore are difficult to define in terms of regional stratigraphy.

3.4.3 Hydrostratigraphy

The following discussion of hydrostratigraphy is based on individual high quality borehole data; grouped by the local geomorphic elements. As outlined in the methods section (3.3.4.1), the following notation is used for K_{sat} values of hydrostratigraphy:

K_{Gm} = Geometric Mean K_{sat} for measured values

K_{Gc} = Geometric Mean K_{sat} for calculated values

K_{Ga} = Geometric Mean K_{sat} for all values (both measured and calculated)

Only K_{Ga} values are discussed in the following text as this incorporates all available data (some layers contained only a measured values or a calculated

value, while others contained both). Appendix D contains $K_{Gm,}$ $K_{Gc,}$ and K_{Ga} values.

As discussed in the methods section, hydrostratigraphic units were delineated based on grouping values within an order or magnitude range.

3.4.3.1 Drumlinized Till Plain

The drumlinized till plain is comprised of the GDC-2B, GDC-1A, and TGI-1A boreholes. Figure 3.5 shows the lithology, grain-size data, K_{sat} values and inferred hydrostratigraphy for each hole. GDC-2B is dominated by K_{sat} values in the range of $1x10^{-7}$ – $1x10^{-6}$ m/s. As such, the entire borehole is treated as a single hydrostratigraphic unit with a K_{Ga} value of $3.23x10^{-7}$ m/s. The lithology shows little variation within the borehole, therefore, little variation was expected in K_{sat} (assuming lithology and K_{sat} are correlated). The small degree of variation in K_{sat}values does not reflect the changes in lithology, but rather reflects changes in grain-size distribution (the relative amount of silt) and sorting. For example, the samples at 1.32m and 2.18m show that differing lithologies (sand and diamict) have similar K_{sat} values when similar grain-size distributions are present. Conversely, a uniformly classified lithology may contain heterogeneity in its grain-size distributions (and resulting sorting characteristics) as seen at 4.01m and 4.52m, which is reflected in K_{sat}. The samples at 4.01m and 4.52m also illustrate the impact of sorting (uniformity) on K_{sat} as the sample at 4.52m has a higher conductivity than the sample at 4.01m, despite having a higher relative amount of silt. This is due to the effect on sample sorting (uniformity) which impacts the

porosity of a sample. As detailed in Sections 2.2.2 and 2.4.2.1, sorting (uniformity) greatly affects porosity (more uniform samples have higher porosities) which directly impacts K_{sat}, this sorting (uniformity) effect can outweigh the influence of grain-size alone. The relationship of K_{sat} variability with changes in grain-size distribution and sorting is expected due to the use of falling head permeameter tests and empirical grain-size methods to calculate K_{sat}, which are both sensitive to these two parameters.

GDC-1A is characterized by K_{sat}values in the range of $1x10^{-8}$ – $1x10^{-6}$ m/s, with most of the measured values being within one order of magnitude. Therefore, the entire borehole is treated as a single hydrostratigraphic unit with a K_{Ga} value of $8.36x10^{-8}$ m/s. There is a relative lack of variability in the lithology, as much of the borehole consists of an extensive diamict unit (with a surficial sand unit and silt/clay unit from 6.5-8.5m). Similar to GDC-2B, the variation in K_{sat} reflects changes in grain-size distribution and sorting within the lithologic units. An example is in the extensive diamict unit from 22.5-37m; which shows K_{sat} variation consistent with the relative amount of clay (higher clay content corresponding to lower K_{sat} values). The effects of sorting (uniformity) is seen in the K_{sat} value of the silt/clay unit at 7.54m, which is similar in conductivity to surrounding diamict units despite its lower average grain-size. Similar to the example seen in GDC-2B, this is due to the effect of uniformity on porosity and its resulting influence on K_{sat}. Whereas there are different lithologies in GDC-1A, the grain size distribution of the matrix of the diamict and gravel are very similar, whereas the silt/clay unit is similarly dominated by silt.

TGI-1A is dominated by values within the $1x10^{-7}$ - $1x10^{-6}$ m/s range. There is insufficient evidence to suggest that the higher K_{sat} value at 13.66m is extensive, as heterogeneity in the outwash plain is likely on the scale of 10's of meters (Section 3.4.1.1), and high and low quality data do not suggest great lateral extent. Additionally, it must be considered that this is an empirically calculated K_{sat} value, which inherently carries a lack of accuracy with values deviating by up to 1.5 orders of magnitude from measured values (Section 2.4.1). As a result, the entire borehole is treated as a single hydrostratigraphic unit with a K_{Ga} value of $4.15x10^{-7}$ m/s. TGI-1A contains a higher degree of lithologic variability than GDC-2B and GDC-1A with the presence of distinct sand units. As with GDC-2B and GDC-1A, the K_{sat} values in TGI-1A are representative of variability in grain-size distribution and sorting, but also of changes in lithology. Higher values are found within sand units (5.5-7.5m and 13-15m), with fairly consistent values throughout the diamict units.

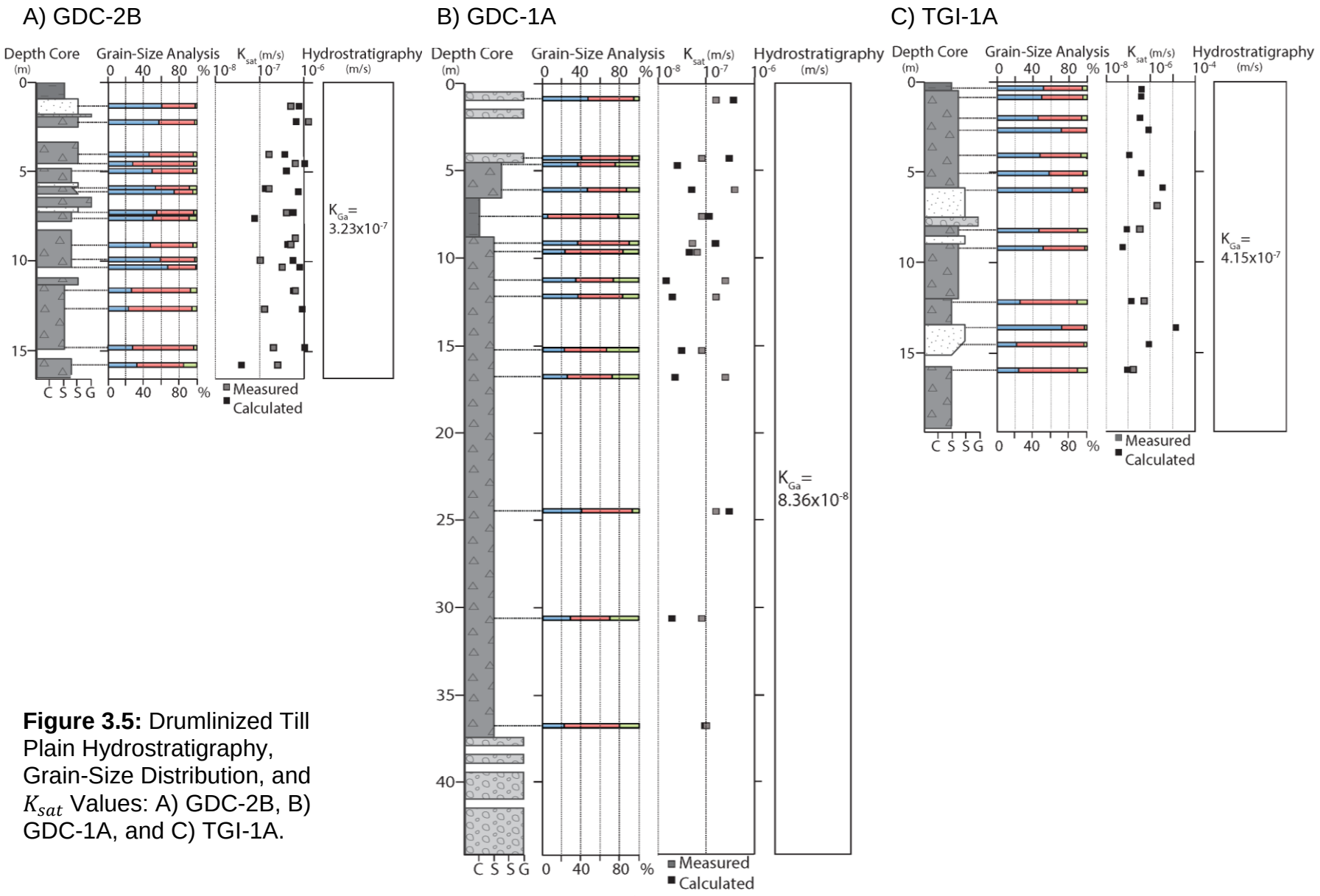

Figure 3.5: Drumlinized Till Plain Hydrostratigraphy, Grain-Size Distribution, and K_{sat} Values: A) GDC-2B, B) GDC-1A, and C) TGI-1A.

3.4.3.2 Outwash Plain

High quality borehole data in the outwash plain is comprised of the GDC-10A, VE-1A, and ARS-1A boreholes. Figure 3.6 shows the lithology and corresponding hydrostratigraphy and K_{sat} values for each hole. GDC-10A is characterized predominantly by K_{sat} values in the range of $1x10^{-7}$ – $1x10^{-6}$ m/s with a distinct higher conductivity value in the uppermost sand unit. Therefore, the borehole is classified as having two hydrostratigraphic units; with a K_{Ga} value of $2.19x10^{-5}$ m/s for the uppermost sand unit (~2.0 – 2.2m), and K_{Ga}= $4.54x10^{-7}$ m/s for the remainder of the borehole. GDC-10A exhibits relatively high variation in lithology which is loosely reflected in K_{sat} values. As with previous boreholes, the K_{sat} values reflect changes in grain-size distribution and sorting, but also the changes in lithology to a lesser degree. The K_{sat} values in the uppermost sand layer and underlying silt/clay layers (2.5 – 4.0m) correlate well with the variability in lithology; with sand and larger grained silt/clay (higher d_{10}) layers having higher K_{sat} values than finer grained silts/clays (lower d_{10}). Below 4m, there is little K_{sat} correlation to the type of lithology as gravel, sand, and silt/clay units all yield similar conductivity values. This is due to the sorting (uniformity effect) discussed throughout Section 3.4.3.1; where more uniform samples (despite having a smaller grain-size) have relatively high K_{sat} values due to the effect of sorting (uniformity) on porosity. For example, the sediment at 4.69m is much finer than the sediment 5.63m however, the high uniformity of the sample (4.69m) results in a higher porosity and thus a higher K_{sat} value; similar to the K_{sat} value of the much coarser (but less uniform) sample at 5.63m. However, these

variations are within an order of magnitude and therefore are not delineated as separate hydrostratigraphic units.

VE-1A is characterized by values in the $1x10^{-7}$ – $1x10^{-6}$ m/s range in the upper 6.45m and $1x10^{-6}$ – $1x10^{-4}$ m/s range below 6.45m, with most of the measured K_{sat} values in the bottom part ranging between 10^{-6} to 10^{-5}m/s. Thus, the borehole is separated into two main hydrostratigraphic units with K_{Ga} values of $2.88x10^{-7}$m/s, in the upper 6.45m, and $1.11x10^{-5}$m/s below 6.45m. In this core, variability in K_{sat} is clearly associated with changes in grain-size distributions and sorting, which is captured by the difference in K_{sat} values seen in the upper sand unit (more fines, and thus lower K_{sat}values) and lowermost sand unit (more sand, and thus higher K_{sat} values).

ARS-1A is characterized by K_{sat} values in the $5x10^{-7}$ – $5x10^{-6}$ m/s range. There are higher K_{sat} values at 1.03m (~1 order of magnitude) and 7.48m (~2 orders of magnitude), which are not delineated as individual hydrostratigraphic units. Based on the lithology, seen in high and low quality borehole data (Figure 3.3), these are likely small-scale local heterogeneities (as there is no evidence of significant lateral extent) from localized high energy flows that resulted in higher sand content. Therefore, these localized high conductivity zones likely present minimal impact on hydrostratigraphic implications. As such, the entire borehole is classified as a single hydrostratigraphic unit with a K_{Ga} value of 1.11×10^{-6}. There is no obvious correlation between lithology and K_{sat} values considering, as with other boreholes, the diamict and gravel have relatively similar matrix texture and hence similar K_{sat} values.

Figure 3.6: Outwash Plain Hydrostratigraphy, Grain-size Distribution and K_{sat} Values: A) GDC-10A, B) VE-1A, and C) ARS-1A.

A) GDC-10A

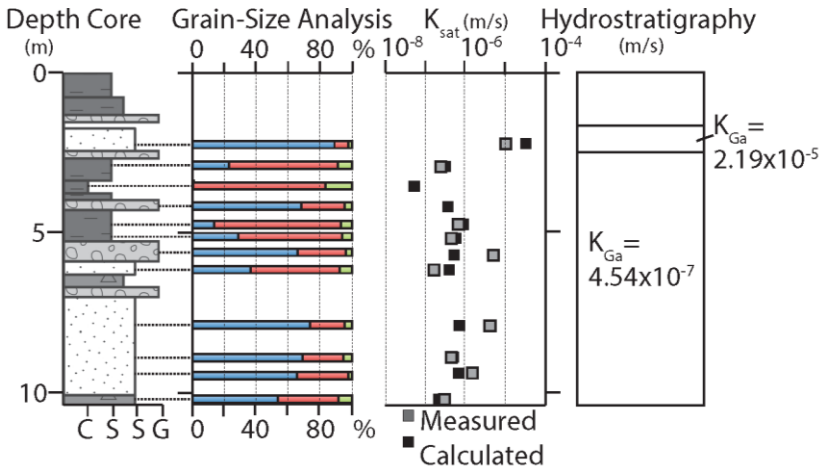

B) VE-1A

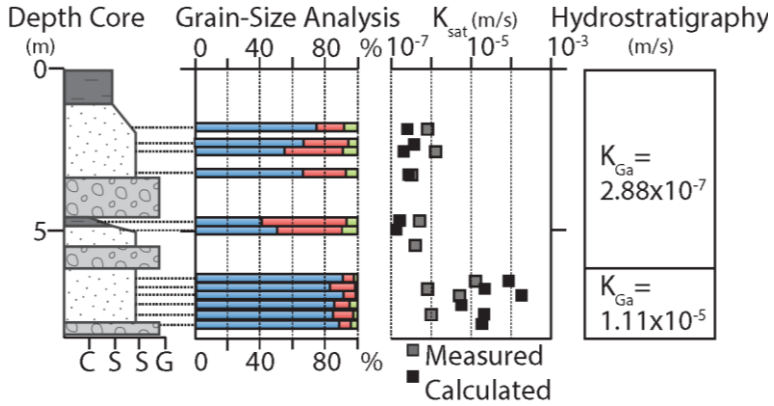

C) ARS-1A

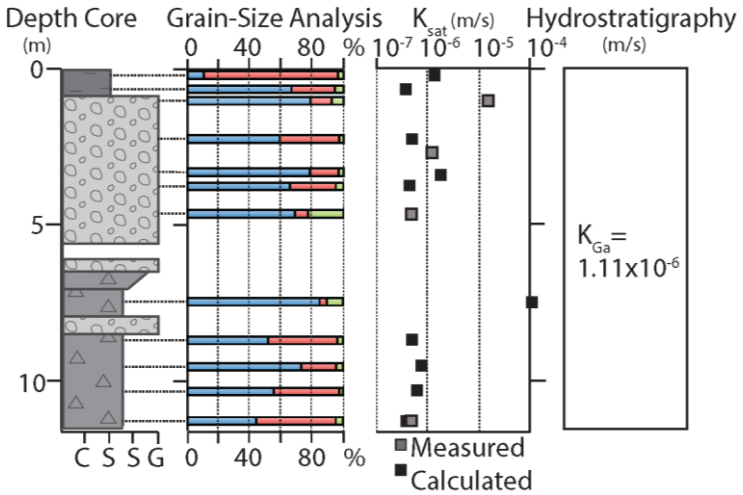

3.4.3.3 Paris Moraine

High quality borehole data in the Paris Moraine is comprised of the VPV-1A, VAN-1A, and FRE-1A boreholes. Figure 3.7 shows the lithology and corresponding hydrostratigraphy and K_{sat} values for each hole. VPV-1A is characterized primarily by K_{sat} values in the $1x10^{-7}$ – $1x10^{-6}$ m/s range. There is a single high K_{sat} sand unit ($1.21x10^{-3}$ m/s) at 11.63m that is not delineated separately as it is likely part of a washed out interval of the borehole. Additionally, due to the highly variable lithology of the Paris Moraine, this value would be a thin discontinuous layer, and would not have significant hydrogeological impact at a regional scale. Therefore, the entire borehole is classified as a single hydrostratigraphic unit with a K_{Ga} value of $1.25x10^{-7}$ m/s. Changes in K_{sat} do not correlate well with changes in lithology as values are fairly similar regardless of lithology (the one exception being the high sand value at 11.63m, which would be expected to be higher than diamict values). As with previous boreholes, the K_{sat} values follow the grain-size distributions and sorting which are often similar across gravel, sand, and diamict lithologies, resulting in the relatively consistent K_{sat} values throughout the borehole.

VAN-1A is characterized predominantly by K_{sat} values in the $1x10^{-8}$ – $1x10^{-5}$ m/s order of magnitude range. Although it is consistent with other boreholes having K_{Ga} values in the $1x10^{-8}$ – $1x10^{-6}$ m/s range, it displays much greater variability compared to other boreholes, with values varying over 5 orders of magnitude. There are higher conductivity values ($1x10^{-3}$ to $1x10^{-4}$ m/s range) at 24.16m and 30.86m. The value at 24.16m is not included separately in

delineation of hydrostratigraphic units as, based on lithological geometries (Figure 3.4), it is likely thin small-scale and discontinuous in nature. The value at 30.86m is delineated as a higher K_{sat} unit as it differs by >1.5 orders of magnitude from adjacent measured values indicating that is it significantly different from surrounding values (Section 3.3.4.1). There are also low K_{sat} values present at 10.20, 12.18, 17.33, 19.35, 23.35, 29.25, 36.10, and 36.96m which all fall in the range of $1x10^{-8}$ – $1x10^{-7}$ m/s. The lows at 12.18,17.33, 19.35, 23.35, 36.10, and 36.96m are all empirically calculated K_{sat} values, which as fully detailed in Section 2.4.1, can deviate by up to ~1.5 orders of magnitude from measured values. This places them within an order of magnitude of nearby values and therefore, they are not delineated as separate hydrostratigraphic units. Additionally, even without accounting for this 1.5 order of magnitude deviation, the values at 10.20, 12.18, 19.35, 23.35, 36.10 and 36.96m already fall within an order of magnitude of adjacent values, and hence are not delineated as separate hydrostratigraphic units as set out in the methods section (3.3.4.1). Therefore, the borehole is separated into 3 hydrostratigraphic units with K_{Ga} values of: $7.47x10^{-7}$ m/s (upper 30m), $8.48x10^{-4}$ m/s (30 – 32.8m), and $3.03x10^{-7}$ m/s (below 32.8m). Variation in K_{sat} values are reflected by heterogeneity seen in grain-size distributions and sorting. These K_{sat} variations are not always reflected by changes in lithology as many lithologies (diamict, silt/clay, sand, and gravel) are poorly sorted and thus have similar grain-size distributions. Rather they are often seen within individual units that exhibit grain-size variability

vertically (ie. diamict unit from 0.25 – 7.0m; gravel unit from 10.1m – 17.0m; sand unit from 25.6 – 32.5m), and therefore contain a range of K_{sat} values.

FRE-1A is characterized by K_{sat} values in the 1x10^{-7} – 1x10^{-6} m/s order of magnitude range with intervals of higher conductivity (1-2.5 orders of magnitude) layers below 7m. These higher K_{sat} layers are consistent with the lithology (ie. sands and gravels generally display higher conductivities than the diamict layers), and are delineated as separate units as they differ from adjacent values by more than an order of magnitude (Section 3.3.4.1). Therefore, the borehole is separated into 5 hydrostratigraphic units with the following K_{Ga} values: 2.8x10^{-7} m/s (0-7m), 8.19x10^{-6} m/s (7-11.55m), 3.64x10^{-7} m/s (11.55-13.13m), 4.32x10^{-5} m/s (13.13-13.75m), and 4.33x10^{-7} m/s (below 13.75m).

3.4.3.4 K_{sat} Variability within Geomorphic Elements

The drumlinized till plain contains a relatively low degree of K_{sat} variability with values ranging from 8.36x10^{-8} – 4.15x10^{-7} m/s. On an individual hole basis, all three boreholes (GDC-2B, GDC-1A, and TGI-1A) are delineated as single hydrostratigraphic units. This is expected based on the relative lack of lithologic variability as much of the high and low quality borehole data consists of extensive diamict units, with some smaller scale stratified sediments. It is interesting to note that despite some variability between diamict units (some having more silt or being more overconsolidated than adjacent diamict units; McGill, 2012), they appear to have fairly consistent hydraulic properties. This may be due to the loss of structure and consolidation effects, due to the use of disturbed samples.

The outwash plain contains a slightly higher degree of K_{sat} variability, with values ranging from 2.88x10^{-7} – 2.19x10^{-5} m/s, when compared to the drumlinized till plain. On an individual hole basis, only ARS-1A is delineated as a single hydrostratigraphic units, while GDC-10A and VE-1A, consists of three and two units respectively. This increase in K_{sat} heterogeneity is expected as these holes contain a much higher degree of lithological variability, with a range of thinner stratified sediments dominating rather than extensive diamict layers. However, as discussed in Sections 3.4.3.1 – 3.4.3.3, there is not as much K_{sat} variability as might be expected with the amount of lithologic variability that is present. This is caused by the relatively similar grain-size distributions and sorting that are found in differing lithologies.

The Paris moraine contains the highest degree of K_{sat} variability with values ranging from 1.25x10^{-7} – 8.48x10^{-4} m/s. On an individual hole basis, only VPV-1A is delineated as a single hydrostratigraphic units, while the other two boreholes consist of three and five units. The lack of heterogeneity in VPV-1A is expected due to its similarity to sediments found in the drumlinized till plain (mostly composed of extensive diamict units). The higher degree of heterogeneity seen in VAN-1A and FRE-1A is expected due to the increased presence of stratified sediment bedding (often in thinner units). As in the outwash plain, there is not as much K_{sat} variability in VAN-1A as might be expected based on lithology and this is likely due to the similar grain-size/sorting charactaristics of those different lithologies. In contrast, there is much clearer relationship between lithology and K_{sat} values in FRE-1A on the backslope of the

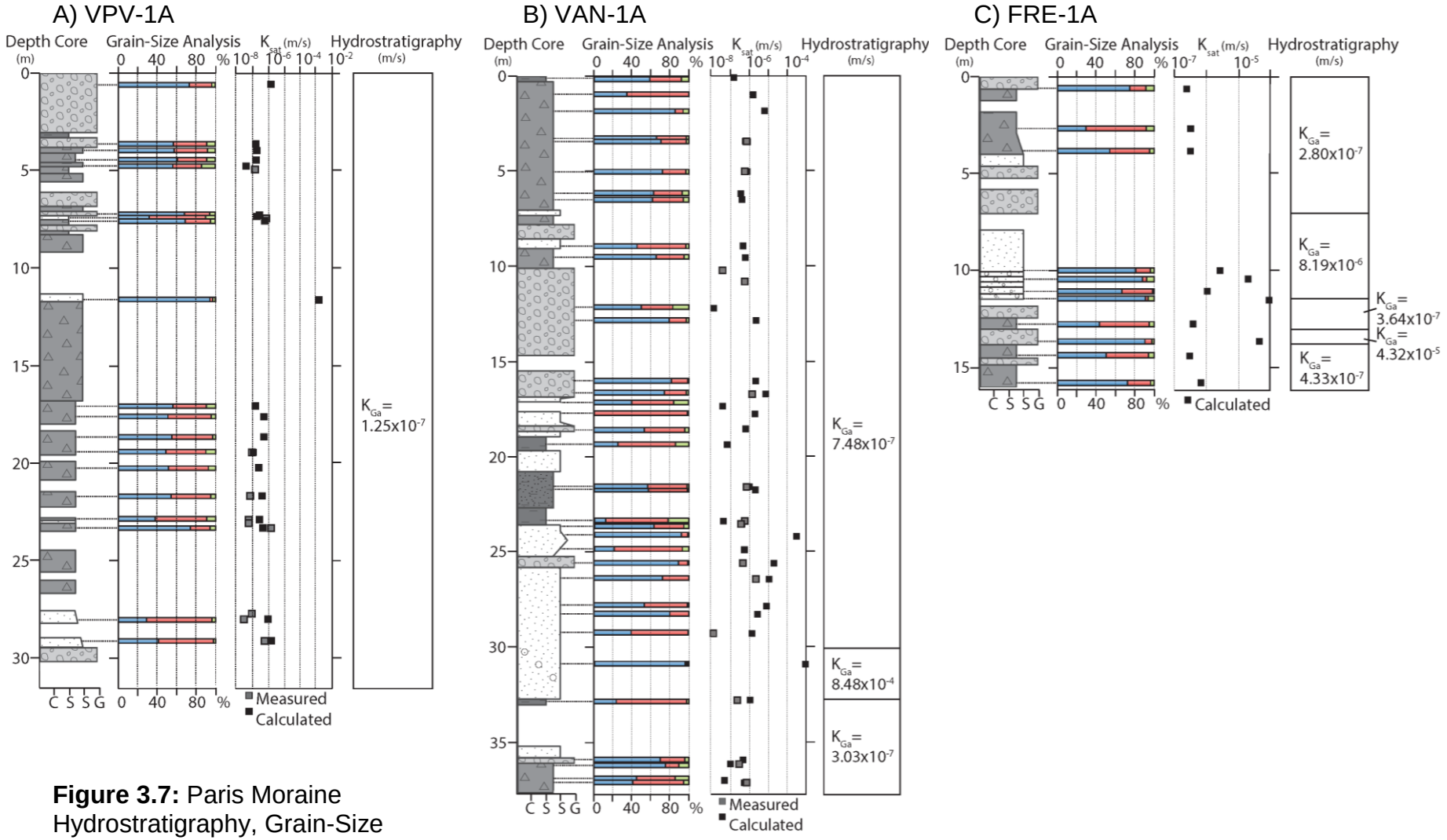

Figure 3.7: Paris Moraine Hydrostratigraphy, Grain-Size Distributions and K_{sat} Values: A) VPV-1A, B) VAN-1A, and C) FRE-1A.

moraine, where gravel units are sandier than diamict units, and sand units have much lower mud content.

3.4.4 Correlation to Lithology

Figures 3.5 – 3.7 reveal that hydrostratigraphy can deviate from variation observed in the lithology, supporting the findings of Maxey (1964) who stated that hydrostratigraphic boundaries often run across lithologic boundaries. K_{sat} values are found to reflect variation in grain-size distributions and sorting which sometimes, but not always, coincide with changes in lithology. This study found K_{sat} values of many unique adjacent lithologic units to have similar K_{sat} values (+/- an order of magnitude), due to the similarity of grain-size distributions and sorting across these differing lithologic units. This study has also found K_{sat} values of similar lithologic units can contain variation, which is reflected in the grain-size distributions and sorting from which the K_{sat} values were calculated. Additionally, there is often significant variation in K_{sat} values within individual lithologic units in correlation with changes in grain-size distribution and sorting.

Variation in K_{sat} values is not always sufficient evidence for delineation of separate hydrostratigraphic units. The lithologic cross section indicates, many of these variations (in grain-size distribution and resulting K_{sat}) are likely thin, discontinuous, small-scale heterogeneities with negligible implication on hydrostratigraphic considerations (K_{sat} variation within an order of magnitude, which is not delineated as a separate hydrostratigraphic unit). It is therefore

advisable to ensure use of appropriate measurement and calculation methods when investigating hydraulic properties of a highly reworked glacial area.

Values measured and calculated in this study vary significantly with those found in the literature (Figure 3.1). Table 3.2 outlines observed K_{Gm}, K_{Gc}, and K_{Ga} values for the range of sediments encountered in this study. These were calculated by: 1) classifying each unit by textural class (ie. gravel, sand, silt/clay, diamict, etc); and 2) taking the K_{sat} values from each unit, in each class, to calculate K_{Gm}, K_{Gc}, and K_{Ga} values for each textural class. Hydrogeologists and sedimentologists are aware of the heterogeneity of K_{sat} values within textural classes. The general assumption is that larger grain-size equates to higher K_{sat} values, and that poorly sorted sediments have lower values due to voids between large grains being filled with fines. However, Table 3.2 shows that there is significant deviation from this in assumption in the study area.

Sediment	K_{Gm} **(n)**	**Max/Min** K_{Gm}	K_{Gc} **(n)**	**Max/Min** K_{Gc}	K_{Ga} **(n)**
Gravel	6.76×10^{-7} (10)	1.75×10^{-5} 3.80×10^{-8}	7.09×10^{-7} (21)	4.32×10^{-5} 1.22×10^{-8}	6.98×10^{-7} (31)
Gravelly Sand	1.46×10^{-6} (11)	1.18×10^{-5} 1.39×10^{-7}	6.98×10^{-6} (16)	8.45×10^{-4} 3.16×10^{-7}	3.69×10^{-6} (27)
Sand	4.61×10^{-7} (7)	2.27×10^{-6} 1.39×10^{-8}	1.64×10^{-6} (17)	2.88×10^{-4} 3.57×10^{-8}	1.13×10^{-6} (24)
Silty Sand	4.13×10^{-7} (3)	1.19×10^{-6} 7.05×10^{-8}	2.19×10^{-7} (5)	3.47×10^{-7} 1.26×10^{-7}	2.77×10^{-7} (8)
Compact Sand	5.68×10^{-8} (2)	9.48×10^{-8} 3.41×10^{-8}	8.22×10^{-7} (1)	8.22×10^{-7} 8.22×10^{-7}	1.54×10^{-7} (3)
Sandy Silt	3.74×10^{-7} (3)	6.55×10^{-7} 1.93×10^{-7}	4.6×10^{-7} (3)	8.07×10^{-7} 2.49×10^{-7}	4.15×10^{-7} (6)
Silt/Clay	3.13×10^{-7} (5)	8.21×10^{-7} 4.62×10^{-8}	2.54×10^{-7} (12)	1.90×10^{-6} 3.29×10^{-8}	1.51×10^{-7} (17)
Diamict	2.23×10^{-7} (39)	1.65×10^{-6} 6.82×10^{-8}	2.85×10^{-7} (69)	1.21×10^{-3} 1.36×10^{-8}	2.61×10^{-7} (108)

Table 3.2: Average hydraulic conductivity (m/s) for sediments from measured, calculated, and all values.

This highlights the necessity of having site-specific information regarding hydraulic parameters. Measurement and calculation of hydraulic parameters is necessary with a high resolution in order to accurately classify hydrostratigraphy.

3.4.5 Measured vs Calculated Values

Both measured and calculated K_{sat} were used in delineation of hydrostratigraphy. In Figures 3.5 - 3.7 it is clear that the calculated and measured values can be similar, but can also differ by >1 order of magnitude. In the case of this study, the values have already been calibrated (Section 2.0) to match measured values as closely as possible ensuring maximum accuracy of values. However, it should be noted that this study did not find the precision of the Kozeny-Carman (Vukovic and Soro, 1992) to be high. As such, the calculated K_{sat} value can range over 1.5 orders of magnitude for a given measured value (Chapter 2.0). It also tends to underestimate measured K_{sat} values higher than $1x10^{-6}$m/s (Figure 2.7). However, it is the most widely used in the literature, has been found to produce the most accurate values compared to other empirical grain-size methods (Kasenow, 2002; Vukovic and Soro, 1993; Carrier, 2003) and is relatively accurate for a wide range of materials (Chapuis and Aubertin, 2003).

When using calculated K_{sat} values this low precision must be understood as a potential source of error and accounted for where possible and necessary.

The low precision is accounted for when delineating hydrostratigraphy by: grouping together values within ~1 order of magnitude (Section 3.3.4.1) and by considering delineation of values on an individual basis in the context of adjacent values and other available data (i.e. grain size distribution, sorting) that can explain the difference between the measured and calculated values; Section 3.4.3).

As such, the observed differences in K_{sat} (differences >1 order of magnitude) are significant and may be attributed to variation in grain-size distribution and sorting characteristics, which are reflected by delineation of distinct hydrostratigraphic units. While differences between measured and calculated K_{sat} values have been accounted for, it is advisable that future studies focus on measured data, which eliminates the potential error in adjusting for these differences.

3.4.6 Effect of Uniformity and Porosity on Calculated K_{sat}

Hydrogeologists and sedimentologists have the common understanding that larger grains tend to have larger pores, resulting in higher conductivity values. This often holds true in the Guelph/Paris Moraine data. However, it must be pointed out that there are data points that do not follow this trend. It is also understood that the more poorly sorted a sample is, the more voids (between large grains) are filled by small grains, thus decreasing conductivity. Analysis reveals that this disconnect between average grain-size of a sample and K_{sat} value is due to the inherent bias built into the empirical grain-size methods,

including the Kozeny-Carman (Vukovic and Soro, 1992) method, with respect to the sorting (uniformity) of the sample. The Kozeny-Carman (Vukovic and Soro, 1992) method puts great significance on the calculated porosity of a sample, as estimated from C_u (uniformity index) (this is outlined in detail in the Empirical Grain-Size Methods Section, Chapter 2). As such, a well-sorted (highly uniform) sample that is primarily a silt/clay may yield higher calculated K_{sat} values than a more poorly sorted (heterogeneous) sand. The effects of the sorting (uniformity index), and resulting porosity values are therefore overrepresented when compared to effects of grain-size on the calculated K_{sat} value.

3.4.7 Hydrostratigraphic Cross Section

Figure 3.8 presents the hydrostratigraphic cross-section crossing the three geomorphic elements in the Guelph area going from the drumlinized till plain in the NW through the outwash plain and the Paris Moraine in the SE. (Figure 3.2). Figure 3.8 displays the hydrostratigraphic logs from Section 3.4.3, a K_{Ga} value for each geomorphic element (See Appendix D for $K_{Gm}$and K_{Gc}), and aquifer and aquitard units for the study area. The K_{Ga} of the geomorphic element is considered the “background” conductivity, providing a reasonable estimation throughout the geomorphic element, whereas the borehole specific hydrostratigraphic units are included as an indication of the degree and presence of localized small-scale variability.

The drumlinized till plain has a background K_{Ga} value of 2.72x10^{-7} m/s (includes GDC-1A and GDC-2B which are not shown on the cross-section).

There is a single aquifer unit seen in GDC-10A (K_{Ga} = 2.19x10^{-5} m/s) which is likely present on the scale of hundreds meters based on the lithologic geometry of Figure 3.4. It exhibits low variability in K_{Ga} between boreholes as they all fall within the range of 8.36x10^{-8} - 6.47x10^{-7} m/s. These likely correspond to the Port Stanley till or older (McGill, 2012).

The outwash plain has a background K_{Ga} value of 1.40x10^{-6} m/s, which is ~1 order of magnitude higher than that of the drumlinized till plain. It contains two aquifer units; one at the base of VE-1A (K_{Ga} = 1.11x10^{-5} m/s) and the second through the entire depth of ARS-1A (K_{Ga} = 1.11x10^{-6} m/s). Based on the lithology of Figure 3.4, the aquifer unit in VE-1A is likely present on the scale of hundreds of meters. This higher conductivity zone likely corresponds to older stratified sediments that have cut into the underlying Catfishcreek Till, which is the oldest regionally extensive till in the area (Karrow, 1987, McGill, 2012). The scale of the ARS-1A aquifer unit is difficult to estimate as the aquifer unit itself does not correspond to a specific lithology in the borehole, but rather consists of multiple lithologies (Figure 3.4 and 3.6). However, it is likely that the aquifer unit is confined to the frontslope outwash fan seen in Figure 3.4. The outwash plain exhibits relatively low variability in K_{Ga} between boreholes as the majority of delineated hydrostratigraphic units fall within the range of 2.88x10^{-7} – 1.11x10^{-6} m/s.

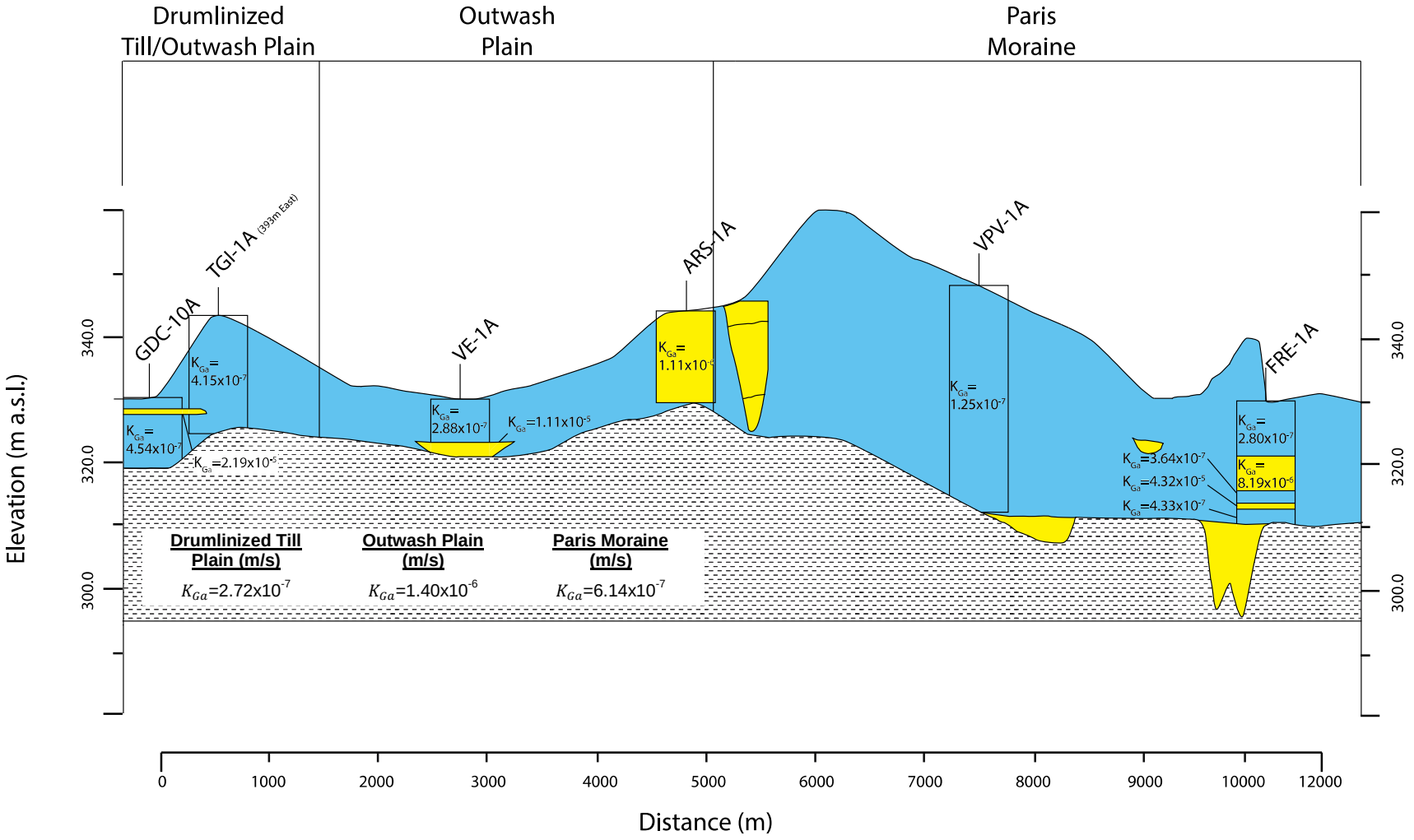

Figure 3.8: Hydrostratigrahpic Cross Section. Vertical Exaggeration is 6x

The Paris Moraine has a background K_{Ga} value of 6.14x10^{-7} m/s, which is >1 order of magnitude higher than that of the outwash plain. Figure 3.7 shows multiple aquifer units present in the Paris Moraine in both high and low quality borehole data. FRE-1A contains upper and lower aquifer units with K_{Ga} values of 8.19x10^{-6} and 4.32x10^{-5} m/s respectively. Based on the lithology in Figure 3.4, these are likely localized, on the tens to hundreds of meters scale. Aquifer units were also delineated in the low quality borehole data at the frontslope, backslope, and bedrock topographic lows of the Paris Moraine. The frontslope aquifer unit corresponds to the sand units in P13 (Figure 3.4), which were delineated as an aquifer unit based on the relatively uniform nature of the sediments which has been identified by this study as an important factor in the conductivity of sediments in the area (Section 3.4.6). The backslope aquifer unit corresponds to the gravel unit in MOE well 6704582 (Figure 3.4). This is delineated as an aquifer unit as it is identified as a relatively uniform gravel (lacking fine-grained components) and, like the frontslope aquifer unit, is therefore likely to have a high conductivity (Section 3.4.6). The centralized bedrock topographic low aquifer unit corresponds to gravel and sand units seen in MOE wells 6705875 and 6702750 (Figure 3.4). These were delineated as an aquifer unit due to the uniform nature of the sediments (stones, sands, and gravels) which, due to their lack of fines (uniformity), are likely to be highly conductive (Section 3.4.6). The backslope bedrock topographic low corresponds to MOE well 6710603 (Figure 3.4). This was delineated as an aquifer unit due to the loosely packed nature of its diamict sediments which would indicate a higher porosity values and hence higher

conductivity (Section 3.4.6). In general, the Paris Moraine exhibits higher variability in K_{Ga} between boreholes as delineated hydrostratigraphic units fall within the range of 8.48×10^{-4} – 1.25×10^{-7} m/s. Two of the three boreholes in the Paris Moraine contain significant hydrostratigraphic variability. The relatively uniform hydraulic conductivity in the upper portions of VAN-1A, VPV-1A and FRE-1A likely corresponds to the Wentworth Till (McGill, 2012).

Overall, there is a general trend of increasing background conductivity, occurrence of aquifer units, and hydrostratigraphic variability with proximity to the Paris Moraine. This is consistent with the increased variability of moraine formation processes within the moraine itself (depression infilling, and glaciolacustrine environments) as well as on its front and backslope (slope failure, debris flows, melt-water streams, and glaciolacustrine environments), that will in turn result in more variable unit geometries, texture and sorting. These processes are discussed in greater detail in Section 2.4.3. Sediment infilling of lows and depressions, during moraine formation, has led to the accumulation (with relatively high frequency) of uniform and loosely packed sediments resulting in the formation of the aforementioned aquifer units.

3.4.7.1 Hydrostratigraphic Overview

The hydrostratigraphic cross section presents a contextual understanding of the Guelph/Paris Moraine area with 3 main implications: 1. The area is dominated by background conductivity values of 2.72×10^{-7}, 1.40×10^{-6}, and 6.14×10^{-7} m/s, in the drumlinized till plain, outwash plain, and Paris Moraine

respectively; 2. This background conductivity framework contains small-scale semi-continuous/expansive aquifer units, on the scale of tens to hundreds of meters, which may form local flow regimes; and, 3. The heterogeneity in K_{sat} values and occurrence of aquifer units increases from the drumlinized till plain, through the outwash plain and onto the most variable in the Paris Moraine.

3.5.0 IMPLICATIONS

As part of the ORF project, this study has produced lithostratigraphic and hydrostratigraphic cross sections for use in vulnerability mapping to inform future expansion and development in the Guelph area. As such, these cross sections can be used to inform the vulnerability of the different physiographic regions. In order to fully characterize vulnerability, multiple cross sections would be required due to the spatial variability of lithology and hydraulic parameters of such a glaciated region.

Based on this work, the lowest vulnerability area is the drumlinized till/outwash plain. Its background conductivity is the lowest of the three geomorphic elements. It also contains the least variability in K_{Ga} values as 3 of 4 boreholes in this area are classified as single hydrostratigraphic units with few aquifer units. Therefore, this area would be more appropriate for higher-risk activities such as industry and high yield farming practices. It should be noted that due to the lithologic heterogeneity and presence of bedrock topographic lows (eg. GDC-1A), higher conductivity windows into the bedrock may be locally present.

The outwash plain is moderately vulnerable. While its background hydraulic conductivity is the highest of the three geomorphic elements (which is a relatively small range), it contains a lower degree of heterogeneity and fewer aquifer units when compared to the Paris Moraine. While it still may contain higher conductivity windows (aquifer units) into the bedrock due to discontinuity of lower till layering, it lacks the bedrock topographic lows seen in the drumlinized

till/outwash plain, and the Paris Moraine (which are often filled with coarse sediments forming high conductivity windows into the underlying bedrock). Therefore, lower-risk activities are appropriate for this area such as minor industry, residential housing, and low yield farming operations.

The most vulnerable area is the Paris Moraine itself, particularly its back slope. Its background conductivity is intermediate compared to the drumlinized till/outwash plain and the outwash plain. However, it contains the highest variability in hydrostratigraphy with a higher frequency of aquifer units. Higher conductivity windows (aquifer units) are likely present due to the depositional conditions during glaciation and deglaciation of the area. It should be noted that Golder (2006) suggests that there may be hydraulic connections between these discrete aquifer units, however, the complexity of the hydrostratigraphy and lithology in the Paris Moraine make it difficult to characterize these connections or lack thereof. Blackport (2009) suggests a variable degree of connectivity between these units, resulting in potential for larger scale-but still relatively localized-groundwater production zones. With variable connectivity between these units, there are likely areas of both higher and lower vulnerability within the Paris Moraine. Additionally, the low relief of this area will cause pooling of water, increasing infiltration. The spatial variability in the Paris Moraine dictates that site- specific studies are undertaken before explicit characterization of a site as high or low vulnerability. However, without such data, low risk activities should be prioritized for this area such as low-density residential housing and recreation.

While background conductivity values for the geomorphic elements provide context and regional scale values, there is significant small-scale variation in K_{sat} within these elements (Figure 3.8). This is reflected in the hydrostratigraphic variability between high quality boreholes in the Paris Moraine; contrasting the uniform nature of K_{sat} values in VPV-1A, with the relatively high variability found in FRE-1A (Figure 3.8). As such, this study provides detailed site-specific data, for the high quality boreholes, and infers the hydrostratigraphic data between high quality boreholes using low quality lithologic data. This provides a reasonable understanding of the regional context and variability, but is not reliable for site-specific applications where there is no high quality borehole data. Therefore, it is highly recommended that site-specific investigations are conducted prior to the commencement of higher-risk activities.

3.6.0 Conclusions

As the demand for ground water resources continues to grow, the management and protection of groundwater resources has become an even more significant consideration, both globally and locally. In order to better manage and understand water quantity and quality issues in the Guelph/Paris Moraine area, this study aimed to characterize the heterogeneity of hydraulic conductivity values, resulting in delineation of hydrostratigraphy in the Quaternary sediments.

Due to the glacial history of the area, the Quaternary sediments are variable in lithology, however, this is not always reflected in their hydraulic properties. Rather, variability in grain-size distributions and sorting dictate the conductivity of sediments (which does not always correlate with variation in lithologic classification). Thus, the following conclusions have been made regarding hydrostratigraphy: 1. Lithology and hydrostratigraphy do not always correlate well in such a reworked glacial setting; 2. A background framework of reasonable K_{Ga} values is applicable for use in each geomorphic element in the area; and, 3. Aquifer units exist, with increased frequency in proximity to the Paris Moraine, forming preferential flow zones through the unconsolidated sediments and into underlying bedrock.

The implications of the hydrostratigraphy dictate the following regarding vulnerability of the study area to contamination: 1. The drumlinized till/outwash plain is the least vulnerable due to its low background conductivity, and lack of variability (high conductivity layers/zones); 2. The outwash plain is more

vulnerable due to its higher background conductivity, while lacking numerous aquifer units; and, 3. The Paris Moraine itself is the most vulnerable due to its relatively similar/high background conductivity, its numerous aquifer units, and low relief/hummocky topography which causes pooling and increased infiltration.

The highly variable nature of the Quaternary sediments dictates that further high quality sampling is needed in order to more accurately characterize the hydrostratigraphy of glaciated areas. A greater resolution of boreholes is required in order to more accurately describe heterogeneities. The fact that lithology alone cannot be used to accurately estimate hydraulic parameters suggests that, while usage of lower quality data is still advisable, it remains more advantageous to have additional grain-size data as it more directly reflects hydraulic properties compared to lithology alone. Therefore, for greater application and use, high resolution grains-size analysis at regular intervals through the borehole should be included in all basic drilling activities.

4.0 CONCLUSIONS

The purpose of this thesis was to study Quaternary sediment deposits in the Guelph area for the purpose of groundwater protection and risk management. Nine high-resolution continuous cores and existing geologic and hydrogeologic data were used to: 1. Assess 19 empirical grain-size methods for their applicability to sediments in the study area; and 2. Delinate higher-resolution hydrostratigraphy with new calculated and measured K_{sat} data.

Comparative analysis of K_{sat} estimations from 19 empirical grain-size methods reveals significant variability between methods. With identical input, estimations range over 0-2 orders of magnitude. When compared to measured K_{sat} values, these empirical methods vary in their ability to reflect the effects of grain-size heterogeneity of samples. The shortcoming of these methods is their ability to quantify heterogeneity of samples with changes in input values.
The locally calibrated form of the Kozeny-Carman (Vukovic and Soro, 1992) was deemed the most appropriate for use in this study as it is the most widely uses and accepted in the liternature (Vukovic and Soro, 1992; Kasenow, 2002; Carrier, 2003), provided accuracy and precision similar to other methods, and will facilitate comparison to literature values.

Quaternary hydrostratigraphy in the Southeast Guelph area is characterized by the following observations: 1. Lithology and hydrostratigraphy sometimes correlate, rather, hydrostragigraphy is dictated by grain-size distributions and sorting charactaristics; 2. General background conductivities of 2.72×10^{-7} m/s, 1.40×10^{-6} m/s, and 6.14×10^{-7} m/s, can be assigned to the

drumlinized till/outwash plain, outwash plain, and Paris Moraine respectively; 3. Aquifer units are present, with increasing frequency in proximity to the Paris Moraine, likely forming preferential flow pathways.

Vulnerability to contamination is summarized by the following: 1. The drumlinized till/outwash plain is least vulnerable due to its low background conductivity and lack aquifer units; 2. The outwash plain is more vulnerable due to its higher background conductivity and relative lack of aquifer units; and, 3. The Paris Moraine is the most vulnerable due to its similar/high conductivity, relatively high number of aquifer units, bedrock topographic lows, and low topographic relief/hummocky topography.

The Quaternary sediments in the Guelph area are highly variable and require further high quality sampling. A greater resolution of boreholes will provide the data necessary to describe the present heterogeneity. The disparity between lithology and hydraulic properties suggests that grain-size analysis should be employed in all drilling activities at regular intervals for more accurate representation of both lithology and hydraulic properties.

5.0 REFERENCES

Alyamani and Sen, 1993. Determination of hydraulic conductivity form complete grain-size distribution curves. Ground Water, 31, 551–555.

Anderson, M.,1989. Hydrogeologic facies models to delineate large-scale spatial trends in glacial and glaciofluvial sediments. Geological Society of America Bulletin, 101, 501–511.

Anderson, M., Aiken, J., Webb, E., Mickelson, D., 1999. Sedimentology and hydrogeology of two braided stream deposits. Sedimentary Geology, 129, 187-199.

Barr, D.W. 2001. Coefficient of permeability determined by measurable parameters. Ground Water 39, no. 3: 356–361.

Best, A., 2013. Non-point source pollution in Quaternary glacial deposits, Guelph, Ontario. M.Sc. thesis, University of Guelph - School of Environmental Science. [Unpublished.]

Beyer, W. 1964. Zur Bestimmung der Wasserdurchlassigkeit von Kieson und Sanduen aus der Kornverteilung [On the determination of hydraulic conductivity of gravels and sands from grain-size distribution]. *Wasserwirtschaft Wassertechnik* 14, 165–169.

Blackport, 2009. Review of the state of knowledge for the Waterloo and Paris/Galt moraines. Blackport Hydrogeology Inc., Blackport and Associates Ltd., AquaResource Inc. Prepared for: Land and Water Policy Branch, Ministry of the Environment.

Brandes, O., and Ferguson, K., 2003. Flushing the future? Examining urban water use in Canada. Polis Project on Ecological Governance, University of Victoria. Victoria, BC. Accessible at: http://www.waterdsm.org/

Brooks, R., and Corey, A., 1964. Hydraulic properties of porous media, Hydrol. Pap. 3, Colo. State Univ., Fort Collins.

Burdine, N.T., 1953. Relative permeability calculations from pore size distribution data. Trans. AIME 198, 71-77.

Burt, A., 2011. The Orangeville moraine project: preliminary results of drilling and section work; in Summary of Field Work and Other Activities 2011, Ontario Geological Survey, Open File Report 6270, 28-1 - 28-34.

Carrier, W., 2003. Goodbye, Hazen; hello, Kozeny-Carman. Journal of geotechnical and geoenvironmental engineering, 129, 1054–1056.

Chapuis, R., and Aubertin, M., 2003. On the use of the Kozeny-Carman equation to predict the hydraulic conductivity of soils. Canadian Geotechincal Journal 40, 616-628.

Chapuis, R., Dallaire, V., Marcotte, D., Chouteau, M., Acevedo, N., and Gagnon, F., 2005. Evaluating the hydraulic conductivity at three different scales within an unconfined sand aquifer at Lachenaie, Quebec. Canadian Geotechnical Journal 42, 1212–1220.

Chapman, L., and Putnam, D., 1984. Physiography of southern Ontario; Ontario Geological Survey.

Cheng, and Chen, 2007. Evaluation of methods for determination of hydraulic properties in an aquifer-aquitard system hydrologically connected to a river. Hydrogeology Journal, 15, 669–678.

Freeze, A., and Cherry, J.,1979. Groundwater. Prentice Hall Inc., New Jersey, USA.

Golder Associates, 2006. Guelph-Puslinch groundwater protection study. Report to the Grand River Conservation Authority, City of Guelph, and Township of Puslinch.

Golder Associates and Blackport Hydrogeology Inc. 2006. Integrated urban study. Undertaken for the Regional Municipality of Waterloo.

GRCA, 2014. Geotechnical Reports Database [computer file]. Sustainable bedrock water supplies for Ontario communities. University of Guelph.

Harleman, D., Melhorn, P., and Rumer, R., 1963. Dispersion-permeability correlation in porous media. Journal of the Hydraulic Division, 89, 67–85.

Hazen, A., 1892. Some physical properties of sands and gravels. Rept. Massachusetts State Board of Health.

Hazen, A., 1911. Discussion. Dams on sand foundations. Trans. ASCE, 73.

Honisch, M., Hellmeier, C., Weiss, K., 2002. Response of surface and subsurface water quality to land use changes. Geoderma 105, 277–298.

Ishaku, J., Gadzama, E., Kaigama, U., 2011. Evaluation of empirical formulae for the determination of hydraulic conductivity based on grain-size analysis. Journal of Geology and Mining Research, 3, 105-113.

Istomina, V., 1957. Seepage Stability of the Soil. Moscow.

Karrow, P.,1968. Pleistocene geology of the Guelph area southern Ontario. Ontario Department of Mines. 38 pp.

Karrow, P.,1987. Quaternary geology of the Hamilton-Cambridge area, southern Ontario. Ontario Geological Survey Report 255.

Kasenow, M., 2002. Determination of hydraulic conductivity from grain size analysis. Denver, Colorado: Water Resources Publications.

Kozeny, J., 1953. Das wasser in boden, grundwasserbewegung. Hydraulik, 380–445.

Kroetsch, D., Wang, C., 2008. Particle Size Distribution, in: Carter, M.R., Gregorich, E.G. (Eds.), Soil sampling and methods of analysis. Taylor & Francis, Boca Raton, 713–725.

Krumbein, W., and Monk, D., 1943. Permeability as a function of the size parameters of unconsolidated sands. Transactions of the American Institute of Mining, Metallurgical and Petroleum Engineers, 151, 153–163.

Kumar C., and Mittal, S., 2010. Determination of soil hydraulic properties in a part of hindon river catchment using SOILPROP software. ISH Journal of Hydrualic Engineering, 16, 13-27.

Lotowater, 1997. Study of the hydrogeology of the Cambridge area. Report to the Regional Municipality of Waterloo.

Maxey, G., 1964. Hydrostratigraphic units. Journal of Hydrology, 2, 124-129.

McGill, M., 2012. A sedimentological and geomorphological investigation of the Paris Moraine in the Guelph area, Ontario, Canada. M.Sc. thesis, University of Guelph - School of Environmental Science. [Unpublished.]

Ministry of Infrastructure, 2012. Growth plan for the greater golden horseshoe 2006 office consolidation, January 2012. Queen's Printer for Ontario. 70 pp.

MOE, 2010. Water Well Database [computer file]. Queen's Printer, Toronto. See: http://www.ene.gov.on.ca/environment/en/resources/collection/data_downloads/index.htm#Well Records

Mualem, Y., 1976. A new model predicting the hydraulic conductivity of unsaturated porous media. Water Resour. Res., 12, 513 - 522.

Mukherjee, S., 2011. Hydrostratigraphy. YES Bulletin, 1, 10-13.

NAVFAC, 1974. *Design Manual* — Soil Mechanics, foundations and earth structures. Washington, D.C., U.S. Government Printing Office.

Ontario Geological Survey, 2003. Surficial Geology of Southern Ontario. Miscellaneous Release-Data 128-REV [computer files]. Using: ArcMap 9.3 [GIS software]. Queen's Printer for Ontario, 2003.

Opazo Gonzalez, T., 2012. Evaluation of sources and processes controlling groundwater nitrate in a silurian bedrock aquifer. M.Sc. Thesis, University of Waterloo, Ontario, Canada. [Unpublished.]

Paul, M., 1984. The supraglacial landsystem. In Eyles, N. ed. Glacial geology an introduction for engineers and earth scientists. Oxford, Pergamon Press. 409 pp.

Pravedny, G., 1966. Design and selection of grain size composition of filter beds for the transition zones of large dams. Moscow.

Provincial Deigital Elevation Model, 2007. [Map]. Ontario Minstiry of Natural Resources (MNR). Tiled Dataset, version 2.0 [computer files]. Using: ArcMap 9.3 [GIS software]. Queen's Printer for Ontario, 2007.

Rosas, J., Lopez, O., Missimer, T., Coulibaly, K., Dehwah, A., Sesler, K., Lujan, L., and Mantilla, D., 2014. Determination of hydraulic conductivity from grain-size distribution for different depositional environments. Groundwater, 52, 399-413.

Russell, H., Sharpe, D., Logan, C. and Brennand, T., 2001. Not without sedimentology: Guiding groundwater studies in the Oak Ridges moraine, Southern Ontario, Illinois State Geological Survey, Open File Series 2000-1, Bloomington-Normal, 38-41.

Sadura, S., Martini, I., Endres, A., Wolf, K., 2006. Morphology and GPR stratigraphy of a frontal part of an end moraine of the laurentide ice sheet: Paris Moraine near Guelph, ON, Canada. Geomorphology, 75, 212-225.

Schapp, M., 1999. ROSETTA. US Salinity Laboratory: http://www.ussl.ars.usda.gov/MODELS/ROSETTA/ROSETTA.html

Schaap, M., Leij, F., 2000. Improved prediction of unsaturated hydraulic conductivity with the Mualem-van Genuchten model. Soil Sci. Soc. Am. J. 64, 843-851.

Schapp, M., Leij, F., and Van Genuchten, M., 2001. ROSETTA: a computer program for estimating soil hydraulic parameters with hierarchical pedotransfer functions. Journal of Hydrology, 251, 163-176.

Seaber, P.,1988. Hydrostratigraphic units, in hydrogeology: Boulder, Colorada, Geological Society of America, The Geology of North America, v.O-2.

Singer, S.N., Cheng, C.K., and Scafe, M.G., 2003. Hydrogeology of southern Ontario, second edition. Ministry of the Environment. Hydrogeology of Ontario Series, Report 1.

Singhal, B., and Gupta, R., 2010. Applied hydrogeology of fractured rocks. Springer. pp. 8, 142.

Slichter, C., 1899. Theoretical investigation of the motion of ground waters. U.S. Geological Survey 19th Annual Report, 2, 322.

SSSA, 2002. Methods of soil analysis: Part 4, Physical Methods. Soil Science Society of America, Inc. Madison, Wisconsin, USA, 264-284, 809-815

Stalker, A. MacS., 1960. Ice-pressed drift forms and associated deposits in Alberta. Geol. Surv. Can. Bull. 57, 38.

Statistics Canada, 2003. Human activity and the environment. Annual Statistics 2003. Catalogue no. 16- 201-XIE.

Terzaghi, C. 1925. Principles of soil mechanics. Engineering News Record, 95, 832.

USGS, 2014. The USGS water science school. See: http://water.usgs.gov/edu/

Van Genuchten, M., 1980. A closed-form equation for predicting the hydraulic conductivity of unsaturated soils. Soil Sci. Am. J., 44, 892-898.

Van Genuchten, M., Leij, F., Yates, S., 1991. The RETC code for quantifying the hydraulic functions of unsaturated soils. U.S. Salinity Laboratory, Department of Agriculture, EPA/600/2-91/065.

Vukovic, M., and Soro, A., 1992. Determination of hydraulic conductivity of porous media from grain-size composition. Littleton, Colorado: Water Resources Publications.

Wada, Y., van Beek, L., van Kempen, C., Reckman, J., Vasak, S., Bierkens, M., 2010. Global depletion of groundwater resources. Geophysical Research Letters 37, 1–5.

Whiteley, H., 1982. Annual Report OMAF project 00394 – The effect of agricultural activities on groundwater quality. School of Engineering, University of Guelph. [Unpublished]

Whiteley, H., 1987. Final Report OMAF Project 00394 – The effects of agricultural activities on levels of nitrate nitrogen and related constituents in groundwater. School of Engineering, University of Guelph. [Unpublished]

Wosten, J., Pachepsky, Y., Rawls, W., Pedotransfer functions: bridging the gap between available basic soil data and missing soil hydraulic characteristics. Journal of Hydrology, 251, 123-150.

6.0 APPENDICIES

Appendix A

Calibrated and measured K_{sat} values (m/s)

Sample ID	Depth (m)	K_{sat} (m/s) Measured	K_{sat} (m/s) Alyamani	K_{sat} (m/s) Beyer	K_{sat} (m/s) Chapuis	K_{sat} (m/s) Harleman	K_{sat} (m/s) Hazen New	K_{sat} (m/s) Hazen Original	K_{sat} (m/s) Kozeny
ARS1A - 1	0.23		1.02E-07	3.63E-07	1.09E-06	3.79E-07	3.79E-07	7.17E-07	5.44E-07
ARS1A - 2	0.66		4.35E-06	5.22E-07	3.94E-07	5.16E-07	5.16E-07	4.15E-07	4.81E-07
ARS1A - 3	1.03	1.75E-05							
ARS1A - 4	2.26		4.91E-06	6.82E-07	4.86E-07	6.74E-07	6.74E-07	5.41E-07	4.70E-07
ARS1A - 5	2.69	1.17E-06							
ARS1A - 6	3.40		9.11E-06	2.37E-06	1.36E-06	2.34E-06	2.34E-06	1.98E-06	1.37E-06
ARS1A - 7	3.75		3.14E-06	5.99E-07	4.46E-07	5.92E-07	5.92E-07	4.83E-07	5.02E-07
ARS1A - 8	4.66	5.10E-07							
ARS1A - 12	7.48		8.64E-06	2.63E-05	3.39E-05	2.75E-05	2.75E-05	5.43E-05	1.97E-05
ARS1A - 14	8.67		2.70E-07	5.18E-07	4.89E-07	5.16E-07	5.16E-07	5.01E-07	4.18E-07
ARS1A - 15	9.51		3.65E-06	9.70E-07	6.81E-07	9.61E-07	9.61E-07	8.16E-07	7.93E-07
ARS1A - 16	10.30		4.01E-07	6.57E-07	5.90E-07	6.55E-07	6.55E-07	6.35E-07	5.33E-07
ARS1A - 17	11.28	4.52E-07	4.60E-08	3.73E-07	4.07E-07	3.73E-07	3.73E-07	3.82E-07	6.17E-07

Sample ID	Depth (m)	K_{sat} (m/s) Kozeny Carman	K_{sat} (m/s) KC (Carrier)	K_{sat} (m/s) Kruger	K_{sat} (m/s) Krumbein	K_{sat} (m/s) NAVFAC	K_{sat} (m/s) Pavchich	K_{sat} (m/s) Sauerbrei
ARS1A - 1	0.23	1.27E-06	5.44E-07	2.90E-07	3.02E-08	4.77E-06	3.10E-07	5.18E-07
ARS1A - 2	0.66			5.87E-07	2.85E-06	2.74E-07	6.04E-07	4.55E-07
ARS1A - 3	1.03							
ARS1A - 4	2.26			5.68E-07	6.13E-06	3.98E-07	3.98E-07	2.94E-07
ARS1A - 5	2.69							
ARS1A - 6	3.40			1.59E-06	1.74E-06	2.53E-06	4.41E-06	4.11E-06
ARS1A - 7	3.75	4.06E-07	5.02E-07	6.06E-07	1.79E-06	3.42E-07	5.21E-07	4.45E-07
ARS1A - 8	4.66							
ARS1A - 12	7.48	1.03E-04	1.97E-05	9.64E-06	1.65E-06	8.59E-04	2.44E-05	4.24E-05
ARS1A - 14	8.67			4.40E-07	3.04E-07	4.26E-07	2.76E-07	2.97E-07
ARS1A - 15	9.51	6.98E-07	7.93E-07	9.27E-07	7.47E-07	7.36E-07	1.11E-06	1.04E-06
ARS1A - 16	10.30			5.59E-07	9.81E-07	5.91E-07	3.65E-07	3.93E-07
ARS1A - 17	11.28	3.61E-07	6.17E-07	6.12E-07	4.33E-07	3.19E-07	1.83E-07	2.05E-07

Sample ID	Depth (m)	K_{sat} (m/s) Slichter	K_{sat} (m/s) Terzaghi	K_{sat} (m/s) USBR	K_{sat} (m/s) Zamarin	K_{sat} (m/s) Zunker
ARS1A - 1	0.23	1.06E-06	1.21E-06	8.57E-08	3.60E-07	3.94E-07
ARS1A - 2	0.66	3.77E-07	3.54E-07	8.30E-07	5.29E-07	5.17E-07
ARS1A - 3	1.03					
ARS1A - 4	2.26	4.93E-07	4.62E-07	3.55E-07	5.17E-07	5.15E-07
ARS1A - 5	2.69					
ARS1A - 6	3.40	1.82E-06	1.74E-06	7.16E-06	1.55E-06	1.58E-06
ARS1A - 7	3.75	4.41E-07	4.16E-07	7.23E-07	5.55E-07	5.47E-07
ARS1A - 8	4.66					
ARS1A - 12	7.48	8.38E-05	9.63E-05	1.20E-05	1.72E-05	3.48E-05
ARS1A - 14	8.67	4.81E-07	4.82E-07	2.62E-07	4.40E-07	4.52E-07
ARS1A - 15	9.51	7.52E-07	7.20E-07	2.10E-06	8.76E-07	8.60E-07
ARS1A - 16	10.30	6.11E-07	6.12E-07	3.69E-07	5.71E-07	6.05E-07
ARS1A - 17	11.28	3.76E-07	3.83E-07	1.44E-07	6.72E-07	7.96E-07

Sample ID	Depth (m)	K_{sat} (m/s) Measured	K_{sat} (m/s) Alyamani	K_{sat} (m/s) Beyer	K_{sat} (m/s) Chapuis	K_{sat} (m/s) Harleman	K_{sat} (m/s) Hazen New	K_{sat} (m/s) Hazen Original	K_{sat} (m/s) Kozeny
FRE1A - 1	0.62		1.00E-05	3.51E-07	2.89E-07	3.47E-07	3.47E-07	2.78E-07	5.58E-07
FRE1A - 2	2.67		4.09E-10	2.02E-07	3.60E-07	2.05E-07	2.05E-07	2.69E-07	2.72E-07
FRE1A - 3	3.83		6.28E-07	4.39E-07	3.56E-07	4.34E-07	4.34E-07	3.59E-07	3.23E-07
FRE1A - 4	4.19								
FRE1A - 5	4.94								
FRE1A - 6	8.31								
FRE1A - 7	9.98		6.56E-06	3.18E-06	1.89E-06	3.16E-06	3.16E-06	2.91E-06	1.49E-06
FRE1A - 8	10.42		9.72E-06	1.99E-05	9.12E-06	1.99E-05	1.99E-05	2.04E-05	2.39E-06
FRE1A - 9	11.05		1.12E-06	1.24E-06	9.19E-07	1.23E-06	1.23E-06	1.15E-06	9.74E-07
FRE1A - 10	11.51		1.48E-06	4.43E-05	3.01E-05	4.54E-05	4.54E-05	6.78E-05	9.47E-06
FRE1A - 11	12.74		2.25E-08	3.74E-07	4.09E-07	3.74E-07	3.74E-07	3.85E-07	3.12E-07
FRE1A - 12	13.64		4.11E-05	4.54E-05	1.72E-05	4.54E-05	4.54E-05	4.60E-05	6.97E-06
FRE1A - 13	14.39		3.09E-07	3.88E-07	3.42E-07	3.85E-07	3.85E-07	3.35E-07	2.96E-07
FRE1A - 14	15.77		6.34E-06	9.27E-07	6.41E-07	9.17E-07	9.17E-07	7.62E-07	7.69E-07

Sample ID	Depth (m)	K_{sat} (m/s) Kozeny Carman	K_{sat} (m/s) KC (Carrier)	K_{sat} (m/s) Kruger	K_{sat} (m/s) Krumbein	K_{sat} (m/s) NAVFAC	K_{sat} (m/s) Pavchich	K_{sat} (m/s) Sauerbrei
FRE1A - 1	0.62	2.33E-07	5.58E-07	6.65E-07	2.54E-06	1.56E-07	1.32E-06	9.58E-07
FRE1A - 2	2.67	3.09E-07	2.72E-07	2.14E-07	2.66E-08	3.37E-07	1.36E-07	1.77E-07
FRE1A - 3	3.83	3.04E-07	3.23E-07	3.80E-07	5.75E-07	2.29E-07	2.33E-07	2.09E-07
FRE1A - 4	4.19							
FRE1A - 5	4.94							
FRE1A - 6	8.31							
FRE1A - 7	9.98	2.58E-06	1.49E-06	1.60E-06	4.52E-06	4.57E-06	6.54E-06	6.73E-06
FRE1A - 8	10.42	1.92E-05	2.39E-06	2.31E-06	1.75E-05	7.17E-05	2.79E-05	3.12E-05
FRE1A - 9	11.05	1.02E-06	9.74E-07	1.03E-06	4.32E-06	1.28E-06	1.02E-06	1.06E-06
FRE1A - 10	11.51	8.84E-05	9.47E-06	6.36E-06	8.88E-06	5.39E-04	4.46E-05	6.27E-05
FRE1A - 11	12.74	3.64E-07	3.12E-07	3.07E-07	8.90E-07	3.22E-07	1.79E-07	2.01E-07
FRE1A - 12	13.64	4.32E-05	6.97E-06	6.68E-06	2.13E-05	2.17E-04	1.02E-04	1.13E-04
FRE1A - 13	14.39	2.90E-07	2.96E-07	3.32E-07	2.33E-06	2.17E-07	1.89E-07	1.84E-07
FRE1A - 14	15.77	6.46E-07	7.69E-07	8.91E-07	3.75E-06	6.58E-07	1.17E-06	1.06E-06

Sample ID	Depth (m)	K_{sat} (m/s) Slichter	K_{sat} (m/s) Terzaghi	K_{sat} (m/s) USBR	K_{sat} (m/s) Zamarin	K_{sat} (m/s) Zunker
FRE1A - 1	0.62	2.53E-07	2.38E-07	3.43E-06	5.84E-07	5.38E-07
FRE1A - 2	2.67	3.01E-07	3.27E-07	6.85E-08	2.29E-07	2.18E-07
FRE1A - 3	3.83	3.29E-07	3.12E-07	2.35E-07	3.47E-07	3.42E-07
FRE1A - 4	4.19					
FRE1A - 5	4.94					
FRE1A - 6	8.31					
FRE1A - 7	9.98	2.74E-06	2.70E-06	1.05E-05	1.58E-06	1.54E-06
FRE1A - 8	10.42	2.00E-05	2.04E-05	5.84E-05	2.27E-06	1.95E-06
FRE1A - 9	11.05	1.09E-06	1.07E-06	1.53E-06	1.09E-06	1.26E-06
FRE1A - 10	11.51	8.25E-05	9.17E-05	4.69E-05	7.91E-06	7.57E-06
FRE1A - 11	12.74	3.79E-07	3.86E-07	1.39E-07	3.05E-07	2.98E-07
FRE1A - 12	13.64	4.51E-05	4.58E-05	2.27E-04	7.14E-06	6.55E-06
FRE1A - 13	14.39	3.11E-07	3.00E-07	1.79E-07	3.08E-07	3.02E-07
FRE1A - 14	15.77	6.99E-07	6.64E-07	2.32E-06	8.37E-07	8.35E-07

Sample ID	Depth (m)	K_{sat} (m/s) Measured	K_{sat} (m/s) Alyamani	K_{sat} (m/s) Beyer	K_{sat} (m/s) Chapuis	K_{sat} (m/s) Harleman	K_{sat} (m/s) Hazen New	K_{sat} (m/s) Hazen Original	K_{sat} (m/s) Kozeny
GDC1A - 1	0.93	1.66E-07	9.90E-08	4.00E-07	3.89E-07	3.99E-07	3.99E-07	3.78E-07	3.01E-07
GDC1A - 2	4.24	8.76E-08	3.07E-08	2.77E-07	3.32E-07	2.77E-07	2.77E-07	2.91E-07	2.52E-07
GDC1A - 3	4.65	0.00E+00	1.19E-07	3.45E-08	4.78E-08	3.41E-08	3.41E-08	2.78E-08	8.38E-08
GDC1A - 4	6.02	4.22E-07	4.75E-07	6.95E-08	8.16E-08	6.86E-08	6.86E-08	5.53E-08	1.45E-07
GDC1A - 5	7.54	8.39E-08	2.24E-09	5.50E-08	1.57E-07	5.64E-08	5.64E-08	8.30E-08	1.29E-07
GDC1A - 6	9.07	4.62E-08	2.12E-08	1.45E-07	1.99E-07	1.46E-07	1.46E-07	1.52E-07	1.91E-07
GDC1A - 7	9.58	6.82E-08	1.63E-08	4.50E-08	7.46E-08	4.49E-08	4.49E-08	4.46E-08	9.99E-08
GDC1A - 8	11.20	2.45E-07	5.50E-08	2.01E-08	3.13E-08	1.98E-08	1.98E-08	1.62E-08	6.66E-08
GDC1A - 9	12.12	1.41E-07	1.33E-07	2.76E-08	3.99E-08	2.73E-08	2.73E-08	2.21E-08	1.01E-07
GDC1A - 10	15.16	8.53E-08	1.95E-10	2.70E-08	5.58E-08	2.71E-08	2.71E-08	2.92E-08	6.86E-08
GDC1A - 11	16.69	2.40E-07	1.06E-08	2.54E-08	4.37E-08	2.53E-08	2.53E-08	2.34E-08	6.70E-08
GDC1A - 13	24.31	1.58E-07	3.07E-08	2.77E-07	3.32E-07	2.77E-07	2.77E-07	2.91E-07	2.53E-07
GDC1A - 14	30.40	8.84E-08	1.20E-08	2.35E-08	3.91E-08	2.33E-08	2.33E-08	2.07E-08	6.22E-08
GDC1A - 15	36.50	1.07E-07	1.35E-11	6.47E-08	1.34E-07	6.55E-08	6.55E-08	8.06E-08	1.10E-07

Sample ID	Depth (m)	K_{sat} (m/s) Kozeny Carman	K_{sat} (m/s) KC (Carrier)	K_{sat} (m/s) Kruger	K_{sat} (m/s) Krumbein	K_{sat} (m/s) NAVFAC	K_{sat} (m/s) Pavchich	K_{sat} (m/s) Sauerbrei
GDC1A - 1	0.93	3.41E-07	3.01E-07	3.23E-07	8.91E-08	2.82E-07	1.88E-07	1.98E-07
GDC1A - 2	4.24	2.79E-07	2.52E-07	2.46E-07	6.89E-08	2.27E-07	1.38E-07	1.57E-07
GDC1A - 3	4.65	2.34E-08	8.38E-08	1.01E-07	4.57E-07	6.18E-09	1.67E-08	1.42E-08
GDC1A - 4	6.02	4.64E-08	1.45E-07	1.79E-07	3.57E-07	1.61E-08	7.48E-08	5.94E-08
GDC1A - 5	7.54	1.07E-07	1.29E-07	9.17E-08	1.85E-08	1.10E-07	3.93E-08	5.49E-08
GDC1A - 6	9.07	1.45E-07	1.91E-07	1.91E-07	1.09E-08	9.33E-08	9.91E-08	1.12E-07
GDC1A - 7	9.58	4.13E-08	9.99E-08	1.07E-07	2.29E-07	1.60E-08	3.78E-08	4.13E-08
GDC1A - 8	11.20	1.36E-08	6.66E-08	8.34E-08	3.21E-08	2.89E-09	9.07E-09	7.77E-09
GDC1A - 9	12.12	1.86E-08	1.01E-07	1.27E-07	1.64E-07	4.47E-09	3.43E-08	2.87E-08
GDC1A - 10	15.16	2.86E-08	6.86E-08	6.66E-08	2.87E-07	1.07E-08	1.11E-08	1.29E-08
GDC1A - 11	16.69	2.09E-08	6.70E-08	7.47E-08	2.86E-07	5.84E-09	9.77E-09	1.01E-08
GDC1A - 13	24.31	2.79E-07	2.53E-07	2.47E-07	6.89E-08	2.28E-07	1.39E-07	1.58E-07
GDC1A - 14	30.40	1.81E-08	6.22E-08	7.21E-08	9.84E-08	4.61E-09	8.16E-09	8.14E-09
GDC1A - 15	36.50	8.72E-08	1.10E-07	9.32E-08	4.20E-08	5.82E-08	3.42E-08	4.28E-08

Sample ID	Depth (m)	K_{sat} (m/s) Slichter	K_{sat} (m/s) Terzaghi	K_{sat} (m/s) USBR	K_{sat} (m/s) Zamarin	K_{sat} (m/s) Zunker
GDC1A - 1	0.93	3.61E-07	3.59E-07	1.62E-07	3.11E-07	3.03E-07
GDC1A - 2	4.24	2.89E-07	2.96E-07	4.39E-08	2.44E-07	2.35E-07
GDC1A - 3	4.65	2.54E-08	2.39E-08	4.96E-09	8.47E-08	7.42E-08
GDC1A - 4	6.02	5.04E-08	4.73E-08	2.54E-08	1.52E-07	1.37E-07
GDC1A - 5	7.54	1.00E-07	1.11E-07	5.94E-09	9.80E-08	8.77E-08
GDC1A - 6	9.07	1.50E-07	1.54E-07	2.93E-08	1.83E-07	1.68E-07
GDC1A - 7	9.58	4.33E-08	4.37E-08	1.23E-08	9.83E-08	8.66E-08
GDC1A - 8	11.20	1.48E-08	1.39E-08	2.15E-09	6.81E-08	5.71E-08
GDC1A - 9	12.12	2.02E-08	1.90E-08	1.54E-08	1.07E-07	9.38E-08
GDC1A - 10	15.16	2.94E-08	3.04E-08	2.09E-09	6.10E-08	5.09E-08
GDC1A - 11	16.69	2.22E-08	2.19E-08	2.21E-09	6.47E-08	5.48E-08
GDC1A - 13	24.31	2.89E-07	2.97E-07	4.39E-08	2.45E-07	2.36E-07
GDC1A - 14	30.40	1.94E-08	1.88E-08	1.75E-09	6.10E-08	5.09E-08
GDC1A - 15	36.50	8.68E-08	9.29E-08	6.64E-09	9.17E-08	7.88E-08

Sample ID	Depth (m)	K_{sat} (m/s) Measured	K_{sat} (m/s) Alyamani	K_{sat} (m/s) Beyer	K_{sat} (m/s) Chapuis	K_{sat} (m/s) Harleman	K_{sat} (m/s) Hazen New	K_{sat} (m/s) Hazen Original	K_{sat} (m/s) Kozeny
GDC2B - 1	1.32	5.13E-07	6.69E-07	8.49E-07	7.04E-07	8.45E-07	8.45E-07	8.05E-07	6.96E-07
GDC2B - 2	2.18	1.18E-06	4.34E-07	7.04E-07	6.29E-07	7.03E-07	7.03E-07	6.87E-07	5.94E-07
GDC2B - 3	4.01	1.63E-07	8.66E-08	3.87E-07	3.98E-07	3.86E-07	3.86E-07	3.80E-07	3.17E-07
GDC2B - 4	4.52	7.04E-07	4.99E-08	4.02E-07	8.89E-07	4.15E-07	4.15E-07	6.77E-07	5.54E-07
GDC2B - 5	4.93		1.80E-07	4.53E-07	4.22E-07	4.51E-07	4.51E-07	4.22E-07	3.43E-07
GDC2B - 6	5.92	1.50E-07	9.87E-07	1.88E-07	1.80E-07	1.86E-07	1.86E-07	1.51E-07	2.07E-07
GDC2B - 7	6.10		3.51E-06	9.94E-07	6.88E-07	9.84E-07	9.84E-07	8.29E-07	7.87E-07
GDC2B - 8	7.26	3.81E-07	3.42E-07	6.00E-07	5.56E-07	5.99E-07	5.99E-07	5.86E-07	5.02E-07
GDC2B - 9	7.59		7.31E-07	1.06E-07	1.16E-07	1.05E-07	1.05E-07	8.59E-08	1.75E-07
GDC2B - 10	8.69	6.67E-07							
GDC2B - 11	9.04	1.04E-07	1.10E-07	4.37E-07	4.47E-07	4.36E-07	4.36E-07	4.37E-07	3.59E-07
GDC2B - 12	9.93	9.41E-08	6.59E-07	6.64E-07	5.54E-07	6.60E-07	6.60E-07	6.05E-07	5.35E-07
GDC2B - 13	10.31	3.35E-07	2.30E-06	1.03E-06	7.27E-07	1.02E-06	1.02E-06	8.81E-07	8.05E-07
GDC2B - 14	11.63	6.18E-07	1.15E-08	2.93E-07	5.63E-07	3.00E-07	3.00E-07	4.34E-07	8.49E-07
GDC2B - 15	12.65	1.28E-07	4.94E-08	3.33E-07	8.05E-07	3.45E-07	3.45E-07	5.77E-07	4.66E-07
GDC2B - 16	14.80	2.19E-07	4.99E-08	4.02E-07	8.89E-07	4.15E-07	4.15E-07	6.77E-07	5.54E-07
GDC2B - 17	15.77	2.35E-07	6.14E-08	4.81E-08	6.73E-08	4.77E-08	4.77E-08	4.18E-08	1.10E-07
GDC2B - 18	10.30	2.44E-07	3.54E-07	9.11E-08	1.02E-07	9.00E-08	9.00E-08	7.36E-08	1.39E-07
GDC2B - 19	xxx	1.01E-07	1.37E-08	3.31E-07	6.24E-07	3.38E-07	3.38E-07	4.92E-07	4.12E-07

Sample ID	Depth (m)	K_{sat} (m/s) Kozeny Carman	K_{sat} (m/s) KC (Carrier)	K_{sat} (m/s) Kruger	K_{sat} (m/s) Krumbein	K_{sat} (m/s) NAVFAC	K_{sat} (m/s) Pavchich	K_{sat} (m/s) Sauerbrei
GDC2B - 1	1.32	7.28E-07	6.96E-07	7.34E-07	3.06E-07	8.01E-07	5.23E-07	5.54E-07
GDC2B - 2	2.18	6.31E-07	5.94E-07	6.11E-07	6.70E-07	6.65E-07	4.22E-07	4.56E-07
GDC2B - 3	4.01	3.51E-07	3.17E-07	3.23E-07	2.10E-07	2.99E-07	1.88E-07	2.05E-07
GDC2B - 4	4.52	9.81E-07	5.54E-07	3.53E-07	2.80E-08	2.26E-06	2.95E-07	4.41E-07
GDC2B - 5	4.93	3.79E-07	3.43E-07	3.69E-07	2.62E-07	3.23E-07	2.17E-07	2.27E-07
GDC2B - 6	5.92	1.27E-07	2.07E-07	2.51E-07	5.52E-07	6.68E-08	1.19E-07	1.01E-07
GDC2B - 7	6.10	7.07E-07	7.87E-07	9.13E-07	3.71E-06	7.48E-07	2.38E-06	2.21E-06
GDC2B - 8	7.26	5.39E-07	5.02E-07	5.20E-07	8.99E-08	5.37E-07	3.48E-07	3.78E-07
GDC2B - 9	7.59	7.24E-08	1.75E-07	2.10E-07	2.74E-06	3.03E-08	7.80E-08	6.71E-08
GDC2B - 10	8.69							
GDC2B - 11	9.04	4.08E-07	3.59E-07	3.63E-07	1.02E-07	3.70E-07	2.19E-07	2.41E-07
GDC2B - 12	9.93	5.37E-07	5.35E-07	5.79E-07	2.21E-06	5.19E-07	3.99E-07	4.10E-07
GDC2B - 13	10.31	7.58E-07	8.05E-07	9.11E-07	9.10E-06	8.27E-07	7.30E-07	6.99E-07
GDC2B - 14	11.63	5.48E-07	8.49E-07	6.06E-07	4.15E-08	8.38E-07	1.90E-07	2.63E-07
GDC2B - 15	12.65	8.65E-07	4.66E-07	2.89E-07	7.78E-08	2.07E-06	2.51E-07	3.82E-07
GDC2B - 16	14.80	9.81E-07	5.54E-07	3.53E-07	2.80E-08	2.26E-06	2.95E-07	4.41E-07
GDC2B - 17	15.77	3.63E-08	1.10E-07	1.27E-07	1.21E-07	1.20E-08	4.86E-08	4.77E-08
GDC2B - 18	10.30	6.20E-08	1.39E-07	1.68E-07	4.54E-07	2.44E-08	5.98E-08	5.15E-08
GDC2B - 19	xxx	6.24E-07	4.12E-07	2.97E-07	1.03E-07	9.97E-07	2.15E-07	2.98E-07

Sample ID	Depth (m)	K_{sat} (m/s) Slichter	K_{sat} (m/s) Terzaghi	K_{sat} (m/s) USBR	K_{sat} (m/s) Zamarin	K_{sat} (m/s) Zunker
GDC2B - 1	1.32	7.69E-07	7.66E-07	6.00E-07	7.62E-07	8.38E-07
GDC2B - 2	2.18	6.63E-07	6.66E-07	4.46E-07	6.34E-07	6.88E-07
GDC2B - 3	4.01	3.68E-07	3.71E-07	1.57E-07	3.17E-07	3.14E-07
GDC2B - 4	4.52	8.83E-07	9.95E-07	1.11E-07	4.23E-07	4.39E-07
GDC2B - 5	4.93	4.01E-07	3.98E-07	1.96E-07	3.56E-07	3.54E-07
GDC2B - 6	5.92	1.38E-07	1.30E-07	1.12E-07	2.18E-07	2.00E-07
GDC2B - 7	6.10	7.63E-07	7.29E-07	4.89E-06	8.67E-07	8.70E-07
GDC2B - 8	7.26	5.66E-07	5.69E-07	3.52E-07	5.33E-07	5.64E-07
GDC2B - 9	7.59	7.85E-08	7.41E-08	7.54E-08	1.83E-07	1.71E-07
GDC2B - 10	8.69					
GDC2B - 11	9.04	4.26E-07	4.32E-07	1.85E-07	3.63E-07	3.66E-07
GDC2B - 12	9.93	5.71E-07	5.62E-07	4.53E-07	5.77E-07	6.12E-07
GDC2B - 13	10.31	8.15E-07	7.85E-07	1.03E-06	8.99E-07	9.63E-07
GDC2B - 14	11.63	5.17E-07	5.72E-07	8.51E-08	7.96E-07	1.06E-06
GDC2B - 15	12.65	7.69E-07	8.69E-07	8.75E-08	3.44E-07	3.51E-07
GDC2B - 16	14.80	8.83E-07	9.95E-07	1.11E-07	4.23E-07	4.39E-07
GDC2B - 17	15.77	3.89E-08	3.76E-08	3.93E-08	1.12E-07	1.01E-07
GDC2B - 18	10.30	6.72E-08	6.35E-08	4.97E-08	1.44E-07	1.30E-07
GDC2B - 19	xxx	5.88E-07	6.51E-07	9.75E-08	3.36E-07	3.30E-07

Sample ID	Depth (m)	K_{sat} (m/s) Measured	K_{sat} (m/s) Alyamani	K_{sat} (m/s) Beyer	K_{sat} (m/s) Chapuis	K_{sat} (m/s) Harleman	K_{sat} (m/s) Hazen New	K_{sat} (m/s) Hazen Original	K_{sat} (m/s) Kozeny
GDC10A - 1	2.19	1.03E-05	3.18E-08	2.63E-05	1.82E-05	2.68E-05	2.68E-05	3.78E-05	7.86E-06
GDC10A - 2	2.90	1.93E-07	4.42E-09	2.04E-07	3.04E-07	2.05E-07	2.05E-07	2.40E-07	2.16E-07
GDC10A - 3	3.51		2.75E-09	2.62E-08	6.23E-08	2.64E-08	2.64E-08	3.13E-08	9.20E-08
GDC10A - 4	4.15		1.94E-05	4.47E-07	3.48E-07	4.41E-07	4.41E-07	3.54E-07	4.62E-07
GDC10A - 5	4.69	6.55E-07	5.00E-08	2.95E-07	7.63E-07	3.06E-07	3.06E-07	5.23E-07	3.97E-07
GDC10A - 6	5.12	4.14E-07	3.55E-08	3.50E-07	5.12E-07	3.54E-07	3.54E-07	4.42E-07	3.37E-07
GDC10A - 7	5.64	6.01E-06	1.08E-05	6.55E-07	4.70E-07	6.46E-07	6.46E-07	5.19E-07	5.25E-07
GDC10A - 8	6.10	1.39E-07	1.80E-09	2.55E-07	3.66E-07	2.57E-07	2.57E-07	3.03E-07	2.65E-07
GDC10A - 9	7.83	5.45E-06	6.23E-06	9.14E-07	6.20E-07	9.03E-07	9.03E-07	7.36E-07	7.34E-07
GDC10A - 10	8.81	4.10E-07	2.87E-06	6.06E-07	4.61E-07	5.99E-07	5.99E-07	4.99E-07	5.58E-07
GDC10A - 11	9.30	1.68E-06	3.14E-06	8.41E-07	6.01E-07	8.32E-07	8.32E-07	6.99E-07	6.44E-07
GDC10A - 12	10.12	2.61E-07	1.40E-06	2.39E-07	2.20E-07	2.36E-07	2.36E-07	1.95E-07	2.39E-07

Sample ID	Depth (m)	K_{sat} (m/s) Kozeny Carman	K_{sat} (m/s) KC (Carrier)	K_{sat} (m/s) Kruger	K_{sat} (m/s) Krumbein	K_{sat} (m/s) NAVFAC	K_{sat} (m/s) Pavchich	K_{sat} (m/s) Sauerbrei
GDC10A - 1	2.19	4.64E-05	7.86E-06	5.73E-06	9.97E-07	2.33E-04	3.55E-05	4.83E-05
GDC10A - 2	2.90	2.49E-07	2.16E-07	1.92E-07	2.28E-08	2.18E-07	1.30E-07	1.58E-07
GDC10A - 3	3.51	3.29E-08	9.20E-08	8.42E-08	1.24E-09	1.50E-08	4.51E-08	5.53E-08
GDC10A - 4	4.15	2.96E-07	4.62E-07	5.65E-07	7.74E-06	2.19E-07	6.17E-07	3.80E-07
GDC10A - 5	4.69	8.07E-07	3.97E-07	2.41E-07	2.58E-08	2.02E-06	2.28E-07	3.52E-07
GDC10A - 6	5.12	4.84E-07	3.37E-07	2.81E-07	4.96E-09	5.67E-07	2.15E-07	2.72E-07
GDC10A - 7	5.64	4.35E-07	5.25E-07	6.40E-07	2.23E-06	3.75E-07	5.22E-07	3.79E-07
GDC10A - 8	6.10	3.16E-07	2.65E-07	2.38E-07	5.67E-08	3.00E-07	1.40E-07	1.71E-07
GDC10A - 9	7.83	6.19E-07	7.34E-07	8.89E-07	5.52E-06	6.18E-07	1.41E-06	1.19E-06
GDC10A - 10	8.81	4.23E-07	5.58E-07	6.63E-07	1.06E-06	3.64E-07	7.23E-07	6.55E-07
GDC10A - 11	9.30	5.95E-07	6.44E-07	7.59E-07	2.06E-06	5.88E-07	5.34E-07	4.92E-07
GDC10A - 12	10.12	1.65E-07	2.39E-07	2.89E-07	1.29E-06	9.65E-08	1.53E-07	1.36E-07

Sample ID	Depth (m)	K_{sat} (m/s) Slichter	K_{sat} (m/s) Terzaghi	K_{sat} (m/s) USBR	K_{sat} (m/s) Zamarin	K_{sat} (m/s) Zunker
GDC10A - 1	2.19	4.42E-05	4.87E-05	3.67E-05	7.03E-06	6.74E-06
GDC10A - 2	2.90	2.51E-07	2.66E-07	7.92E-08	2.05E-07	2.11E-07
GDC10A - 3	3.51	3.30E-08	3.50E-08	3.06E-08	8.29E-08	7.27E-08
GDC10A - 4	4.15	3.22E-07	3.02E-07	6.69E-07	4.97E-07	4.62E-07
GDC10A - 5	4.69	7.10E-07	8.04E-07	7.46E-08	2.91E-07	3.04E-07
GDC10A - 6	5.12	4.80E-07	5.15E-07	1.34E-07	3.22E-07	3.60E-07
GDC10A - 7	5.64	4.72E-07	4.43E-07	5.50E-07	5.74E-07	5.49E-07
GDC10A - 8	6.10	3.18E-07	3.36E-07	8.59E-08	2.44E-07	2.28E-07
GDC10A - 9	7.83	6.71E-07	6.33E-07	2.97E-06	8.17E-07	7.91E-07
GDC10A - 10	8.81	4.58E-07	4.35E-07	1.29E-06	6.15E-07	6.03E-07
GDC10A - 11	9.30	6.43E-07	6.13E-07	6.75E-07	7.18E-07	7.26E-07
GDC10A - 12	10.12	1.78E-07	1.69E-07	1.52E-07	2.55E-07	2.39E-07

Sample ID	Depth (m)	K_{sat} (m/s) Measured	K_{sat} (m/s) Alyamani	K_{sat} (m/s) Beyer	K_{sat} (m/s) Chapuis	K_{sat} (m/s) Harleman	K_{sat} (m/s) Hazen New	K_{sat} (m/s) Hazen Original	K_{sat} (m/s) Kozeny
TGI1A - 1	0.41		3.01E-07	4.82E-07	4.45E-07	4.80E-07	4.80E-07	4.51E-07	3.78E-07
TGI1A - 2	0.81		2.07E-07	4.42E-07	4.39E-07	4.41E-07	4.41E-07	4.32E-07	3.66E-07
TGI1A - 4	2.00		1.05E-07	3.68E-07	3.95E-07	3.68E-07	3.68E-07	3.72E-07	3.09E-07
TGI1A - 5	2.67		3.72E-06	1.17E-06	7.96E-07	1.16E-06	1.16E-06	9.94E-07	9.31E-07
TGI1A - 6	4.07		3.95E-07	1.62E-07	1.66E-07	1.60E-07	1.60E-07	1.35E-07	1.97E-07
TGI1A - 7	5.07		9.15E-07	5.42E-07	4.39E-07	5.37E-07	5.37E-07	4.63E-07	4.23E-07
TGI1A - 8	5.87		4.43E-06	3.73E-06	2.45E-06	3.73E-06	3.73E-06	3.80E-06	2.07E-06
TGI1A -9	6.88	1.88E-06							
TGI1A - 10	8.19	3.07E-07	3.68E-07	1.29E-07	1.36E-07	1.27E-07	1.27E-07	1.05E-07	1.77E-07
TGI1A - 11	9.19		9.01E-07	8.73E-08	9.75E-08	8.62E-08	8.62E-08	6.95E-08	1.74E-07
TGI1A - 13	12.18	5.07E-07	7.72E-09	1.28E-07	1.96E-07	1.28E-07	1.28E-07	1.42E-07	1.70E-07
TGI1A - 15b	13.66		2.16E-07	5.81E-06	7.30E-06	6.00E-06	6.00E-06	9.88E-06	1.21E-05
TGI1A - 16	14.59		2.87E-08	4.28E-07	8.20E-07	4.39E-07	4.39E-07	6.66E-07	4.69E-07
TGI1A - 52.5	16.00	1.60E-07	4.27E-09	7.72E-08	1.39E-07	7.77E-08	7.77E-08	8.96E-08	1.70E-07

Sample ID	Depth (m)	K_{sat} (m/s) Kozeny Carman	K_{sat} (m/s) KC (Carrier)	K_{sat} (m/s) Kruger	K_{sat} (m/s) Krumbein	K_{sat} (m/s) NAVFAC	K_{sat} (m/s) Pavchich	K_{sat} (m/s) Sauerbrei
TGI1A - 1	0.41	4.06E-07	3.78E-07	4.05E-07	4.20E-07	3.56E-07	2.44E-07	2.56E-07
TGI1A - 2	0.81	3.98E-07	3.66E-07	3.82E-07	1.22E-07	3.54E-07	2.34E-07	2.54E-07
TGI1A - 4	2.00	3.48E-07	3.09E-07	3.17E-07	5.01E-08	3.00E-07	1.88E-07	2.08E-07
TGI1A - 5	2.67	8.53E-07	9.31E-07	1.06E-06	4.04E-06	9.74E-07	1.03E-06	9.79E-07
TGI1A - 6	4.07	1.15E-07	1.97E-07	2.33E-07	3.46E-07	5.86E-08	1.16E-07	1.07E-07
TGI1A - 7	5.07	3.99E-07	4.23E-07	4.83E-07	7.92E-07	3.37E-07	3.12E-07	3.00E-07
TGI1A - 8	5.87	3.58E-06	2.07E-06	2.04E-06	3.76E-06	7.25E-06	9.38E-06	1.05E-05
TGI1A -9	6.88							
TGI1A - 10	8.19	8.93E-08	1.77E-07	2.12E-07	6.15E-07	4.09E-08	1.06E-07	9.51E-08
TGI1A - 11	9.19	5.83E-08	1.74E-07	2.13E-07	1.86E-06	2.22E-08	6.82E-08	5.40E-08
TGI1A - 13	12.18	1.42E-07	1.70E-07	1.59E-07	1.39E-07	9.64E-08	7.90E-08	9.30E-08
TGI1A - 15b	13.66	1.45E-05	1.21E-05	6.72E-06	3.17E-06	6.21E-05	7.21E-06	1.08E-05
TGI1A - 16	14.59	8.84E-07	4.69E-07	3.23E-07	2.45E-08	1.68E-06	2.91E-07	4.14E-07
TGI1A - 52.5	16.00	9.19E-08	1.70E-07	1.56E-07	3.12E-08	5.64E-08	7.34E-08	8.85E-08

Sample ID	Depth (m)	K_{sat} (m/s) Slichter	K_{sat} (m/s) Terzaghi	K_{sat} (m/s) USBR	K_{sat} (m/s) Zamarin	K_{sat} (m/s) Zunker
TGI1A - 1	0.41	4.29E-07	4.26E-07	2.30E-07	3.96E-07	3.99E-07
TGI1A - 2	0.81	4.18E-07	4.20E-07	2.12E-07	3.80E-07	3.83E-07
TGI1A - 4	2.00	3.63E-07	3.69E-07	1.55E-07	3.14E-07	3.09E-07
TGI1A - 5	2.67	9.18E-07	8.81E-07	1.70E-06	1.03E-06	1.07E-06
TGI1A - 6	4.07	1.24E-07	1.18E-07	1.06E-07	2.08E-07	1.95E-07
TGI1A - 7	5.07	4.29E-07	4.13E-07	3.49E-07	4.57E-07	4.63E-07
TGI1A - 8	5.87	3.73E-06	3.80E-06	1.88E-05	2.10E-06	1.96E-06
TGI1A -9	6.88					
TGI1A - 10	8.19	9.66E-08	9.17E-08	9.41E-08	1.85E-07	1.72E-07
TGI1A - 11	9.19	6.33E-08	5.95E-08	6.01E-08	1.82E-07	1.66E-07
TGI1A - 13	12.18	1.45E-07	1.51E-07	4.84E-08	1.60E-07	1.52E-07
TGI1A - 15b	13.66	1.30E-05	1.46E-05	5.57E-06	1.18E-05	2.77E-05
TGI1A - 16	14.59	8.21E-07	9.14E-07	1.27E-07	3.97E-07	4.51E-07
TGI1A - 52.5	16.00	9.30E-08	9.79E-08	4.06E-08	1.55E-07	1.41E-07

Sample ID	Depth (m)	K_{sat} (m/s) Measured	K_{sat} (m/s) Alyamani	K_{sat} (m/s) Beyer	K_{sat} (m/s) Chapuis	K_{sat} (m/s) Harleman	K_{sat} (m/s) Hazen New	K_{sat} (m/s) Hazen Original	K_{sat} (m/s) Kozeny
VAN1A - M1	0.08		1.03E-06	2.03E-07	1.90E-07	2.01E-07	2.01E-07	1.62E-07	2.52E-07
VAN1A - 3	0.99		7.29E-08	5.84E-07	1.19E-06	6.03E-07	6.03E-07	9.84E-07	9.01E-07
VAN1A - 4	1.84		8.61E-06	7.20E-06	3.62E-06	7.16E-06	7.16E-06	6.62E-06	1.65E-06
VAN1A - M2	3.43	7.68E-07	1.93E-06	7.65E-07	5.74E-07	7.57E-07	7.57E-07	6.52E-07	6.29E-07
VAN1A - 6	3.46		2.62E-06	9.98E-07	7.03E-07	9.89E-07	9.89E-07	8.47E-07	7.76E-07
VAN1A - 8	5.01	6.33E-07	2.87E-06	9.34E-07	6.74E-07	9.26E-07	9.26E-07	7.99E-07	7.89E-07
VAN1A - M3	6.17		1.63E-06	4.56E-07	3.74E-07	4.51E-07	4.51E-07	3.81E-07	4.32E-07
VAN1A - 9	6.48		1.25E-06	4.96E-07	4.10E-07	4.91E-07	4.91E-07	4.24E-07	4.41E-07
VAN1A - 12	8.92		1.74E-08	4.60E-07	4.59E-07	4.60E-07	4.60E-07	4.56E-07	3.44E-07
VAN1A - M4	9.53		1.39E-06	7.31E-07	5.82E-07	7.26E-07	7.26E-07	6.51E-07	6.22E-07
VAN1A - 33.2-33.7	10.20	3.80E-08							
VAN1A - 14	10.79	6.23E-07							
VAN1A - 15	12.18		1.10E-06	1.84E-08	2.87E-08	1.81E-08	1.81E-08	1.46E-08	1.16E-07
VAN1A - M5	12.82		5.48E-06	2.75E-06	1.60E-06	2.73E-06	2.73E-06	2.40E-06	1.56E-06
VAN1A - M6	15.62								
VAN1A - 17	16.00		5.98E-05	2.95E-06	1.53E-06	2.91E-06	2.91E-06	2.34E-06	2.20E-06
VAN1A - 18	16.69	1.66E-06	5.73E-05	3.36E-06	4.03E-06	3.45E-06	3.45E-06	5.17E-06	3.19E-06
VAN1A - 56.2-56.7	17.33		1.26E-07	5.23E-08	6.64E-08	5.16E-08	5.16E-08	4.23E-08	1.13E-07
VAN1A - 58-58.4	17.74		1.64E-07	4.09E-07	1.43E-06	4.30E-07	4.30E-07	8.87E-07	6.28E-07
VAN1A - M7	18.52		2.30E-07	5.52E-07	6.01E-07	5.54E-07	5.54E-07	6.04E-07	5.71E-07
VAN1A - 20	19.35		1.45E-08	6.31E-08	1.03E-07	6.31E-08	6.31E-08	6.55E-08	1.27E-07
VAN1A - 21	21.56	8.21E-07	2.30E-07	8.19E-07	8.42E-07	8.24E-07	8.24E-07	9.16E-07	7.84E-07
VAN1A - M8	21.72		3.18E-08	1.22E-06	1.49E-06	1.24E-06	1.24E-06	1.64E-06	1.37E-06
VAN1A - 23	23.35	6.02E-07	9.81E-10	3.12E-08	7.18E-08	3.14E-08	3.14E-08	3.74E-08	8.71E-08
VAN1A - 23.51	23.51	4.30E-07	1.71E-06	5.08E-07	4.09E-07	5.02E-07	5.02E-07	4.26E-07	4.51E-07

Sample ID	Depth (m)	K_{sat} (m/s) Kozeny Carman	K_{sat} (m/s) KC (Carrier)	K_{sat} (m/s) Kruger	K_{sat} (m/s) Krumbein	K_{sat} (m/s) NAVFAC	K_{sat} (m/s) Pavchich	K_{sat} (m/s) Sauerbrei
VAN1A - M1	0.08	1.36E-07	2.52E-07	3.03E-07	5.57E-06	7.33E-08	1.53E-07	1.25E-07
VAN1A - 3	0.99	1.43E-06	9.01E-07	5.64E-07	1.95E-06	3.58E-06	4.29E-07	6.41E-07
VAN1A - 4	1.84	5.90E-06	1.65E-06	1.80E-06	2.29E-06	1.44E-05	1.38E-05	1.43E-05
VAN1A - M2	3.43	5.61E-07	6.29E-07	7.15E-07	9.46E-06	5.44E-07	6.37E-07	6.11E-07
VAN1A - 6	3.46	7.27E-07	7.76E-07	8.91E-07	4.58E-06	7.80E-07	1.19E-06	1.13E-06
VAN1A - 8	5.01	6.89E-07	7.89E-07	9.03E-07	8.87E-07	7.24E-07	1.03E-06	9.91E-07
VAN1A - M3	6.17	3.25E-07	4.32E-07	5.05E-07	7.16E-07	2.52E-07	3.95E-07	3.67E-07
VAN1A - 9	6.48	3.65E-07	4.41E-07	5.10E-07	4.92E-07	2.99E-07	3.85E-07	3.71E-07
VAN1A - 12	8.92	4.22E-07	3.44E-07	3.50E-07	4.01E-07	3.86E-07	2.10E-07	2.30E-07
VAN1A - M4	9.53	5.71E-07	6.22E-07	6.96E-07	1.33E-06	5.62E-07	6.55E-07	6.58E-07
VAN1A - 33.2-33.7	10.20							
VAN1A - 14	10.79							
VAN1A - 15	12.18	1.22E-08	1.16E-07	1.45E-07	1.48E-06	2.44E-09	2.19E-08	1.37E-08
VAN1A - M5	12.82	2.08E-06	1.56E-06	1.74E-06	5.84E-06	3.40E-06	4.93E-06	4.85E-06
VAN1A - M6	15.62							
VAN1A - 17	16.00	1.96E-06	2.20E-06	2.61E-06	1.96E-05	3.14E-06	4.29E-06	3.35E-06
VAN1A - 18	16.69	6.77E-06	3.19E-06	2.18E-06	1.94E-08	2.13E-05	8.44E-06	1.19E-05
VAN1A - 56.2-56.7	17.33	3.57E-08	1.13E-07	1.35E-07	1.31E-06	1.12E-08	1.63E-09	1.42E-09
VAN1A - 58-58.4	17.74	1.80E-06	6.28E-07	3.03E-07	3.11E-10	9.94E-06	3.79E-07	6.86E-07
VAN1A - M7	18.52	5.95E-07	5.71E-07	5.33E-07	7.69E-08	6.55E-07	4.52E-07	5.27E-07
VAN1A - 20	19.35	6.24E-08	1.27E-07	1.28E-07	1.33E-07	2.95E-08	6.30E-08	7.11E-08
VAN1A - 21	21.56	9.16E-07	7.84E-07	7.19E-07	6.17E-08	1.18E-06	5.70E-07	6.73E-07
VAN1A - M8	21.72	1.90E-06	1.37E-06	1.05E-06	3.90E-08	3.63E-06	1.37E-06	1.79E-06
VAN1A - 23	23.35	3.94E-08	8.71E-08	8.01E-08	7.98E-08	1.92E-08	2.83E-08	3.47E-08
VAN1A - 23.51	23.51	3.64E-07	4.51E-07	5.27E-07	3.79E-07	2.96E-07	4.00E-07	3.74E-07

Sample ID	Depth (m)	K_{sat} (m/s) Slichter	K_{sat} (m/s) Terzaghi	K_{sat} (m/s) USBR	K_{sat} (m/s) Zamarin	K_{sat} (m/s) Zunker
VAN1A - M1	0.08	1.48E-07	1.39E-07	1.65E-07	2.64E-07	2.44E-07
VAN1A - 3	0.99	1.28E-06	1.45E-06	1.70E-07	7.03E-07	7.79E-07
VAN1A - 4	1.84	6.27E-06	6.18E-06	2.59E-05	1.71E-06	1.52E-06
VAN1A - M2	3.43	6.04E-07	5.81E-07	9.50E-07	6.90E-07	7.15E-07
VAN1A - 6	3.46	7.82E-07	7.52E-07	2.33E-06	8.63E-07	8.95E-07
VAN1A - 8	5.01	7.40E-07	7.13E-07	1.89E-06	8.62E-07	8.58E-07
VAN1A - M3	6.17	3.50E-07	3.35E-07	5.57E-07	4.70E-07	4.68E-07
VAN1A - 9	6.48	3.93E-07	3.78E-07	5.15E-07	4.82E-07	4.85E-07
VAN1A - 12	8.92	4.42E-07	4.46E-07	1.72E-07	3.48E-07	3.49E-07
VAN1A - M4	9.53	6.10E-07	5.95E-07	9.96E-07	6.85E-07	7.11E-07
VAN1A - 33.2-33.7	10.20					
VAN1A - 14	10.79					
VAN1A - 15	12.18	1.32E-08	1.24E-08	1.47E-08	1.21E-07	1.04E-07
VAN1A - M5	12.82	2.23E-06	2.17E-06	8.22E-06	1.74E-06	1.80E-06
VAN1A - M6	15.62					
VAN1A - 17	16.00	2.13E-06	2.00E-06	2.90E-05	2.48E-06	2.40E-06
VAN1A - 18	16.69	6.31E-06	7.02E-06	6.03E-06	3.02E-06	4.09E-06
VAN1A - 56.2-56.7	17.33	3.87E-08	3.65E-08	3.50E-08	1.15E-07	1.02E-07
VAN1A - 58-58.4	17.74	1.43E-06	1.64E-06	8.89E-08	3.83E-07	4.35E-07
VAN1A - M7	18.52	6.11E-07	6.34E-07	4.72E-07	5.88E-07	6.65E-07
VAN1A - 20	19.35	6.48E-08	6.63E-08	3.95E-08	1.21E-07	1.10E-07
VAN1A - 21	21.56	9.35E-07	9.76E-07	5.49E-07	8.20E-07	9.66E-07
VAN1A - M8	21.72	1.85E-06	2.01E-06	1.33E-06	1.40E-06	1.97E-06
VAN1A - 23	23.35	3.95E-08	4.20E-08	1.33E-08	7.75E-08	6.56E-08
VAN1A - 23.51	23.51	3.92E-07	3.76E-07	5.40E-07	4.92E-07	4.88E-07

Sample ID	Depth (m)	Ksat (m/s) Measured	Ksat (m/s) Alyamani	Ksat (m/s) Beyer	Ksat (m/s) Chapuis	Ksat (m/s) Harleman	Ksat (m/s) Hazen New	Ksat (m/s) Hazen Original	Ksat (m/s) Kozeny
VAN1A - 24	24.16		4.94E-06	1.16E-04	7.59E-05	1.20E-04	1.20E-04	1.97E-04	2.63E-05
VAN1A - M9	24.86		8.53E-09	2.78E-07	5.26E-07	2.84E-07	2.84E-07	4.04E-07	3.09E-07
VAN1A - 25	25.56	5.58E-07	3.61E-05	2.15E-05	8.71E-06	2.14E-05	2.14E-05	2.02E-05	5.32E-06
VAN1A - 86.4-86.8	26.40	2.27E-06	1.15E-07	4.24E-06	5.53E-06	4.37E-06	4.37E-06	7.07E-06	5.11E-06
VAN1A - M10	27.81		2.54E-07	2.51E-06	4.31E-06	2.61E-06	2.61E-06	4.60E-06	2.75E-06
VAN1A - 26	28.25		3.37E-06	2.68E-06	1.84E-06	2.68E-06	2.68E-06	2.67E-06	2.85E-06
VAN1A - 27	29.25	1.39E-08	2.37E-09	7.38E-07	1.10E-06	7.53E-07	7.53E-07	1.06E-06	8.50E-07
VAN1A - M11	30.86		7.04E-05	1.83E-04	1.76E-04	1.92E-04	1.92E-04	4.04E-04	4.87E-05
VAN1A - 29	32.75	2.80E-07	2.16E-08	5.08E-07	9.01E-07	5.21E-07	5.21E-07	7.71E-07	5.40E-07
VAN1A - M12	35.89		4.16E-05	6.50E-07	4.67E-07	6.42E-07	6.42E-07	5.15E-07	5.77E-07
VAN1A - 31	36.10	3.40E-07	5.69E-06	1.36E-07	1.37E-07	1.34E-07	1.34E-07	1.08E-07	4.37E-07
VAN1A - M13	36.96		4.56E-07	6.50E-08	7.80E-08	6.42E-08	6.42E-08	5.21E-08	1.35E-07
VAN1A - 32	37.08	8.71E-07	1.03E-08	4.18E-07	5.25E-07	4.22E-07	4.22E-07	4.87E-07	3.78E-07

Sample ID	Depth (m)	Ksat (m/s) Kozeny Carman	Ksat (m/s) KC (Carrier)	Ksat (m/s) Kruger	Ksat (m/s) Krumbein	Ksat (m/s) NAVFAC	Ksat (m/s) Pavchich	Ksat (m/s) Sauerbrei
VAN1A - 24	24.16	2.88E-04	2.63E-05	1.61E-05	5.21E-06	2.42E-03	1.89E-04	2.84E-04
VAN1A - M9	24.86	5.01E-07	3.09E-07	2.28E-07	2.56E-08	7.26E-07	1.77E-07	2.42E-07
VAN1A - 25	25.56	1.81E-05	5.32E-06	5.54E-06	6.21E-06	6.76E-05	5.29E-05	5.56E-05
VAN1A - 86.4-86.8	26.40	1.01E-05	5.11E-06	3.18E-06	1.21E-07	3.92E-05	9.07E-06	1.35E-05
VAN1A - M10	27.81	7.38E-06	2.75E-06	1.55E-06	3.08E-08	3.12E-05	8.70E-06	1.38E-05
VAN1A - 26	28.25	2.48E-06	2.85E-06	2.86E-06	5.88E-06	4.36E-06	2.88E-06	3.16E-06
VAN1A - 27	29.25	1.29E-06	8.50E-07	6.22E-07	2.63E-08	2.37E-06	5.41E-07	7.33E-07
VAN1A - M11	30.86	8.45E-04	4.87E-05	2.27E-05	1.66E-06	1.02E-02	2.38E-04	4.40E-04
VAN1A - 29	32.75	9.98E-07	5.40E-07	3.77E-07	2.76E-09	1.87E-06	3.40E-07	4.77E-07
VAN1A - M12	35.89	4.31E-07	5.77E-07	7.10E-07	5.48E-06	3.71E-07	6.37E-07	4.10E-07
VAN1A - 31	36.10	9.00E-08	4.37E-07	5.37E-07	9.17E-07	4.08E-08	1.46E-06	1.03E-06
VAN1A - M13	36.96	4.38E-08	1.35E-07	1.65E-07	4.09E-07	1.49E-08	5.60E-08	4.66E-08
VAN1A - 32	37.08	5.00E-07	3.78E-07	3.44E-07	7.62E-08	5.44E-07	2.23E-07	2.70E-07

Sample ID	Depth (m)	Ksat (m/s) Slichter	Ksat (m/s) Terzaghi	Ksat (m/s) USBR	Ksat (m/s) Zamarin	Ksat (m/s) Zunker
VAN1A - 24	24.16	2.59E-04	2.92E-04	1.92E-04	2.21E-05	2.04E-05
VAN1A - M9	24.86	4.76E-07	5.25E-07	8.12E-08	2.62E-07	2.70E-07
VAN1A - 25	25.56	1.92E-05	1.90E-05	1.28E-04	5.74E-06	5.32E-06
VAN1A - 86.4-86.8	26.40	9.16E-06	1.03E-05	5.58E-06	5.03E-06	8.85E-06
VAN1A - M10	27.81	6.40E-06	7.28E-06	4.52E-06	2.53E-06	5.19E-06
VAN1A - 26	28.25	2.59E-06	2.62E-06	8.39E-06	3.17E-06	3.36E-06
VAN1A - 27	29.25	1.23E-06	1.36E-06	3.24E-07	8.09E-07	1.08E-06
VAN1A - M11	30.86	6.62E-04	7.64E-04	1.38E-04	3.11E-05	2.79E-05
VAN1A - 29	32.75	9.35E-07	1.04E-06	1.60E-07	4.74E-07	5.72E-07
VAN1A - M12	35.89	4.69E-07	4.40E-07	6.30E-07	6.20E-07	5.59E-07
VAN1A - 31	36.10	9.78E-08	9.18E-08	4.85E-06	4.64E-07	4.14E-07
VAN1A - M13	36.96	4.75E-08	4.47E-08	4.75E-08	1.41E-07	1.28E-07
VAN1A - 32	37.08	5.06E-07	5.34E-07	1.53E-07	3.65E-07	3.67E-07

Sample ID	Depth (m)	K_{sat} (m/s) Measured	K_{sat} (m/s) Alyamani	K_{sat} (m/s) Beyer	K_{sat} (m/s) Chapuis	K_{sat} (m/s) Harleman	K_{sat} (m/s) Hazen New	K_{sat} (m/s) Hazen Original	K_{sat} (m/s) Kozeny
VE1A - 1	1.83	8.37E-07	1.00E-05	3.51E-07	2.89E-07	3.47E-07	3.47E-07	2.78E-07	5.58E-07
VE1A - 2	2.30		4.35E-06	5.22E-07	3.94E-07	5.16E-07	5.16E-07	4.15E-07	4.81E-07
VE1A - 3	2.51	1.19E-06	6.70E-07	2.53E-07	2.48E-07	2.51E-07	2.51E-07	2.21E-07	3.14E-07
VE1A - 4	3.22	7.05E-08	4.09E-06	3.81E-07	3.10E-07	3.76E-07	3.76E-07	3.04E-07	4.32E-07
VE1A - 5	4.62	4.75E-07	1.31E-07	1.80E-07	2.07E-07	1.79E-07	1.79E-07	1.69E-07	2.10E-07
VE1A - 6	4.89		5.78E-07	1.77E-07	1.78E-07	1.75E-07	1.75E-07	1.48E-07	2.34E-07
VE1A - 7	5.36	4.41E-07							
VE1A - 8	6.45	1.18E-05	2.09E-06	5.07E-05	2.82E-05	5.15E-05	5.15E-05	6.94E-05	9.39E-06
VE1A - 9	6.69	8.77E-07	1.98E-07	9.79E-06	9.66E-06	1.01E-05	1.01E-05	1.54E-05	4.75E-06
VE1A - 10	6.89	4.55E-06	1.31E-05	4.29E-05	5.10E-05	4.49E-05	4.49E-05	8.99E-05	2.29E-05
VE1A - 11	7.19		2.67E-06	6.94E-06	3.32E-06	6.89E-06	6.89E-06	6.08E-06	1.58E-06
VE1A - 12	7.47	1.10E-06	1.02E-07	1.31E-05	9.37E-06	1.33E-05	1.33E-05	1.74E-05	4.85E-06
VE1A - 13	7.76		5.99E-04	2.64E-05	8.48E-06	2.61E-05	2.61E-05	2.09E-05	2.54E-06

Sample ID	Depth (m)	K_{sat} (m/s) Kozeny Carman	K_{sat} (m/s) KC (Carrier)	K_{sat} (m/s) Kruger	K_{sat} (m/s) Krumbein	K_{sat} (m/s) NAVFAC	K_{sat} (m/s) Pavchich	K_{sat} (m/s) Sauerbrei
VE1A - 1	1.83	2.33E-07	5.58E-07	6.65E-07	2.54E-06	1.56E-07	1.32E-06	9.58E-07
VE1A - 2	2.30	3.47E-07	4.81E-07	5.87E-07	2.85E-06	2.74E-07	6.04E-07	4.55E-07
VE1A - 3	2.51	1.92E-07	3.14E-07	3.50E-07	1.38E-07	1.22E-07	2.21E-07	2.17E-07
VE1A - 4	3.22	2.55E-07	4.32E-07	5.13E-07	8.55E-07	1.78E-07	4.74E-07	3.86E-07
VE1A - 5	4.62	1.52E-07	2.10E-07	2.21E-07	3.45E-09	9.18E-08	1.18E-07	1.24E-07
VE1A - 6	4.89	1.26E-07	2.34E-07	2.70E-07	4.55E-08	6.69E-08	1.47E-07	1.36E-07
VE1A - 7	5.36							
VE1A - 8	6.45	8.15E-05	9.39E-06	7.05E-06	2.81E-06	4.76E-04	1.05E-04	1.39E-04
VE1A - 9	6.69	2.07E-05	4.75E-06	3.12E-06	6.51E-06	8.86E-05	1.45E-05	2.08E-05
VE1A - 10	6.89	1.73E-04	2.29E-05	1.11E-05	8.75E-07	1.60E-03	5.60E-05	9.84E-05
VE1A - 11	7.19	5.29E-06	1.58E-06	1.73E-06	2.35E-06	1.24E-05	1.32E-05	1.30E-05
VE1A - 12	7.47	1.99E-05	4.85E-06	3.73E-06	3.21E-06	7.61E-05	1.52E-05	1.98E-05
VE1A - 13	7.76	1.75E-05	2.54E-06	2.98E-06	2.56E-05	6.85E-05	3.76E-05	2.39E-05

Sample ID	Depth (m)	K_{sat} (m/s) Slichter	K_{sat} (m/s) Terzaghi	K_{sat} (m/s) USBR	K_{sat} (m/s) Zamarin	K_{sat} (m/s) Zunker
VE1A - 1	1.83	2.53E-07	2.38E-07	3.43E-06	5.84E-07	5.38E-07
VE1A - 2	2.30	3.77E-07	3.54E-07	8.30E-07	5.29E-07	5.17E-07
VE1A - 3	2.51	2.06E-07	1.99E-07	2.68E-07	3.33E-07	3.43E-07
VE1A - 4	3.22	2.77E-07	2.61E-07	7.29E-07	4.63E-07	4.49E-07
VE1A - 5	4.62	1.61E-07	1.60E-07	9.70E-08	2.11E-07	2.06E-07
VE1A - 6	4.89	1.36E-07	1.30E-07	1.45E-07	2.47E-07	2.44E-07
VE1A - 7	5.36					
VE1A - 8	6.45	7.88E-05	8.60E-05	1.51E-04	8.43E-06	7.52E-06
VE1A - 9	6.69	1.91E-05	2.13E-05	1.27E-05	4.05E-06	4.46E-06
VE1A - 10	6.89	1.40E-04	1.61E-04	2.92E-05	1.63E-05	1.92E-05
VE1A - 11	7.19	5.66E-06	5.50E-06	2.29E-05	1.65E-06	1.55E-06
VE1A - 12	7.47	1.95E-05	2.11E-05	1.95E-05	4.57E-06	4.84E-06
VE1A - 13	7.76	1.90E-05	1.79E-05	8.09E-05	2.77E-06	2.56E-06

Sample ID	Depth (m)	K_{sat} (m/s) Measured	K_{sat} (m/s) Alyamani	K_{sat} (m/s) Beyer	K_{sat} (m/s) Chapuis	K_{sat} (m/s) Harleman	K_{sat} (m/s) Hazen New	K_{sat} (m/s) Hazen Original	K_{sat} (m/s) Kozeny
VPV1A - 1	xx	2.53E-06							
VPV1A - 2	xx	3.85E-06	2.26E-06	4.78E-07	3.74E-07	4.72E-07	4.72E-07	3.85E-07	4.01E-07
VPV1A - 3	xx	5.87E-06	2.11E-06	4.08E-07	3.28E-07	4.03E-07	4.03E-07	3.27E-07	3.55E-07
VPV1A - 4	xx	1.12E-05	2.05E-05	1.42E-06	8.62E-07	1.40E-06	1.40E-06	1.13E-06	9.99E-07
VPV1A - 5	xx	8.77E-06	5.47E-05	9.18E-07	6.12E-07	9.06E-07	9.06E-07	7.27E-07	7.53E-07
VPV1A - 6	xx	1.12E-06	1.10E-05	3.65E-07	2.98E-07	3.61E-07	3.61E-07	2.90E-07	4.22E-07
VPV1A - 7	xx	2.12E-06	3.25E-06	3.26E-07	2.73E-07	3.22E-07	3.22E-07	2.59E-07	3.51E-07
VPV1A - 8	xx	3.57E-07	2.23E-06	4.69E-07	3.68E-07	4.63E-07	4.63E-07	3.77E-07	4.03E-07
VPV1A - 9	xx	2.78E-07							
VPV1A - 11	xx	4.65E-06	1.88E-06	4.00E-07	3.27E-07	3.95E-07	3.95E-07	3.24E-07	3.51E-07
VPV1A - 12	xx	4.01E-08	5.64E-06	1.82E-06	1.14E-06	1.80E-06	1.80E-06	1.56E-06	1.05E-06
VPV1A - 13	xx	5.13E-06	5.44E-06	8.76E-07	6.05E-07	8.66E-07	8.66E-07	7.11E-07	7.41E-07
VPV1A - 14	xx	7.75E-06	1.46E-05	4.91E-07	3.75E-07	4.85E-07	4.85E-07	3.89E-07	5.07E-07
VPV1A - 15	xx	2.51E-07							
VPV1A - 16	xx	3.87E-06	8.51E-05	3.93E-06	1.91E-06	3.88E-06	3.88E-06	3.12E-06	2.19E-06
VPV1A - 17	xx	3.14E-06	2.79E-05	4.88E-07	3.73E-07	4.82E-07	4.82E-07	3.87E-07	5.54E-07
VPV1A - 18	xx	7.17E-06	5.36E-06	3.00E-07	2.55E-07	2.96E-07	2.96E-07	2.38E-07	3.69E-07
VPV1A - 19	xx	4.22E-06	5.66E-06	2.65E-07	2.32E-07	2.62E-07	2.62E-07	2.10E-07	3.03E-07
VPV1A - 20	xx	1.44E-05	8.40E-05	1.54E-07	1.51E-07	1.52E-07	1.52E-07	1.22E-07	6.42E-07
VPV1A - 21	xx	1.23E-05	6.88E-05	2.99E-06	1.55E-06	2.95E-06	2.95E-06	2.38E-06	1.46E-06
VPV1A - 22	xx	1.12E-05	9.97E-05	1.66E-06	9.74E-07	1.64E-06	1.64E-06	1.32E-06	1.17E-06
VPV1A - 23	0.56		1.97E-06	1.63E-06	1.08E-06	1.62E-06	1.62E-06	1.44E-06	1.07E-06
VPV1A - 26	3.62		2.50E-06	2.14E-07	1.96E-07	2.12E-07	2.12E-07	1.70E-07	2.49E-07
VPV1A - 27	3.96		1.89E-06	2.45E-07	2.19E-07	2.42E-07	2.42E-07	1.95E-07	2.64E-07

Sample ID	Depth (m)	K_{sat} (m/s) Kozeny Carman	K_{sat} (m/s) KC (Carrier)	K_{sat} (m/s) Kruger	K_{sat} (m/s) Krumbein	K_{sat} (m/s) NAVFAC	K_{sat} (m/s) Pavchich	K_{sat} (m/s) Sauerbrei
VPV1A - 1	xx							
VPV1A - 2	xx	3.24E-07	4.01E-07	4.87E-07	1.50E-06	2.49E-07	3.52E-07	3.00E-07
VPV1A - 3	xx	2.74E-07	3.55E-07	4.31E-07	1.79E-06	1.97E-07	2.97E-07	2.45E-07
VPV1A - 4	xx	9.44E-07	9.99E-07	1.21E-06	2.40E-06	1.12E-06	2.94E-06	2.27E-06
VPV1A - 5	xx	6.09E-07	7.53E-07	9.08E-07	2.80E-06	6.03E-07	1.04E-06	6.30E-07
VPV1A - 6	xx	2.42E-07	4.22E-07	5.18E-07	3.21E-06	1.65E-07	5.37E-07	3.38E-07
VPV1A - 7	xx	2.17E-07	3.51E-07	4.30E-07	1.73E-06	1.41E-07	3.21E-07	2.48E-07
VPV1A - 8	xx	3.18E-07	4.03E-07	4.87E-07	1.10E-06	2.42E-07	3.63E-07	3.09E-07
VPV1A - 9	xx							
VPV1A - 11	xx	2.74E-07	3.51E-07	4.23E-07	2.98E-06	1.97E-07	2.74E-07	2.39E-07
VPV1A - 12	xx	1.35E-06	1.05E-06	1.20E-06	5.31E-06	1.85E-06	5.78E-06	5.60E-06
VPV1A - 13	xx	6.01E-07	7.41E-07	8.89E-07	3.53E-06	5.93E-07	2.38E-06	2.08E-06
VPV1A - 14	xx	3.26E-07	5.07E-07	6.20E-07	2.76E-06	2.50E-07	7.27E-07	4.83E-07
VPV1A - 15	xx							
VPV1A - 16	xx	2.61E-06	2.19E-06	2.60E-06	8.49E-06	4.69E-06	7.28E-06	5.51E-06
VPV1A - 17	xx	3.24E-07	5.54E-07	6.77E-07	3.10E-06	2.48E-07	1.03E-06	6.32E-07
VPV1A - 18	xx	1.99E-07	3.69E-07	4.54E-07	1.87E-06	1.25E-07	3.58E-07	2.64E-07
VPV1A - 19	xx	1.76E-07	3.03E-07	3.73E-07	3.01E-06	1.05E-07	2.84E-07	1.76E-07
VPV1A - 20	xx	1.02E-07	6.42E-07	7.87E-07	9.88E-06	4.86E-08	1.43E-05	6.67E-06
VPV1A - 21	xx	1.99E-06	1.46E-06	1.74E-06	2.85E-06	3.20E-06	8.46E-06	6.37E-06
VPV1A - 22	xx	1.10E-06	1.17E-06	1.41E-06	3.04E-06	1.39E-06	5.20E-06	3.45E-06
VPV1A - 23	0.56	1.26E-06	1.07E-06	1.18E-06	1.51E-06	1.69E-06	2.73E-06	2.73E-06
VPV1A - 26	3.62	1.42E-07	2.49E-07	3.04E-07	2.31E-06	7.79E-08	1.87E-07	1.32E-07
VPV1A - 27	3.96	1.63E-07	2.64E-07	3.21E-07	1.91E-06	9.46E-08	1.86E-07	1.46E-07

Sample ID	Depth (m)	K_{sat} (m/s) Slichter	K_{sat} (m/s) Terzaghi	K_{sat} (m/s) USBR	K_{sat} (m/s) Zamarin	K_{sat} (m/s) Zunker
VPV1A - 1	xx					
VPV1A - 2	xx	3.52E-07	3.32E-07	4.24E-07	4.41E-07	4.28E-07
VPV1A - 3	xx	2.98E-07	2.80E-07	3.32E-07	3.86E-07	3.71E-07
VPV1A - 4	xx	1.03E-06	9.63E-07	5.62E-06	1.10E-06	1.06E-06
VPV1A - 5	xx	6.61E-07	6.20E-07	1.08E-06	8.24E-07	8.04E-07
VPV1A - 6	xx	2.63E-07	2.47E-07	6.09E-07	4.53E-07	4.18E-07
VPV1A - 7	xx	2.36E-07	2.21E-07	3.84E-07	3.80E-07	3.58E-07
VPV1A - 8	xx	3.44E-07	3.25E-07	4.49E-07	4.42E-07	4.31E-07
VPV1A - 9	xx					
VPV1A - 11	xx	2.97E-07	2.81E-07	3.14E-07	3.81E-07	3.65E-07
VPV1A - 12	xx	1.45E-06	1.40E-06	9.31E-06	1.14E-06	1.08E-06
VPV1A - 13	xx	6.51E-07	6.16E-07	5.05E-06	8.17E-07	7.85E-07
VPV1A - 14	xx	3.54E-07	3.32E-07	9.47E-07	5.48E-07	5.10E-07
VPV1A - 15	xx					
VPV1A - 16	xx	2.84E-06	2.66E-06	1.50E-05	2.52E-06	2.59E-06
VPV1A - 17	xx	3.52E-07	3.30E-07	1.47E-06	5.93E-07	5.44E-07
VPV1A - 18	xx	2.17E-07	2.03E-07	4.47E-07	3.96E-07	3.64E-07
VPV1A - 19	xx	1.91E-07	1.80E-07	2.44E-07	3.22E-07	2.94E-07
VPV1A - 20	xx	1.11E-07	1.04E-07	1.90E-05	6.58E-07	5.48E-07
VPV1A - 21	xx	2.16E-06	2.03E-06	1.72E-05	1.59E-06	1.49E-06
VPV1A - 22	xx	1.20E-06	1.12E-06	1.08E-05	1.26E-06	1.15E-06
VPV1A - 23	0.56	1.35E-06	1.32E-06	4.83E-06	1.20E-06	1.32E-06
VPV1A - 26	3.62	1.55E-07	1.45E-07	1.56E-07	2.62E-07	2.39E-07
VPV1A - 27	3.96	1.77E-07	1.67E-07	1.81E-07	2.80E-07	2.60E-07

Sample ID	Depth (m)	Ksat (m/s) Measured	Ksat (m/s) Alyamani	Ksat (m/s) Beyer	Ksat (m/s) Chapuis	Ksat (m/s) Harleman	Ksat (m/s) Hazen New	Ksat (m/s) Hazen Original	Ksat (m/s) Kozeny
VPV1A - 28	4.45		6.63E-06	2.20E-07	2.00E-07	2.17E-07	2.17E-07	1.75E-07	2.87E-07
VPV1A - 29	4.76		2.43E-06	5.41E-08	6.68E-08	5.34E-08	5.34E-08	4.29E-08	1.85E-07
VPV1A - 30	4.93	1.57E-07							
VPV1A - 31	5.33								
VPV1A - 34	7.28		1.13E-05	3.70E-07	3.01E-07	3.65E-07	3.65E-07	2.93E-07	4.37E-07
VPV1A - 35	7.34		6.85E-09	1.45E-07	2.21E-07	1.46E-07	1.46E-07	1.65E-07	1.92E-07
VPV1A - 36	7.44	7.59E-07							
VPV1A - 37	7.57		3.31E-06	7.38E-07	5.34E-07	7.30E-07	7.30E-07	6.04E-07	6.15E-07
VPV1A - 44	11.63		2.24E-05	4.71E-04	2.33E-04	4.87E-04	4.87E-04	8.12E-04	2.12E-05
VPV1A - 50	17.07		1.15E-06	2.02E-07	1.91E-07	1.99E-07	1.99E-07	1.63E-07	2.66E-07
VPV1A - 51	17.63		2.31E-07	5.12E-07	4.82E-07	5.10E-07	5.10E-07	4.93E-07	4.13E-07
VPV1A - 52	18.66		8.56E-07	6.13E-07	4.99E-07	6.08E-07	6.08E-07	5.38E-07	4.48E-07
VPV1A - 53	19.46	9.10E-08	5.40E-07	1.44E-07	1.49E-07	1.42E-07	1.42E-07	1.18E-07	2.02E-07
VPV1A - 54	20.24		4.94E-07	2.87E-07	2.70E-07	2.84E-07	2.84E-07	2.47E-07	2.60E-07
VPV1A - 55	21.69	7.17E-08	5.30E-07	4.47E-07	3.95E-07	4.44E-07	4.44E-07	3.97E-07	3.65E-07
VPV1A - 57	22.91	6.91E-08	6.91E-08	2.07E-07	2.96E-07	2.08E-07	2.08E-07	2.37E-07	2.48E-07
VPV1A - 58	23.09	6.91E-08							
VPV1A - 59	23.34	1.65E-06	5.08E-06	5.92E-07	4.35E-07	5.84E-07	5.84E-07	4.71E-07	6.14E-07
VPV1A - 61	25.30								
VPV1A - 63	27.74	9.48E-08							
VPV1A - 64	28.02	3.41E-08	1.94E-08	4.30E-07	7.74E-07	4.40E-07	4.40E-07	6.43E-07	4.91E-07
VPV1A - 65	29.13	6.01E-07	1.60E-08	7.56E-07	1.11E-06	7.70E-07	7.70E-07	1.07E-06	8.55E-07

Sample ID	Depth (m)	Ksat (m/s) Kozeny Carman	Ksat (m/s) KC (Carrier)	Ksat (m/s) Kruger	Ksat (m/s) Krumbein	Ksat (m/s) NAVFAC	Ksat (m/s) Pavchich	Ksat (m/s) Sauerbrei
VPV1A - 28	4.45	1.46E-07	2.87E-07	3.50E-07	2.78E-06	8.08E-08	2.56E-07	1.55E-07
VPV1A - 29	4.76	3.59E-08	1.85E-07	2.25E-07	2.41E-06	1.12E-08	9.77E-08	5.93E-08
VPV1A - 30	4.93							
VPV1A - 31	5.33							
VPV1A - 34	7.28	2.45E-07	4.37E-07	5.27E-07	7.96E-06	1.68E-07	5.10E-07	3.41E-07
VPV1A - 35	7.34	1.66E-07	1.92E-07	1.76E-07	2.22E-07	1.21E-07	9.16E-08	1.09E-07
VPV1A - 36	7.44							
VPV1A - 37	7.57	5.12E-07	6.15E-07	7.26E-07	1.19E-06	4.74E-07	7.13E-07	6.38E-07
VPV1A - 44	11.63	1.21E-03	2.12E-05	1.25E-05	8.46E-07	1.40E-02	1.02E-03	1.54E-03
VPV1A - 50	17.07	1.37E-07	2.66E-07	3.21E-07	1.29E-06	7.43E-08	1.84E-07	1.58E-07
VPV1A - 51	17.63	4.49E-07	4.13E-07	4.30E-07	5.26E-07	4.14E-07	2.65E-07	2.84E-07
VPV1A - 52	18.66	4.69E-07	4.48E-07	4.97E-07	1.36E-06	4.26E-07	2.92E-07	2.89E-07
VPV1A - 53	19.46	1.00E-07	2.02E-07	2.40E-07	5.03E-07	4.83E-08	1.20E-07	1.08E-07
VPV1A - 54	20.24	2.14E-07	2.60E-07	3.00E-07	7.10E-07	1.42E-07	1.62E-07	1.57E-07
VPV1A - 55	21.69	3.48E-07	3.65E-07	4.07E-07	6.27E-07	2.83E-07	2.49E-07	2.50E-07
VPV1A - 57	22.91	2.41E-07	2.48E-07	2.25E-07	5.54E-08	2.01E-07	1.18E-07	1.41E-07
VPV1A - 58	23.09							
VPV1A - 59	23.34	3.94E-07	6.14E-07	7.42E-07	3.78E-06	3.27E-07	2.25E-06	1.74E-06
VPV1A - 61	25.30							
VPV1A - 63	27.74							
VPV1A - 64	28.02	8.22E-07	4.91E-07	3.47E-07	3.20E-08	1.43E-06	2.82E-07	3.92E-07
VPV1A - 65	29.13	1.30E-06	8.55E-07	6.29E-07	5.08E-09	2.35E-06	7.49E-07	1.01E-06

Sample ID	Depth (m)	Ksat (m/s) Slichter	Ksat (m/s) Terzaghi	Ksat (m/s) USBR	Ksat (m/s) Zamarin	Ksat (m/s) Zunker
VPV1A - 28	4.45	1.59E-07	1.49E-07	2.04E-07	3.01E-07	2.73E-07
VPV1A - 29	4.76	3.90E-08	3.66E-08	7.14E-08	1.90E-07	1.68E-07
VPV1A - 30	4.93					
VPV1A - 31	5.33					
VPV1A - 34	7.28	2.67E-07	2.50E-07	6.14E-07	4.62E-07	4.28E-07
VPV1A - 35	7.34	1.69E-07	1.77E-07	5.60E-08	1.75E-07	1.62E-07
VPV1A - 36	7.44					
VPV1A - 37	7.57	5.54E-07	5.25E-07	1.14E-06	6.77E-07	6.75E-07
VPV1A - 44	11.63	1.08E-03	1.22E-03	1.28E-03	1.52E-05	1.30E-05
VPV1A - 50	17.07	1.49E-07	1.40E-07	1.99E-07	2.85E-07	2.73E-07
VPV1A - 51	17.63	4.73E-07	4.73E-07	2.47E-07	4.29E-07	4.41E-07
VPV1A - 52	18.66	5.02E-07	4.87E-07	2.91E-07	4.77E-07	4.86E-07
VPV1A - 53	19.46	1.09E-07	1.03E-07	1.13E-07	2.14E-07	2.02E-07
VPV1A - 54	20.24	2.29E-07	2.22E-07	1.62E-07	2.75E-07	2.64E-07
VPV1A - 55	21.69	3.72E-07	3.63E-07	2.59E-07	3.88E-07	3.89E-07
VPV1A - 57	22.91	2.44E-07	2.56E-07	7.79E-08	2.29E-07	2.19E-07
VPV1A - 58	23.09					
VPV1A - 59	23.34	4.28E-07	4.02E-07	4.76E-06	6.75E-07	6.52E-07
VPV1A - 61	25.30					
VPV1A - 63	27.74					
VPV1A - 64	28.02	7.73E-07	8.57E-07	1.31E-07	4.14E-07	4.51E-07
VPV1A - 65	29.13	1.24E-06	1.36E-06	5.60E-07	8.40E-07	1.21E-06

Appendix B

Grain-size analysis values, and calculated and lab measured porosity values. (Blank values indicate there insufficient sample to perform; sieve analysis, for calculated porosity; permeameter analysis, for measured porosity)

Sample ID	Depth (m)	% Sand	% Silt	% Clay	Calculated Porosity	Measured Porosity
ARS1A - 1	0.23	11	86	4	0.38	
ARS1A - 2	0.66	67	28	6	0.26	
ARS1A - 3	1.03	79	14	8	0.26	0.23
ARS1A - 4	2.26	59	38	3	0.26	
ARS1A - 5	2.69					0.45
ARS1A - 6	3.40	79	18	3	0.26	
ARS1A - 7	3.75	66	29	5	0.26	
ARS1A - 8	4.66	69	8	23		0.36
ARS1A - 12	7.48	85	5	11	0.39	
ARS1A - 14	8.67	52	44	4	0.27	
ARS1A - 15	9.51	73	22	5	0.26	
ARS1A - 16	10.30	55	42	3	0.27	
ARS1A - 17	11.28	44	51	5	0.28	0.28

Sample ID	Depth (m)	% Sand	% Silt	% Clay	Calculated Porosity	Measured Porosity
FRE1A - 1	0.62	75	17	8	0.26	
FRE1A - 2	2.67	30	62	8	0.32	
FRE1A - 3	3.83	54	41	5	0.26	
FRE1A - 4	4.19					
FRE1A - 5	4.94					
FRE1A - 6	8.31					
FRE1A - 7	9.98	81	15	4	0.27	
FRE1A - 8	10.42	88	4	8	0.28	
FRE1A - 9	11.05	67	32	1	0.27	
FRE1A - 10	11.51	91	2	6	0.34	
FRE1A - 11	12.74	43	52	5	0.28	
FRE1A - 12	13.64	91	7	2	0.28	
FRE1A - 13	14.39	50	44	6	0.26	
FRE1A - 14	15.77	72	24	4	0.26	

Sample ID	Depth (m)	% Sand	% Silt	% Clay	Calculated Porosity	Measured Porosity
GDC1A - 1	0.93	47	47	6	0.27	0.42
GDC1A - 2	4.24	40	53	7	0.28	0.32
GDC1A - 3	4.65	37	39	25	0.26	
GDC1A - 4	6.02	47	40	13	0.26	0.33
GDC1A - 5	7.54	5	73	22	0.33	0.43
GDC1A - 6	9.07	37	53	10	0.28	0.37
GDC1A - 7	9.58	23	60	17	0.28	0.40
GDC1A - 8	11.20	35	39	27	0.26	0.44
GDC1A - 9	12.12	37	46	17	0.26	0.40
GDC1A - 10	15.16	22	44	34	0.29	0.41
GDC1A - 11	16.69	25	47	28	0.27	
GDC1A - 13	24.31	40	53	7	0.28	0.44
GDC1A - 14	30.40	28	41	30	0.27	0.44
GDC1A - 15	36.50	23	57	21	0.31	0.44

Sample ID	Depth (m)	% Sand	% Silt	% Clay	Calculated Porosity	Measured Porosity
GDC2B - 1	1.32	60	38	2	0.27	
GDC2B - 2	2.18	57	40	3	0.28	0.34
GDC2B - 3	4.01	46	50	4	0.28	0.46
GDC2B - 4	4.52	28	69	4	0.35	0.43
GDC2B - 5	4.93	49	46	5	0.27	
GDC2B - 6	5.92	53	38	9	0.26	0.35
GDC2B - 7	6.10	74	21	5	0.26	
GDC2B - 8	7.26	55	42	4	0.28	0.36
GDC2B - 9	7.59	50	41	9	0.26	
GDC2B - 10	8.69					0.45
GDC2B - 11	9.04	47	48	4	0.28	0.40
GDC2B - 12	9.93	58	39	3	0.27	0.36
GDC2B - 13	10.31	67	32	1	0.26	0.36
GDC2B - 14	11.63	26	67	7	0.33	0.38
GDC2B - 15	12.65	23	72	6	0.36	0.43
GDC2B - 16	14.80	28	69	4	0.35	0.49
GDC2B - 17	15.77	32	53	15	0.26	
GDC2B - 18	10.30	45	42	13	0.26	0.36
GDC2B - 19	xxx	32	61	7	0.33	0.49

Sample ID	Depth (m)	% Sand	% Silt	% Clay	Calculated Porosity	Measured Porosity
GDC10A - 1	2.19	89	9	2	0.33	0.30
GDC10A - 2	2.90	23	68	9	0.30	0.50
GDC10A - 3	3.51	1	83	17	0.30	0.50
GDC10A - 4	4.15	68	27	5	0.26	
GDC10A - 5	4.69	14	79	7	0.36	0.49
GDC10A - 6	5.12	29	65	6	0.31	0.52
GDC10A - 7	5.64	66	30	4	0.26	0.40
GDC10A - 8	6.10	37	56	8	0.30	0.41
GDC10A - 9	7.83	74	22	5	0.26	0.23
GDC10A - 10	8.81	69	25	5	0.26	0.35
GDC10A - 11	9.30	65	32	2	0.26	0.31
GDC10A - 12	10.12	53	38	8	0.26	0.32

Sample ID	Depth (m)	% Sand	% Silt	% Clay	Calculated Porosity	Measured Porosity
TGI1A - 1	0.41	52	43	5	0.27	
TGI1A - 2	0.81	49	46	5	0.28	
TGI1A - 4	2.00	45	49	6	0.28	
TGI1A - 5	2.67	71	28	1	0.26	
TGI1A - 6	4.07	47	46	7	0.26	
TGI1A - 7	5.07	58	38	5	0.26	
TGI1A - 8	5.87	83	14	3	0.28	
TGI1A -9	6.88					0.50
TGI1A - 10	8.19	46	43	11	0.26	0.34
TGI1A - 11	9.19	51	46	3	0.26	
TGI1A - 13	12.18	25	64	11	0.29	0.34
TGI1A - 15b	13.66	72	25	3	0.35	
TGI1A - 16	14.59	21	75	3	0.34	
TGI1A - 52.5	16.00	24	65	11	0.30	0.40

Sample ID	Depth (m)	% Sand	% Silt	% Clay	Calculated Porosity	Measured Porosity
VAN1A - M1	0.08	59	33	8	0.26	
VAN1A - 3	0.99	35	65	0	0.35	
VAN1A - 4	1.84	86	8	6	0.27	
VAN1A - M2	3.43	66	31	3	0.26	0.40
VAN1A - 6	3.46	71	27	2	0.26	
VAN1A - 8	5.01	72	25	3	0.26	0.33
VAN1A - M3	6.17	63	30	7	0.26	
VAN1A - 9	6.48	62	33	6	0.26	
VAN1A - 12	8.92	46	51	3	0.28	
VAN1A - M4	9.53	66	30	5	0.27	
VAN1A - 33.2-33.7	10.20					0.50
VAN1A - 14	10.79					0.44
VAN1A - 15	12.18	50	33	17	0.26	
VAN1A - M5	12.82	79	18	3	0.26	
VAN1A - M6	15.62	94	6	0	0.40	
VAN1A - 17	16.00	82	17	1	0.26	
VAN1A - 18	16.69	74	23	2	0.34	0.45
VAN1A - 56.2-56.7	17.33	40	44	16	0.26	
VAN1A - 58-58.4	17.74	1	98	1	0.40	
VAN1A - M7	18.52	53	43	4	0.29	
VAN1A - 20	19.35	25	60	14	0.28	
VAN1A - 21	21.56	56	42	2	0.29	0.34
VAN1A - M8	21.72	57	41	1	0.32	
VAN1A - 23	23.35	12	66	22	0.30	0.46
VAN1A - 23.51	23.51	63	32	5	0.26	0.65
VAN1A - 24	24.16	92	7	1	0.35	
VAN1A - M9	24.86	21	72	7	0.33	
VAN1A - 25	25.56	89	10	1	0.27	0.43
VAN1A - 86.4-86.8	26.40	72	28	0	0.35	
VAN1A - M10	27.81	53	45	2	0.37	
VAN1A - 26	28.25	80	20	0	0.28	
VAN1A - 27	29.25	39	60	0	0.33	0.46
VAN1A - M11	30.86	96	2	2	0.41	
VAN1A - 29	32.75	24	74	2	0.34	0.54
VAN1A - M12	35.89	70	26	4	0.26	
VAN1A - 31	36.10	76	14	10	0.26	0.46
VAN1A - M13	36.96	45	41	14	0.26	
VAN1A - 32	37.08	41	54	5	0.30	0.36

Sample ID	Depth (m)	% Sand	% Silt	% Clay	Calculated Porosity	Measured Porosity
VE1A - 1	1.83	75	17	8	0.26	0.27
VE1A - 2	2.30	67	28	6	0.26	
VE1A - 3	2.51	55	36	9	0.26	0.51
VE1A - 4	3.22	66	26	7	0.26	0.37
VE1A - 5	4.62	41	52	7	0.27	0.45
VE1A - 6	4.89	50	40	10	0.26	
VE1A - 7	5.36	43	48	9	0.28	0.48
VE1A - 8	6.45	91	7	2	0.32	0.39
VE1A - 9	6.69	83	16	2	0.34	0.40
VE1A - 10	6.89	91	8	1	0.40	0.36
VE1A - 11	7.19	85	9	5	0.26	
VE1A - 12	7.47	85	13	3	0.31	0.38
VE1A - 13	7.76	89	7	4	0.26	

Sample ID	Depth (m)	% Sand	% Silt	% Clay	Calculated Porosity	Measured Porosity
VPV1A - 1	xxx					0.56
VPV1A - 2	xxx	62	32	6	0.26	0.49
VPV1A - 3	xxx	60	33	6	0.26	0.38
VPV1A - 4	xxx	78	19	4	0.26	0.34
VPV1A - 5	xxx	71	27	2	0.26	0.65
VPV1A - 6	xxx	68	25	7	0.26	0.18
VPV1A - 7	xxx	63	29	7	0.26	0.48
VPV1A - 8	xxx	62	32	6	0.26	0.44
VPV1A - 9	xxx					0.37
VPV1A - 11	xxx	60	33	7		0.45
VPV1A - 12	xxx	80	17	3	0.26	0.44
VPV1A - 13	xxx	76	19	5	0.26	0.35
VPV1A - 14	xxx	70	24	6	0.26	0.28
VPV1A - 15	xxx					
VPV1A - 16	xxx	82	17	1	0.26	
VPV1A - 17	xxx	73	22	6	0.26	0.31
VPV1A - 18	xxx	66	26	8	0.26	0.25
VPV1A - 19	xxx	62	30	8	0.26	0.27
VPV1A - 20	xxx	83	7	10	0.26	0.27
VPV1A - 21	xxx	83	14	3	0.26	0.21
VPV1A - 22	xxx	81	15	4	0.26	0.29
VPV1A - 23	0.56	73	23	4	0.27	
VPV1A - 26	3.62	57	35	9	0.26	
VPV1A - 27	3.96	57	34	8	0.26	
VPV1A - 28	4.45	61	30	9	0.26	
VPV1A - 29	4.76	56	30	14	0.26	
VPV1A - 30	4.93					0.36
VPV1A - 31	5.33					
VPV1A - 34	7.28	68	26	6	0.26	
VPV1A - 35	7.34	32	58	10	0.29	
VPV1A - 36	7.44					0.40
VPV1A - 37	7.57	69	26	5	0.26	
VPV1A - 44	11.63	94	3	3	0.36	

Sample ID	Depth (m)	% Sand	% Silt	% Clay	Calculated Porosity	Measured Porosity
VPV1A - 50	17.07	56	34	9	0.26	
VPV1A - 51	17.63	51	45	4	0.27	
VPV1A - 52	18.66	55	42	3	0.26	
VPV1A - 53	19.46	49	41	10	0.26	0.36
VPV1A - 54	20.24	52	41	7	0.26	
VPV1A - 55	21.69	54	41	5	0.27	0.27
VPV1A - 57	22.91	38	53	9	0.29	0.29
VPV1A - 58	23.09					
VPV1A - 59	23.34	74	21	5	0.26	0.40
VPV1A - 61	25.30					
VPV1A - 63	27.74					
VPV1A - 64	28.02	29	67	4	0.33	0.39
VPV1A - 65	29.13	41	56	2	0.32	0.41

Appendix C

Unsaturated soil hydraulic parameters

Sample ID	Depth m	θr (cm^3/cm^3)	θ s (cm^3/cm^3)	α (1/cm)	η (-)
ARS1A - 1	0.23	0.05	0.51	0.01	1.67
ARS1A - 2	0.66	0.03	0.39	0.03	1.42
ARS1A - 3	1.03	0.04	0.38	0.04	1.61
ARS1A - 4	2.26	0.03	0.41	0.02	1.46
ARS1A - 6	3.40	0.03	0.39	0.05	1.66
ARS1A - 7	3.75	0.03	0.39	0.03	1.42
ARS1A - 8	4.66	0.06	0.38	0.03	1.33
ARS1A - 12	7.48	0.06	0.37	0.03	1.81
ARS1A - 14	8.67	0.03	0.41	0.01	1.47
ARS1A - 15	9.51	0.03	0.39	0.04	1.49
ARS1A - 16	10.30	0.03	0.41	0.02	1.45
ARS1A - 17	11.28	0.03	0.42	0.01	1.57

Sample ID	Depth m	θr (cm^3/cm^3)	θs (cm^3/cm^3)	α (1/cm)	η (-)
FRE1A - 1	0.62	0.04	0.38	0.04	1.50
FRE1A - 2	2.67	0.05	0.43	0.00	1.70
FRE1A - 3	3.83	0.03	0.40	0.02	1.45
FRE1A - 7	4.19	0.04	0.39	0.04	1.78
FRE1A - 8	4.94	0.05	0.37	0.03	2.16
FRE1A - 9	8.31	0.03	0.41	0.04	1.43
FRE1A - 10	9.98	0.06	0.37	0.03	0.59
FRE1A - 11	10.42	0.03	0.42	0.01	1.57
FRE1A - 12	11.05	0.05	0.38	0.04	2.72
FRE1A - 13	11.51	0.03	0.40	0.01	1.48
FRE1A - 14	12.74	0.03	0.39	0.04	1.49

Sample ID	Depth m	θr (cm^3/cm^3)	θs (cm^3/cm^3)	α (1/cm)	η (-)
GDC1A - 1	0.93	0.03	0.41	0.01	1.52
GDC1A - 2	4.24	0.04	0.41	0.01	1.60
GDC1A - 3	4.65	0.07	0.42	0.01	1.47
GDC1A - 4	6.02	0.05	0.39	0.01	1.49
GDC1A - 5	7.54	0.08	0.46	0.01	1.60
GDC1A - 6	9.07	0.05	0.41	0.01	1.63
GDC1A - 7	9.58	0.06	0.53	0.00	1.67
GDC1A - 8	11.20	0.07	0.42	0.01	1.47
GDC1A - 9	12.12	0.06	0.41	0.01	1.56
GDC1A - 10	15.16	0.09	0.46	0.01	1.46
GDC1A - 11	16.69	0.08	0.44	0.01	1.52
GDC1A - 13	24.31	0.04	0.41	0.01	1.60
GDC1A - 14	30.40	0.08	0.44	0.01	1.46
GDC1A - 15	36.50	0.07	0.43	0.01	1.63

Sample ID	Depth m	θr (cm^3/cm^3)	θs (cm^3/cm^3)	α (1/cm)	η (-)
GDC2B - 1	1.32	0.03	0.41	0.03	1.42
GDC2B - 2	2.18	0.03	0.41	0.02	1.44
GDC2B - 3	4.01	0.03	0.42	0.01	1.54
GDC2B - 4	4.52	0.04	0.46	0.00	1.72
GDC2B - 5	4.93	0.03	0.41	0.01	1.50
GDC2B - 6	5.92	0.04	0.39	0.02	1.45
GDC2B - 7	6.10	0.03	0.39	0.04	1.52
GDC2B - 8	7.26	0.03	0.41	0.02	1.45
GDC2B - 9	7.59	0.04	0.39	0.01	1.47
GDC2B - 11	9.04	0.03	0.41	0.01	1.53
GDC2B - 12	9.93	0.03	0.41	0.02	1.43
GDC2B - 13	10.31	0.03	0.41	0.04	1.44
GDC2B - 14	11.63	0.05	0.44	0.00	1.72
GDC2B - 15	12.65	0.04	0.46	0.00	1.72
GDC2B - 16	14.80	0.04	0.46	0.00	1.72
GDC2B - 17	15.77	0.06	0.41	0.01	1.63
GDC2B - 18	10.30	0.05	0.40	0.01	1.50
GDC2B - 19	xxx	0.04	0.43	0.00	1.69

Sample ID	Depth m	θr (cm^3/cm^3)	θs (cm^3/cm^3)	α (1/cm)	η (-)
GDC10A - 1	2.19	0.04	0.38	0.04	2.49
GDC10A - 2	2.90	0.05	0.44	0.00	1.72
GDC10A - 3	3.51	0.07	0.48	0.01	1.60
GDC10A - 4	4.15	0.03	0.39	0.04	1.43
GDC10A - 5	4.69	0.05	0.48	0.01	1.70
GDC10A - 6	5.12	0.04	0.44	0.00	1.71
GDC10A - 7	5.64	0.03	0.40	0.03	1.42
GDC10A - 8	6.10	0.04	0.42	0.01	1.64
GDC10A - 9	7.83	0.03	0.39	0.04	1.51
GDC10A - 10	8.81	0.03	0.39	0.04	1.44
GDC10A - 11	9.30	0.03	0.40	0.04	1.43
GDC10A - 12	10.12	0.04	0.39	0.02	1.45

Sample ID	Depth m	θr (cm^3/cm^3)	θs (cm^3/cm^3)	α (1/cm)	η (-)
TGI1A - 1	0.41	0.03	0.40	0.01	1.47
TGI1A - 2	0.81	0.03	0.41	0.01	1.50
TGI1A - 4	2.00	0.04	0.41	0.01	1.54
TGI1A - 5	2.67	0.03	0.41	0.05	1.49
TGI1A - 6	4.07	0.04	0.40	0.01	1.51
TGI1A - 7	5.07	0.03	0.40	0.02	1.43
TGI1A - 8	5.87	0.04	0.39	0.04	1.94
TGI1A - 10	8.19	0.04	0.40	0.01	1.51
TGI1A - 11	9.19	0.03	0.42	0.01	1.48
TGI1A - 13	12.18	0.05	0.43	0.00	1.71
TGI1A - 16	14.59	0.04	0.48	0.01	1.72
TGI1A - 52.5	16.00	0.05	0.43	0.00	1.71

Sample ID	Depth m	θr (cm^3/cm^3)	θs (cm^3/cm^3)	α (1/cm)	η (-)
VAN1A - M1	0.08	0.04	0.39	0.02	1.42
VAN1A - 3	0.99	0.03	0.47	0.01	1.66
VAN1A - 4	1.84	0.05	0.38	0.04	2.02
VAN1A - M2	3.43	0.03	0.40	0.04	1.43
VAN1A - 6	3.46	0.03	0.40	0.04	1.47
VAN1A - 8	5.01	0.03	0.40	0.04	1.49
VAN1A - M3	6.17	0.04	0.39	0.03	1.41
VAN1A - 9	6.48	0.03	0.39	0.03	1.41
VAN1A - 12	8.92	0.03	0.43	0.01	1.55
VAN1A - M4	9.53	0.03	0.39	0.03	1.42
VAN1A - 15	12.18	0.06	0.39	0.02	1.43
VAN1A - M5	12.82	0.03	0.39	0.05	1.71
VAN1A - M6	15.62	0.05	0.38	0.04	3.41
VAN1A - 17	16.00	0.03	0.39	0.05	1.87
VAN1A - 18	16.69	0.03	0.40	0.05	1.54
VAN1A - 56.2-56.7	17.33	0.06	0.40	0.01	1.54
VAN1A - 58-58.4	17.74	0.05	0.57	0.01	1.62
VAN1A - M7	18.52	0.03	0.41	0.02	1.46
VAN1A - 20	19.35	0.06	0.42	0.00	1.68
VAN1A - 21	21.56	0.03	0.42	0.02	1.44
VAN1A - M8	21.72	0.03	0.42	0.02	1.44
VAN1A - 23	23.35	0.08	0.45	0.01	1.62
VAN1A - 23.51	23.51	0.03	0.39	0.03	1.41
VAN1A - 24	24.16	0.05	0.38	0.04	3.03
VAN1A - M9	24.86	0.05	0.46	0.00	1.72
VAN1A - 25	25.56	0.04	0.39	0.04	2.57
VAN1A - 86.4-86.8	26.40	0.03	0.41	0.05	1.51
VAN1A - M10	27.81	0.03	0.42	0.02	1.47
VAN1A - 26	28.25	0.03	0.40	0.05	1.77
VAN1A - 27	29.25	0.03	0.46	0.01	1.63
VAN1A - M11	30.86	0.05	0.38	0.03	3.63
VAN1A - 29	32.75	0.04	0.48	0.01	1.71
VAN1A - M12	35.89	0.03	0.39	0.04	1.45
VAN1A - 31	36.10	0.05	0.38	0.04	1.50
VAN1A - M13	36.96	0.05	0.40	0.01	1.50
VAN1A - 32	37.08	0.04	0.42	0.01	1.60

Sample ID	Depth m	θr (cm^3/cm^3)	θs (cm^3/cm^3)	α (1/cm)	η (-)
VE1A - 1	1.83	0.04	0.38	0.04	1.50
VE1A - 2	2.30	0.03	0.39	0.03	1.42
VE1A - 3	2.51	0.04	0.39	0.02	1.43
VE1A - 4	3.22	0.04	0.39	0.03	1.42
VE1A - 5	4.62	0.04	0.41	0.01	1.60
VE1A - 6	4.89	0.04	0.39	0.01	1.47
VE1A - 7	5.36	0.04	0.40	0.01	1.56
VE1A - 8	6.45	0.05	0.38	0.04	2.76
VE1A - 9	6.69	0.04	0.39	0.05	1.93
VE1A - 10	6.89	0.04	0.38	0.04	2.85
VE1A - 11	7.19	0.05	0.38	0.04	2.04
VE1A - 12	7.47	0.04	0.39	0.04	2.05
VE1A - 13	7.76	0.05	0.38	0.04	2.36

Sample ID	Depth m	θr (cm^3/cm^3)	θs (cm^3/cm^3)	α (1/cm)	η (-)
VPV1A - 2	xx	0.03	0.39	0.03	1.41
VPV1A - 3	xx	0.03	0.39	0.03	1.41
VPV1A - 4	xx	0.03	0.39	0.04	1.62
VPV1A - 5	xx	0.03	0.40	0.04	1.47
VPV1A - 6	xx	0.04	0.39	0.03	1.42
VPV1A - 7	xx	0.04	0.39	0.03	1.41
VPV1A - 8	xx	0.03	0.39	0.03	1.41
VPV1A - 11	xx	0.04	0.39	0.03	1.41
VPV1A - 12	xx	0.04	0.39	0.05	1.74
VPV1A - 13	xx	0.04	0.39	0.04	1.54
VPV1A - 14	xx	0.04	0.39	0.04	1.44
VPV1A - 16	xx	0.03	0.39	0.05	1.87
VPV1A - 17	xx	0.04	0.39	0.04	1.48
VPV1A - 18	xx	0.04	0.39	0.03	1.41
VPV1A - 19	xx	0.04	0.39	0.03	1.41
VPV1A - 20	xx	0.05	0.38	0.03	1.73
VPV1A - 21	xx	0.04	0.39	0.04	1.87
VPV1A - 22	xx	0.04	0.39	0.04	1.74
VPV1A - 23	0.56	0.03	0.39	0.04	1.50
VPV1A - 26	3.62	0.04	0.39	0.02	1.42
VPV1A - 27	3.96	0.04	0.39	0.02	1.42
VPV1A - 28	4.45	0.04	0.39	0.03	1.41
VPV1A - 29	4.76	0.05	0.39	0.02	1.41
VPV1A - 34	7.28	0.03	0.39	0.04	1.43
VPV1A - 35	7.34	0.05	0.42	0.00	1.68
VPV1A - 37	7.57	0.03	0.39	0.04	1.44
VPV1A - 44	11.63	0.05	0.38	0.03	3.21
VPV1A - 50	17.07	0.04	0.39	0.02	1.43
VPV1A - 51	17.63	0.03	0.41	0.01	1.48
VPV1A - 52	18.66	0.03	0.41	0.02	1.45
VPV1A - 53	19.46	0.04	0.39	0.01	1.48
VPV1A - 54	20.24	0.04	0.40	0.01	1.47
VPV1A - 55	21.69	0.03	0.40	0.02	1.45
VPV1A - 57	22.91	0.04	0.41	0.01	1.62
VPV1A - 59	23.34	0.04	0.39	0.04	1.51
VPV1A - 64	28.02	0.04	0.46	0.00	1.71
VPV1A - 65	29.13	0.03	0.44	0.01	1.60

Appendix D

K_{Gm}, K_{Gc}, and K_{Ga} (m/s) values for high quality boreholes and geomorphic elements

ARS-1A

Depth (m)	K_{Gm} (m/s)	K_{Gc} (m/s)	K_{Ga} (m/s)
0 - 11.28	1.47×10^{-6}	9.94×10^{-7}	1.11×10^{-6}

FRE-1A

Depth (m)	K_{Gm} (m/s)	K_{Gc} (m/s)	K_{Ga} (m/s)
0 - 7	0	2.80×10^{-7}	2.80×10^{-7}
7 - 11.51	0	8.19×10^{-6}	8.19×10^{-6}
11.51 - 13	0	3.64×10^{-7}	3.64×10^{-7}
13 - 14	0	4.32×10^{-5}	4.32×10^{-5}
Below 14	0	4.33×10^{-7}	4.33×10^{-7}

GDC-1A

Depth (m)	K_{Gm} (m/s)	K_{Gc} (m/s)	K_{Ga} (m/s)
0 – 36.5	1.24×10^{-7}	5.76×10^{-8}	8.34×10^{-8}

GDC-2B

Depth (m)	K_{Gm} (m/s)	K_{Gc} (m/s)	K_{Ga} (m/s)
0 – 10.3	2.71×10^{-7}	3.76×10^{-7}	3.23×10^{-7}

GDC-10A

Depth (m)	K_{Gm} (m/s)	K_{Gc} (m/s)	K_{Ga} (m/s)
0 – 2.5	1.03×10^{-5}	4.64×10^{-5}	2.19×10^{-5}
Below 2.5	7.04×10^{-7}	3.18×10^{-7}	4.54×10^{-7}

TGI-1A

Depth (m)	K_{Gm} (m/s)	K_{Gc} (m/s)	K_{Ga} (m/s)
0 – 16	4.65×10^{-7}	4.00×10^{-7}	4.15×10^{-7}

VAN-1A

Depth (m)	K_{Gm} (m/s)	K_{Gc} (m/s)	K_{Ga} (m/s)
0 - 30	4.20×10^{-7}	9.28×10^{-7}	7.46×10^{-7}
30 - 32.5	0	8.45×10^{-4}	8.45×10^{-4}
Below 32.5	4.36×10^{-7}	2.43×10^{-7}	3.03×10^{-7}

VE-1A

Depth (m)	K_{Gm} (m/s)	K_{Gc} (m/s)	K_{Ga} (m/s)
0 – 6	4.30×10^{-7}	2.06×10^{-7}	2.88×10^{-7}
Below 6	2.68×10^{-6}	2.85×10^{-5}	1.11×10^{-5}

VPV-1A

Depth (m)	K_{Gm} (m/s)	K_{Gc} (m/s)	K_{Ga} (m/s)
0 – 29.13	1.61×10^{-7}	1.10×10^{-7}	1.25×10^{-7}

Drumlinized Till/Outwash Plain

K_{Gm} (m/s)	K_{Gc} (m/s)	K_{Ga} (m/s)
2.30×10^{-7}	2.53×10^{-7}	2.71×10^{-7}

Outwash Plain

K_{Gm} (m/s)	K_{Gc} (m/s)	K_{Ga} (m/s)
1.10×10^{-6}	1.61×10^{-6}	1.40×10^{-6}

Paris Moraine

K_{Gm} (m/s)	K_{Gc} (m/s)	K_{Ga} (m/s)
2.83×10^{-7}	8.17×10^{-7}	6.14×10^{-7}